Geo. P Newton 621

GCA-TR-67-1-N

COLD CATHODE GAUGE DEVELOPMENT

Wallace S. Kreisman

GCA CORPORATION
Bedford, Massachusetts

FINAL REPORT
CONTRACT NO. NAS5-9180
(29 April 1965 - 20 December 1966)

PREPARED FOR
NATIONAL AERONAUTICS AND SPACE ADMINISTRATION
GODDARD SPACE FLIGHT CENTER
GREENBELT, MARYLAND

DECEMBER 1968

GCA-TR-67-1-N

Final Report

for

COLD CATHODE GAUGE DEVELOPMENT

(29 April 1965 - 20 December 1966)

Contract No.: NAS5-9180

Goddard Space Flight Center

Contracting Officer: J.L. Turner
Technical Monitor: George Newton 621

Prepared by:

GCA CORPORATION
GCA TECHNOLOGY DIVISION
Bedford, Massachusetts

Project Manager: Wallace S. Kreisman

for

Goddard Space Flight Center
Greenbelt, Maryland

ABSTRACT

Studies were made of basic characteristics of magnetron type cold cathode ionization gauges. Specialized equipment was developed and used to determine the distribution of nitrogen and helium positive ion energies and to provide data for the calculation of positive ion origins and trajectories. The trajectory equations were applied to the design of a magnetron gauge mass spectrometer. Gauge pumping and re-emission characteristics for nitrogen were studied. The response of a cold cathode gauge to cycling pressures was determined with the aid of a unique "cycling valve" and a special test system. Gauge stability, noise and calibration experiments were performed.

TABLE OF CONTENTS

LIST OF ILLUSTRATIONS

LIST OF ILLUSTRATIONS (continued)

LIST OF ILLUSTRATIONS (continued)

LIST OF ILLUSTRATIONS (continued)

LIST OF ILLUSTRATIONS (continued)

LIST OF TABLES

I. INTRODUCTION

The objective of this research program was to continue the study and development of cold cathode gauges that was initiated in an earlier program [1]*. Some of the specific tasks undertaken in the program were: (1) a study of gauge pumping and re-emission, (2) measurement of gauge response to cycling pressures, (3) measurement of positive ion energies under various gauge operating conditions, (4) a study of gauge output current stability, and (5) investigation of the feasibility of using a cold cathode gauge as a low resolution mass spectrometer.

Cold cathode ionization gauges have several applications in the space program. Some of these gauges (the GCA model R-5 gauge, for example) have been flown on satellites to measure total ambient densities of the Earth's atmosphere. The low pressure capability of these gauges makes them ideal for measuring the lunar atmospheric density and the low pressures achieved in ultra high vacuum space simulation chambers. A quite recent application of these gauges has been made in the design of spacecraft orientation and attitude control systems [2].

A cold cathode ionization gauge is a vacuum measurement device that consists essentially of two electrodes, and anode and a cathode, with a potential of several kilovolts between them. The electrodes are positioned relative to an external magnetic field of about one kilogauss. The low pressure gas within the interelectrode region breaks down as a result of the strong electric and magnetic fields, and a relatively stable discharge results. It has been found that the discharge current is a direct measure of the number density of gas molecules within the gauge and the gas density is directly related to the gas pressure at a constant temperature.

The first cold cathode gauge was developed by Penning in 1937 [3]. The original Penning type gauges utilized plane parallel circular plates for cathodes and a wire ring as an anode. These gauges would measure pressures only as low as 10^{-6} or 10^{-7} torr. In the late 1950's, a number of improved cold cathode gauges were developed, notably the magnetron-type gauge of Redhead [4]. The essential elements of this new device were a spool-shaped cathode, a surrounding concentric, cylindrical anode, and an auxiliary cathode or shield ring interposed between the edges of the anode and cathode. The shield ring facilitates the initiation of the discharge and separates the discharge initiating current from the positive ion current to the ion collector. Recently, a Penning type discharge gauge has been constructed that is allegedly capable of measuring pressures as low as 10^{-14} torr [5]. A filament is used to start this gauge at low pressures. The design of this gauge is such that it may be operated with an electron multiplier to increase its sensitivity.

---

*Number in [ ] throughout text indicate reference numbers.

In spite of the many advances made in the design of new cold cathode gauges for low pressure operation, little is known about the detailed manner in which they operate. The discharge in the gauge is believed to be a self-sustained Townsend discharge. Although the theory of the discharge initiation has been developed by Beck and Brisbane [6], Haefer [7], and Redhead [8], a detailed theory of the gauge's steady state operation has not been worked out.

Lacking a definite, detailed theory of gauge operation, the logical procedure to be used to understand and improve the operating characteristics of cold cathode gauges is to study their behavior experimentally. Specifically, it would be most valuable to know the electronic space charge distribution within the gauge, the energies and trajectories of the electrons, the rate at which secondary electrons are generated at the electrode surfaces, the electric field distribution within the gauge, the energies and trajectories of the positive ions, and such specialized phenomena as gauge pumping and re-emission. A portion of the research work reported herein deals with a determination of positive ion energies and trajectories and gauge pumping and re-emission.

Positive ion energies were measured for both nitrogen gas and helium gas within a specially constructed cold cathode gauge. A second experimental gauge was used to obtain information concerning the trajectories of positive ions. An attempt was made to determine the origin of positive ions.

Some pumping and re-emission measurements were made for nitrogen gas using a standard magnetron type cold cathode gauge. Pumping speeds and re-emission rates were measured.

In addition to the above studies, which might be termed "fundamental" studies, there are a number of other research areas that involve applications of cold cathode gauges. Two important applications that are discussed in this report are the potential use of a magnetron type cold cathode gauge as a low resolution mass spectrometer and the use of cold cathode gauges to measure cycling gas pressures. The use of a cold cathode gauge as a mass spectrometer would offer the advantages of simplicity, low cost and the absence of a filament with its many limitations.

The reason for studying the response of cold cathode gauges to time varying pressures may not be immediately evident, but there are at least two important applications in the Space program: The first application is the use of such a gauge to measure ambient densities in the Earth's atmosphere (and other planetary atmospheres) from a spinning satellite. The second application is the use of such gauges to determine the orientation of a satellite or space vehicle with respect to the relative wind.

In addition to the above studies, some limited experimental work was performed to look at cold cathode gauge noise and to study the adsorption of nitrogen gas during cold cathode gauge calibration at low pressures.

II. ION ENERGY DISTRIBUTIONS IN A MAGNETRON-TYPE COLD CATHODE IONIZATION GAUGE

The Test System

An all-pyrex glass vacuum test system was used in measuring the energies of positive ions in a magnetron type cold cathode ionization gauge. This same test system was used in the research concerned with a determination of electronic space charge, the determination of positive ion trajectories and positive ion origins, and the design of a magnetron type cold cathode low resolution mass spectrometer. This test system is shown in block diagram form in Figure 1. Figure 2 is a photograph of the complete apparatus.

The glass test system used an H.S. Martin Company model 40-1100 mercury diffusion pump, a three jet pump with a nominal pumping speed of about 50 liters/sec, as the main pump. The Martin pump was backed up with a second glass diffusion pump, Eck and Krebs model 4000 pump, having a speed of about 5 liters/sec. The second pump decreased the forepressure of the large Martin pump and permitted lower pressures to be attained in the test chamber. The backing diffusion pump exhaused into a Welch model 1400 mechanical pump that had a speed of 21 liters/min. A single, demountable glass vacuum trap cooled with dry ice was located between the mechanical pump and the backing diffusion pump. A dual glass vacuum trap cooled with liquid nitrogen was postioned between the two diffusion pumps. A conventional thoriated iridium filament Bayard-Alpert type ionization gauge was connected between the two single sections of the dual trap. This ionization gauge indicated the forepressure of the Martin pump and was used to monitor the system pressure during bakeout.

Two additional liquid nitrogen cooled vacuum traps separated the Martin diffusion pump from the test chamber. The first of these was a conventional single trap 30 cm long and 5 cm in outer diameter with a 3-cm diameter inner tube. The second trap was of the spherical variety, designed to have a high vacuum conductance. The inner bulb, which held the liquid nitrogen, had a capacity of 500 ml. The outer bulb was constructed from a 1-liter spherical flask. The tubulations joining the two cold traps and the test chamber were 3.5 cm in diameter.

The test chamber was constructed from a length of 7.5 cm O.D. pyrex glass tubing. Essentially, it was a cylinder about 25 cm long, closed at one end and tubulated with 3.5 cm diameter tubing at the other end that connected to the spherical cold trap. At the center of the cylinder, there were four 2.5-cm diameter tubulations spaced 90 degrees apart to which various experimental gauges could be attached.

Pure gases were introduced into the test system from a glass manifold to which three 1-liter flasks of reagent grade gases were attached. The manifold was separated from the system by a Hoke model 411 all-metal diaphragm

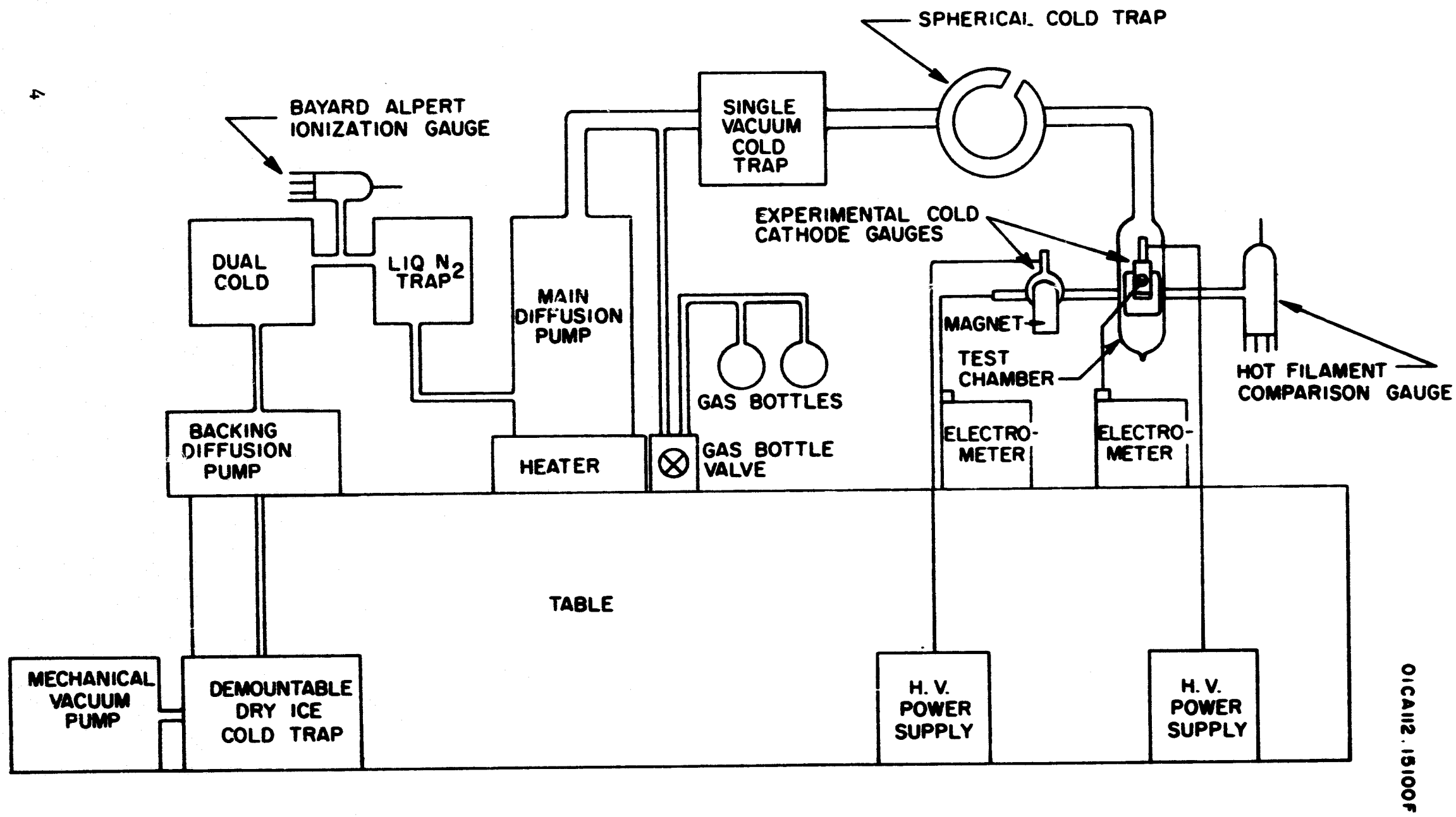

Figure 1. Block diagram of glass vacuum test system.

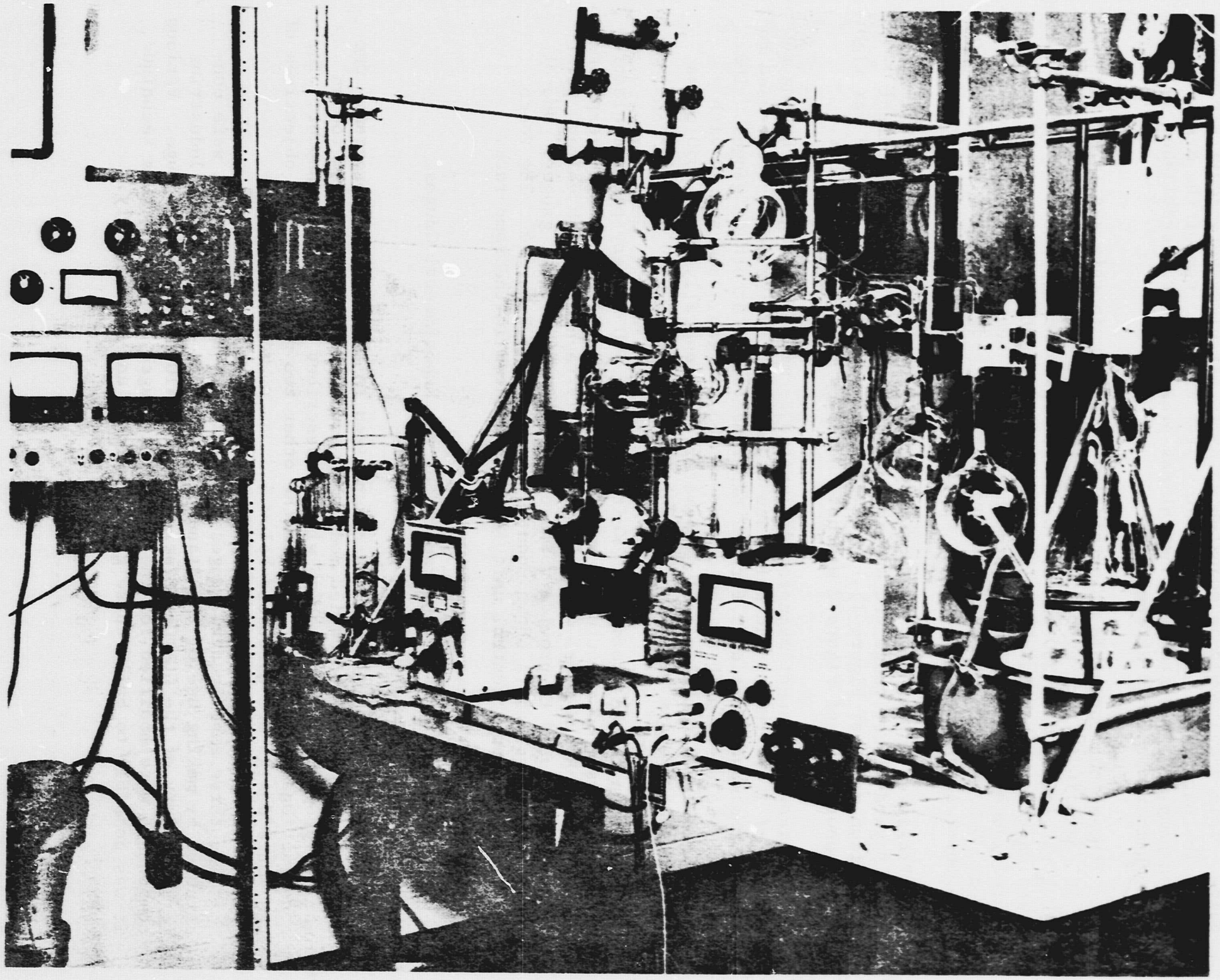

Figure 2. Photograph of vacuum test system.

valve. This valve could be adjusted so as to establish very small flows of gas. The pure gases entered the test system near the top of the Martin diffusion pump. Fairly stable, constant gas pressures were established in the test chamber with this arrangement.

It was found possible to obtain low pressures in this system of the order of 10^{-9} and 10^{-10} torr by baking all of the high vacuum components at temperatures ranging between 250 and 350°C. Bakeout was accomplished by using heating tapes wherever possible and using a heat gun to heat portions of the experimental gauges and other components that were not heated sufficiently by the tapes. Generally, several days of pumping were required after bakeout to reduce the test chamber pressure to its lowest equilibrium value.

Pressures in the test chamber were measured with a hot filament Veeco RG-75 Bayard-Alpert gauge and associated control unit (the hot filament comparison gauge of Figure 1). The large McLeod gauge shown at the far right in the photograph of Figure 2 was not connected to the test chamber.

Alnico V permanent magnets (designated as model M-5 magnets) having an air gap of 1 1/4 inches and pole face diameters of 1 1/4 inches were used to provide the magnetic fields for the experimental cold cathode gauges. The magnetic field strength at the center of the air gap, as measured with a Rawson model 501 rotating coil gaussmeter, was generally about 1050 gauss. Two of these magnets are shown resting on the table top in Figure 2.

As shown in the photograph, Keithley model 600 battery-powered electrometers were used to measure the small dc currents generated in the experimental gauges. John Fluke model 408A and 408B highly regulated high voltage power supplies were used to provide voltages to the experimental gauges. One of these power supplies is shown mounted in a rack in Figure 2. The Veeco Bayard-Alpert gauge control unit is shown mounted in the same rack.

Design and Construction of the Experimental Gauges

Three experimental gauges were utilized in this research program. One of these gauges, the so-called model X-1 gauge, had been designed for an earlier program. The X-1 gauge will be described in the next chapter. The constructional features of each of the other two gauges and the objectives of the gauge design are discussed below.

The three experimental gauges, the X-1, Y-1 and Y-2 gauges, were constructed by making use of the standard components of the Vacuum Industries (a subsidiary of the GCA Corporation) model 1410 cold cathode gauge. Various components were modified for the different gauges. By using this technique, it was possible to build these gauges quickly and economically.

The Model Y-1 Experimental Gauge. The model Y-1 gauge was designed specifically to measure positive ion energies. The salient features of this gauge, as shown in Figure 3, were the placement of a relatively large diameter (.060 inches) wire probe inside the hollow cathode and the provision of a small .010 inches diameter aperture in the side wall of the hollow cathode on the gauge centerline. The small diameter aperture was constructed in the following fashion: A hole 1/8-inch in diameter was drilled through the center of the cylindrical portion of the cathode. This hole was then covered with a sheet of thin wall (.002 inches thick) stainless steel in which a .010-inch diameter hole had been drilled. The thin sheet was welded to the cathode so as to as to center the small aperture with respect to the 1/8-inch diameter hole. The inner diameter of the hollow cathode was .187 inch and the distance from the .010-inch aperture to the center of the hollow cathode was .156 inch.

As can be seen in Figure 3, the gauge cathode was spool shaped. The cathode and plates were 1.0 inch in diameter and the height of the cathode was 13/16 inch. The gauge anode was a cylinder having a length of 1/2 inch and an inner diameter slightly greater than 1 inch so that it could be slipped over the cathode. The gauge envelope was a cylinder 1.9 inches in outer diameter and 1 7/32 inches high overall. A 3/4-inch O.D. tubulation utilizing a Kovar-to-pyrex graded seal permitted the gauge to be attached to the system test chamber. The length of this tubulation was about 9 inches. All metal portions of the gauge were made of type 304 stainless steel that had been vacuum fired to reduce their outgassing rates.

The lower part of the gauge cathode was held in position by resting on a 1/4-inch diameter ceramic sphere that was accurately positioned with respect to the bottom cover of the envelope. The top of the cathode was fastened to the central conductor of a cable end seal as shown. In this way, access was provided to the top, open end of the hollow cathode. A probe wire .060-inch in diameter was centered within the hollow cathode and connected to the central conductor of a separate cable end seal. Short lengths of pyrex glass tubing were used to insulate this probe at all points except the portion within the hollow cathode. The anode cylinder was held in position by the central conductor of a third cable end seal. The conductors provided electrical connections to the cathode, probe and anode as well as serving as mechanical supports.

The central probe that was inserted within the hollow cathode was chosen to have a diameter of .060 inch because experimentation with a similar gauge that had been developed earlier (the model X-1 gauge, to be described in the next chapter) had shown that such a wide probe would effectively collect all of the positive ions that entered the hollow cathode through a .010-inch diameter aperture.

The Model Y-2 Experimental Gauge. The model Y-2 gauge was designed to measure the relative radial electronic space charge distribution within a cold cathode gauge without disturbing the discharge. The unusual element of this experimental gauge was a special cathode in which a series of eleven

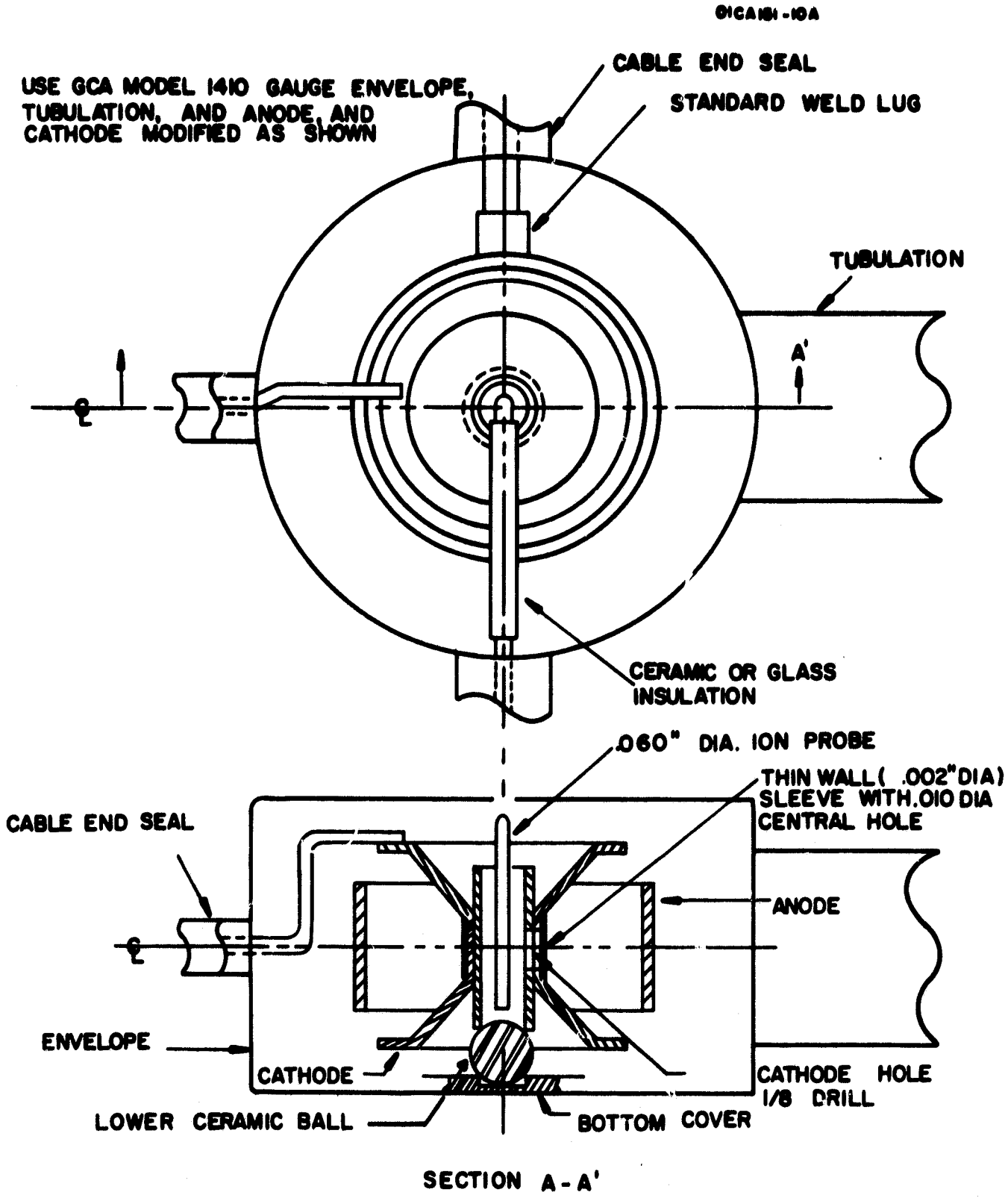

Figure 3. Model Y-1 experimental cold cathode gauge.

small holes had been drilled along a radial line in the upper cathode end plate. The holes were .010 inches in diameter and were spaced .030 inches apart. A bellows-sealed micrometer movement feedthrough was used to move a .010 inches diameter wire probe in a radial direction just above the series of holes in the cathode end plate. In its radial motion, the probe moved successively over each of the eleven holes. Figure 4 is a schematic drawing of this gauge.

In this particular gauge, the cathode end plates were built to overlap the top and bottom edges of the standard cylindrical anode. The cathode end plates were made of .015 inches thick type 304 stainless steel. The central portion of the cathode was a pure cylinder in contrast to the partly conical standard cathode. The cathode was positively positioned by means of two ceramic spheres as shown in Figure 4.

The movable probe wire and its electrical connection to a cable end seal was insulated with short lengths of glass tubing. Only the portion of the probe extending over the series of eleven cathode holes was left uninsulated. A separate cable end seal was used to provide an electrical connection to the cathode while heavy stainless wire conductors that were welded to two diametrially opposite cable end seals were used to support the standard anode and provide an electrical connection to this electrode. The same standard gauge envelope and tubulation was used for this gauge as was used for the Y-1 gauge.

The bellows-sealed motion feedthrough that was used to effect movement of the probe wire is described schematically in Figure 5. A welded metal bellows was used in order to provide the maximum amount of movement for a given bellows length. All of the vacuum seams were T.I.G. heliarc welded. The micrometer thread provided a measured movement of .025 inches per revolution. The micrometer scale was graduated with .001 inches divisions. This motion feedthrough provided a total travel of about 7/16 inch. Since it was constructed entirely of stainless steel, it could be baked out in the same fashion as the other components of the gauge.

Experimental Results

Ion Energy Measurements. The Y-1 experimental gauge was sealed to the test chamber of the glass vacuum test system described earlier and was connected electrically as shown in Figure 6. A J. Fluke model 408A power supply was used to furnish high voltage to the gauge anode while a J. Fluke model 408B power supply, in which the output voltage is variable from 0 volts up to 6 kV, was used to furnish the retarding or bias potential to the gauge cathode. The central ion collecting probe within the hollow cathode was connected to ground through a Keithley model 600 electrometer. Since the voltage input to the Keithley was never more than 1 volt, the potential of the ion probe was never more than 1 volt positive above ground (zero) potential. A second Keithley model 600 electrometer was used to measure the current drawn from the gauge anode high voltage supply. This supply current is predominantly due to the current flow between the gauge anode and cathode, although there can be a small current flow between the anode and the grounded envelope of the gauge.

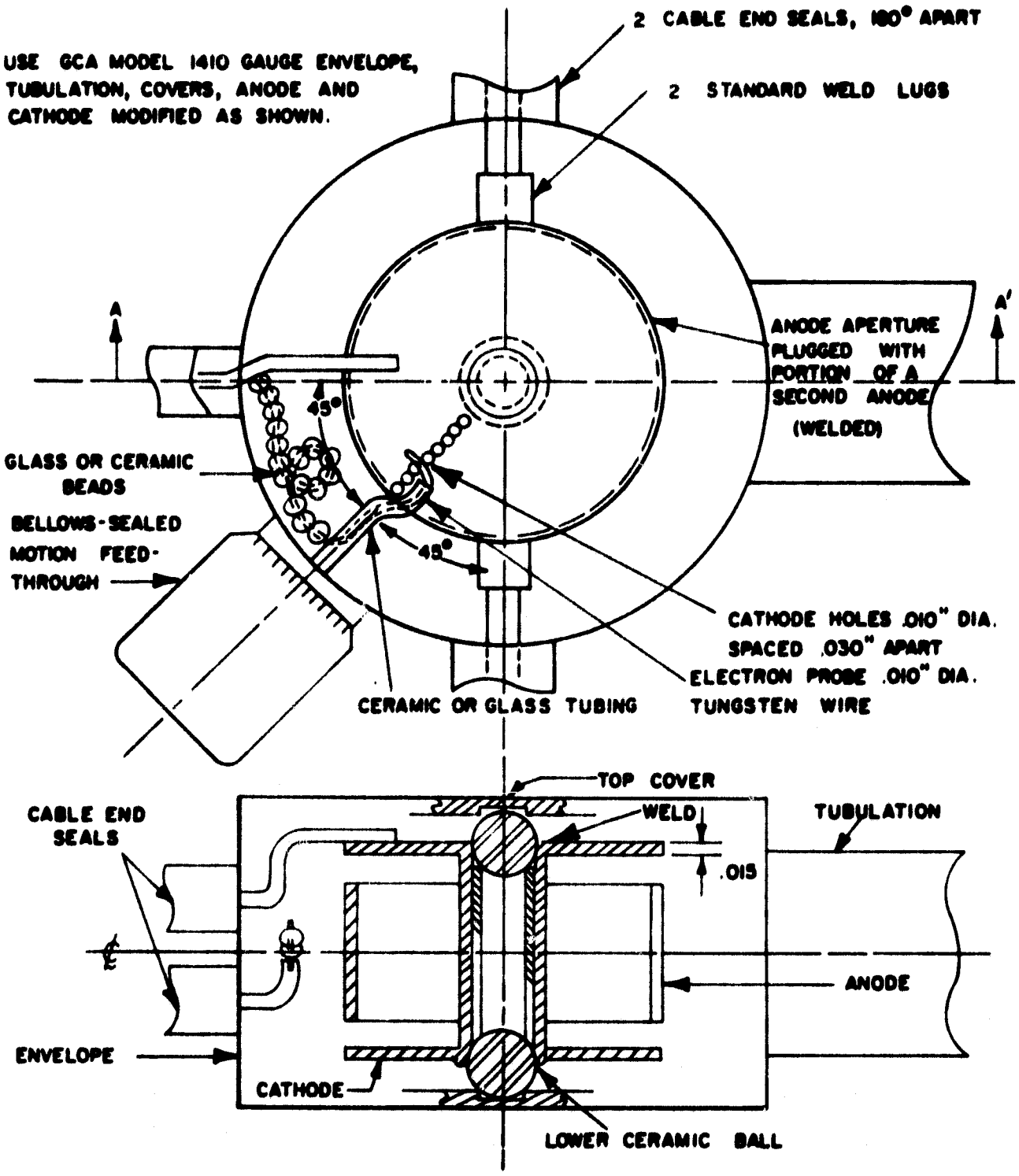

Figure 4. Model Y-2 experimental cold cathode gauge.

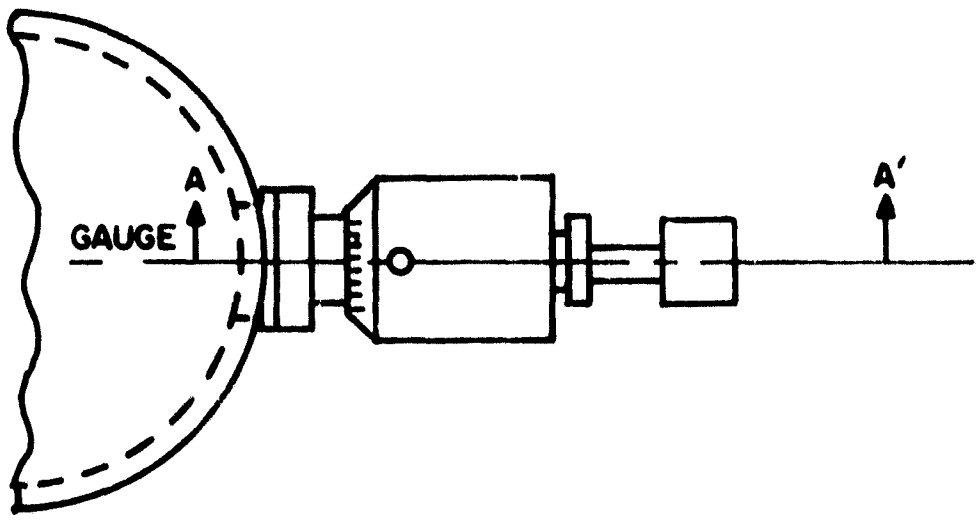

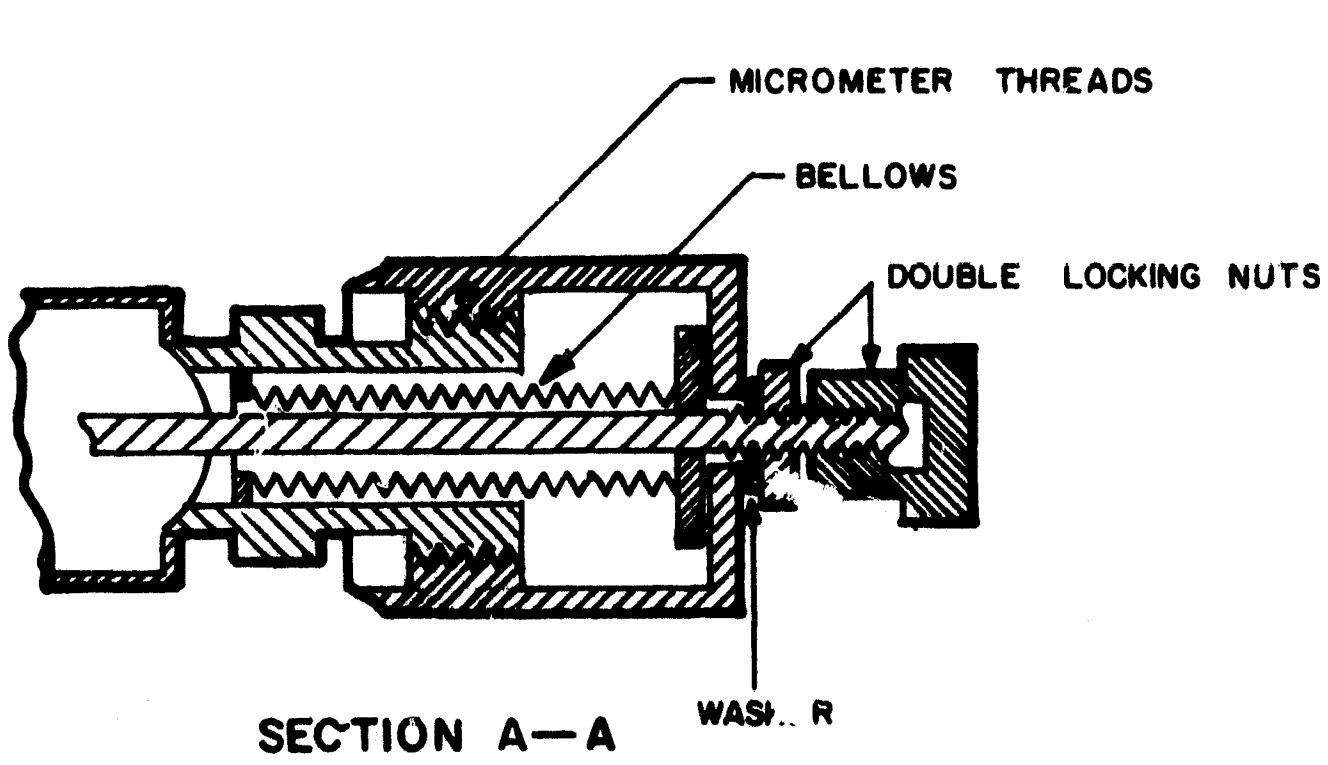

Figure 5. Bellows-sealed motion feedthrough.

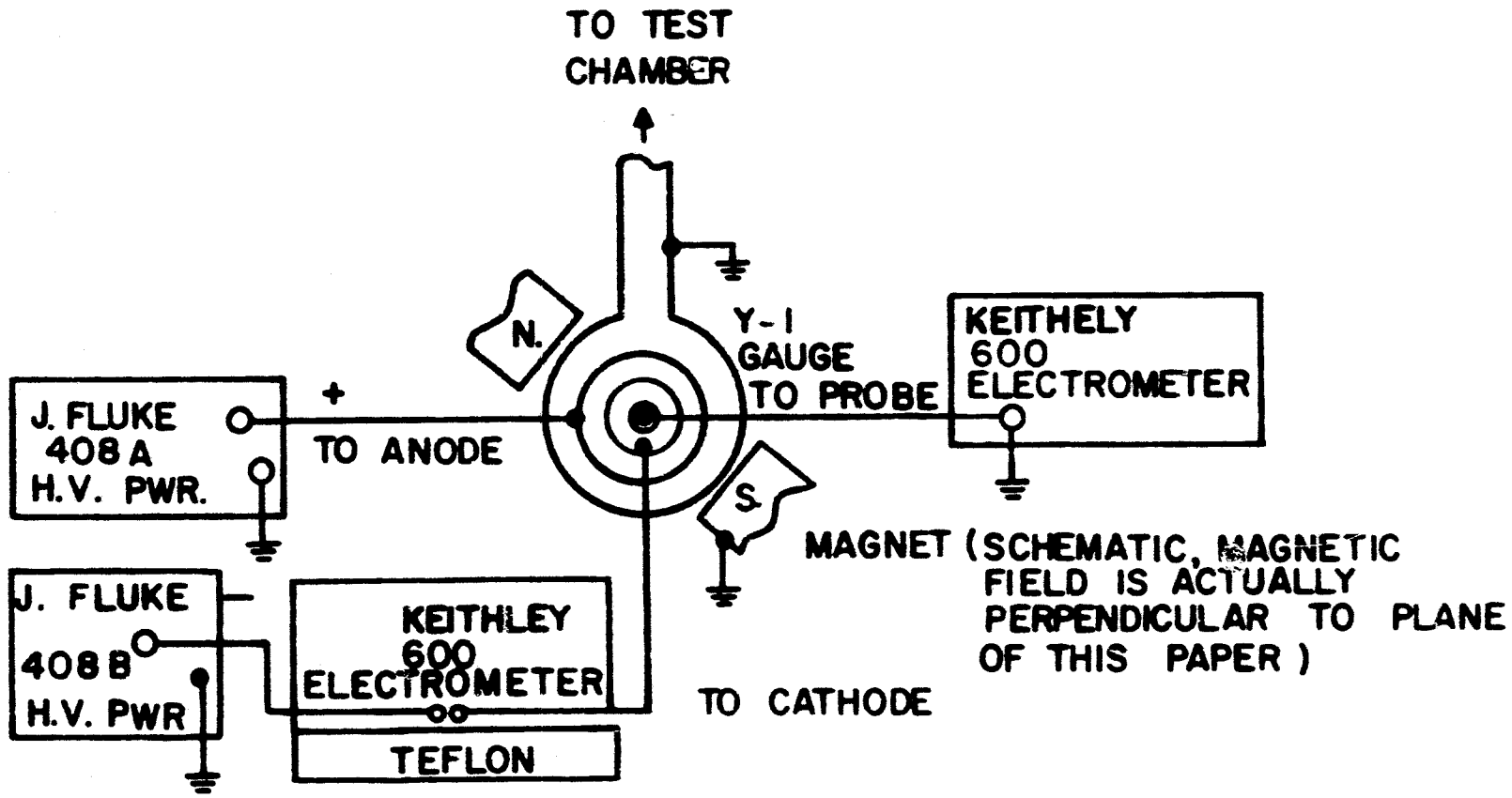

Figure 6. Electrical connections used to measure positive ion energies with the Y-1 experimental gauge.

The resistance between the cathode and ion probe of the Y-1 gauge was measured many times and was always found to be greater than 1×10^{13} ohms, the limit of the measurement capability of the Keithley model 600 electrometer when used as an ohmmeter. During each series of ion energy measurements, the actual ohmic leakage current between the cathode and the ion probe was measured by turning off the anode voltage to extinguish the discharge and then recording the current measured by the ion probe electrometer for all values of the negative retarding potential applied to the gauge cathode. The values of leakage current obtained in this way were never more than about 4×10^{-14} amperes, approximately the measurement limit of the Keithley electrometer. Corrections for these small leakage currents were made wherever necessary.

The method used to make positive ion energy measurements was the standard retarding potential method in which successively fewer and fewer ions were permitted to reach the central ion probe by biasing the cathode more and more negative with respect to the ion probe. The cathode negative bias was changed in steps of 50 volts starting with zero (ground) potential. Simultaneous with the change in the cathode bias potential, the anode potential was also changed to maintain a fixed anode-to-cathode potential. In this way, the main discharge between the anode and cathode was held constant as evidenced by the constancy of the current collected by the cathode. In those cases where the cathode current did change slightly despite the constant anode-to-cathode voltage, corrections for the changes were made. The pressure in the test chamber was monitored continuously and remained constant for ion energy measurements at each pressure level. The ion probe current for each value of cathode bias was recorded and constituted the basic data of the measurement were also recorded for each 50-volt change in cathode bias potential was adopted. All measurements were made using the same timing.

The positive ion probe currents that were measured for increasing negative retarding potentials formed a decreasing sequence representing an "or more" cumulative frequency distribution or ogive. The derivative of this cumulative distribution represents the relative positive ion current density as a function of ion energy. The differentiation of the cumulative distribution was actually approximated by a step-by-step differencing using the data points taken at 50-volt ion energy intervals. For convenience of display and interpretation, the cumulative ion probe current was normalized to unity for zero retarding potential and the probe ion current per energy interval (ion current density) was normalized to unity for the maximum ion current density. Corrections for leakage current and variations in the anode-to-cathode discharge current were made.

An unexpected result of the ion energy measurements was the discovery that the positive ion probe current was reduced to zero for a value of retarding bias potential that was considerably less than the anode-to-cathode potential. Not only did the probe current fall to zero at this point, but it would become negative as the retarding potential was made even more negative. Evidently, the ion prove would start collecting electrons when the gauge cathode became sufficiently negative.

A few auxiliary experiments were made to determine the origin of the negative current to the ion probe. At first, ohmic leakage of the probe insulation was suspected. Measurements made with the high voltage to the anode off but with large negative voltages applied to the cathode, with the probe placed at ground (zero) potential via an electrometer, showed that leakage currents were not greater than 10^{-14} amperes. Another possible source of electrons would be a secondary gas discharge between either the central ion probe and the negative cathode or between the negative cathode and the grounded metal envelope. In order to test this possibility, the metal envelope was first placed at the same potential as the cathode. As the cathode was placed at a greater and greater negative potential, it was found that the negative current to the ion probe started much earlier at a smaller negative cathode potential (-500 volts) than for the case where the metal envelope was at ground potential (-900 volts). Evidently the negatively-biased envelope made it easier for the ion probe to collect electrons. When the metal envelope was placed at the same positive potential as the anode (+1.5 kV), the negative current to the ion probe started later at a larger negative cathode potential (-1000 volts).

In all cases it was found that an increase of gas pressure within the gauge had two separate effects. Increasing pressure tended to shift the onset of probe electron collection to larger values of cathode negative potential. This was a very small effect but was consistent with the result, to be described later, that positive ion energies increased with increasing gas pressure. The second effect was that increased gas pressures resulted in much larger negative currents to the ion probe per unit increase in cathode retarding potential. This result confirmed the notion that the undesired electrons were coming from a gas discharge process. The unresolved question to date centers whether the electrons were originating in the main discharge and were somehow finding their way to the ion probe, or whether they were formed in a secondary discharge outside the main anode-to-cathode discharge. Future experimental gauges designed to measure positive ion energies would have to take this phenomenon into account. Despite the shortcoming mentioned above, the ion energy data that was obtained with the Y-1 experimental gauge accounted for about 95 percent of the ions present in the discharge.

Certain system preparations were made prior to making ion energy measurements. The system was baked out and allowed to pump down to a low equilibrium background pressure that was generally in the 10^{-9} torr region. After this, the experimental Y-1 gauge was allowed to operate overnight at the value of anode voltage that would be used for the experiments.

Before ion energy measurements were made, voltage-current characteristics of the Y-1 gauge were determined, using the background gas in the test system. Both the gauge cathode and ion probe currents were measured as a function of the anode voltage for voltages ranging between 1.0 and 4.2 kV. Measurements were made every 100 volts. The gauge cathode and ion probe were essentially at ground (zero) potential. The results of the measurements are displayed in Figure 7. It can be seen that the ion probe current generally followed the cathode current, but that for anode voltages between 2.0 and 3.0 kV, the ion

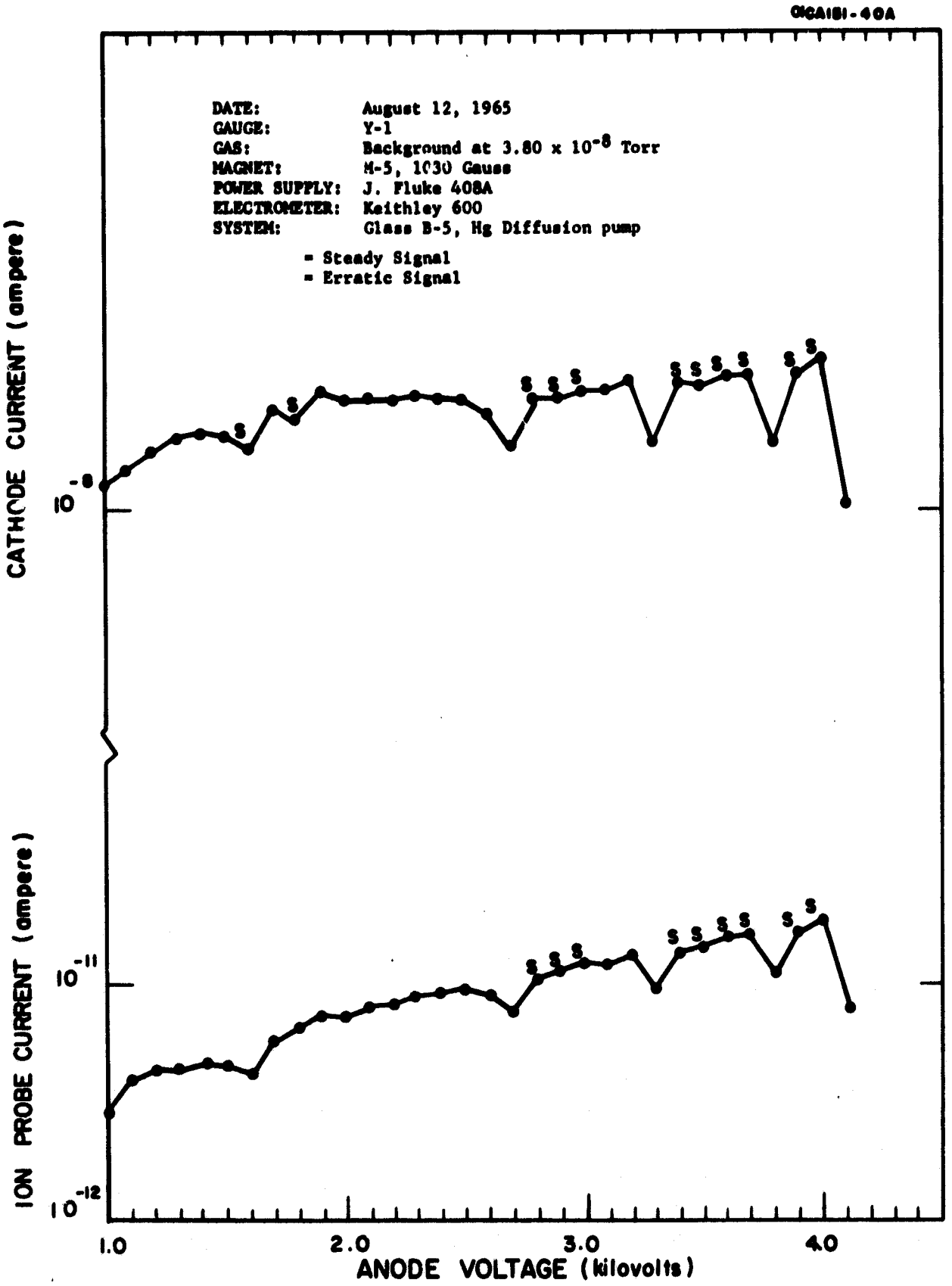

Figure 7. Voltage-current characteristics of the Y-1 experimental gauge.

probe current had a generally increasing value with increasing voltage while the cathode current was relatively constant. The negative dips in both currents coincided as did the regions of steady and unsteady signals. The ion probe does appear to be measuring a constant fraction of the total discharge current.

The first careful ion energy measurement was made with 1.5 kV on the gauge anode using nitrogen gas at a pressure of 8.6×10^{-6} torr. The results of this measurement are shown in Figure 8. The cumulative ion probe currents are plotted in two different ways in this graph. The ratio of each ion probe current i_+ measured in sequence to the maximum ion probe current i_{+MAX} (measured for zero retarding potential) yields an "or more" ogive. This distribution has a value of unity for zero ion energy and decreases to almost zero for higher ion energies. The complementary "less than" cumulative frequency distribution is obtained by subtracting the ratio i_+/i_{+MAX} from unity. The derivative of either ogive, normalized to unity for the maximum value of the derivative, yields the relative ion current density, that is, the ion current per ion energy interval.

As can be seen in Figure 8, the mode of the ion energy distribution occurs at 550 volts. Since this distribution is skewed to the left, the median is some value less than 550 volts and the arithmetic mean will be less than the median. Thus, the mean ion energy is of the order of one third of the anode-to-cathode potential. The ion energy distribution here is basically unimodal.

The second careful ion energy measurement was made with 3.5 kV on the gauge anode using nitrogen gas at a pressure of 8.5×10^{-6} torr. The results of this measuremnnt are shown in Figure 9. Here it is seen that the unimodal distribution obtained with 1.5 kV on the gauge anode has become a multimodal distribution at the higher anode voltage of 3.5kV. There are at least six peaks in the ion current distribution, and there is a distinct valley or near absence of ions having energies between 250 and 400 volts. This data shows clearly the possibility of the existence of "bands of ion energy."

In order to make a systematic stduy of ion energy distributions in a magnetron type cold cathode ionization gauge, several series of related ion energy measurements were made. First, measurements were made with nitrogen gas using an anode voltage of 3.0 kV. The nitrogen gas pressure was increased in steps, starting with a low pressure of 8.5×10^{-8} torr. Second, measurements were made with nitrogen gas using an anode voltage of 1.5 kV, again for a series of increasing pressures. Finally, measurements were made with helium gas at an anode voltage of 1.5 kV.

The results of the systematic positive ion energy measurements are displayed in Figures 10 through 22. A study of these results leads to a number of interesting observations and conclusions. First, the positive ions appear to be grouped into energy bands. The energy bands vary in energy spread from about 100 volts to 200 or 300 volts. For all pressures of nitrogen gas there is an initial energy band of energy spread from zero to 150 volts.

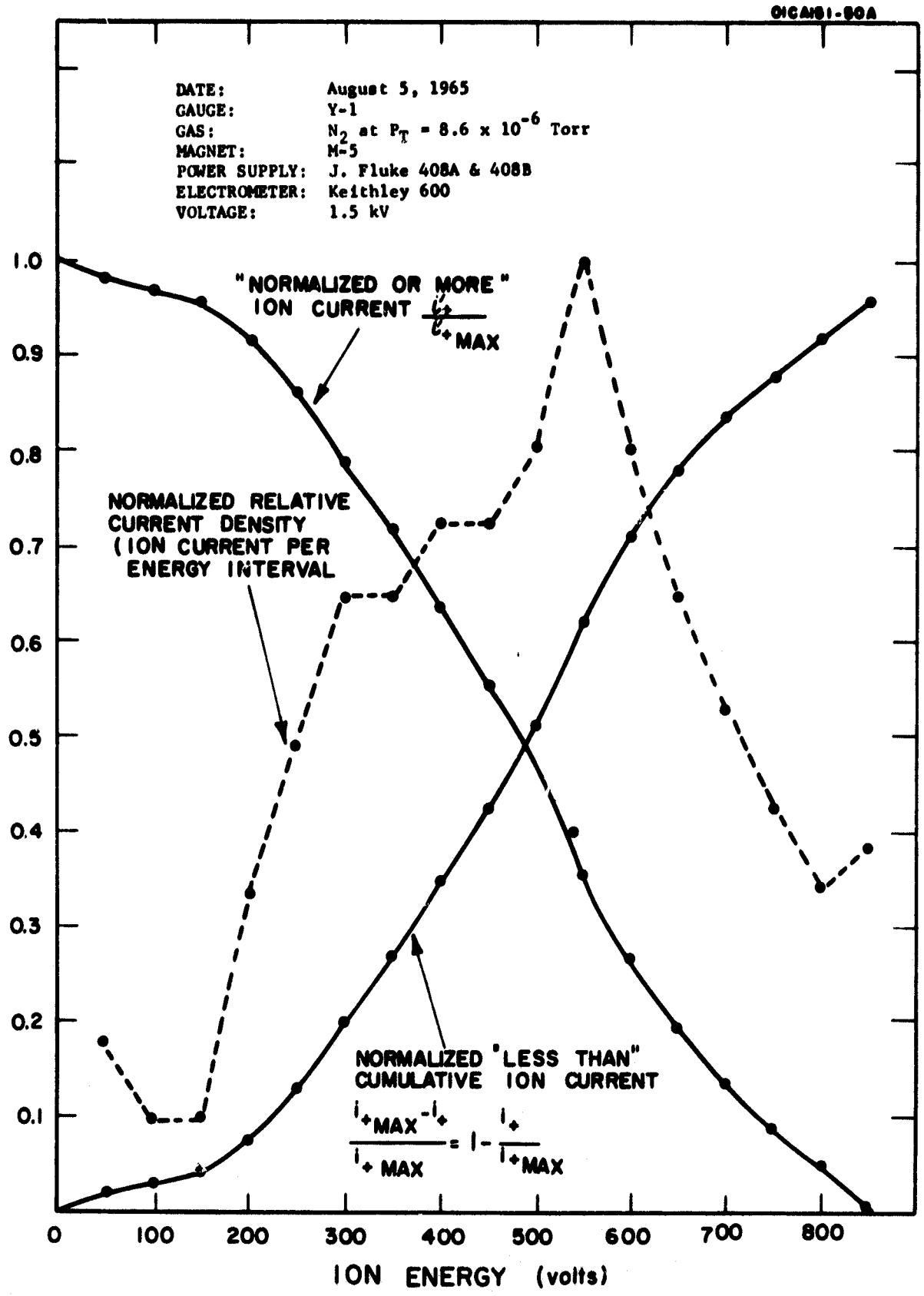

Figure 8. Fractional cumulative ion probe currents and relative ion current density at 1.5 kV for nitrogen gas at 8.6 x 10^{-6} torr.

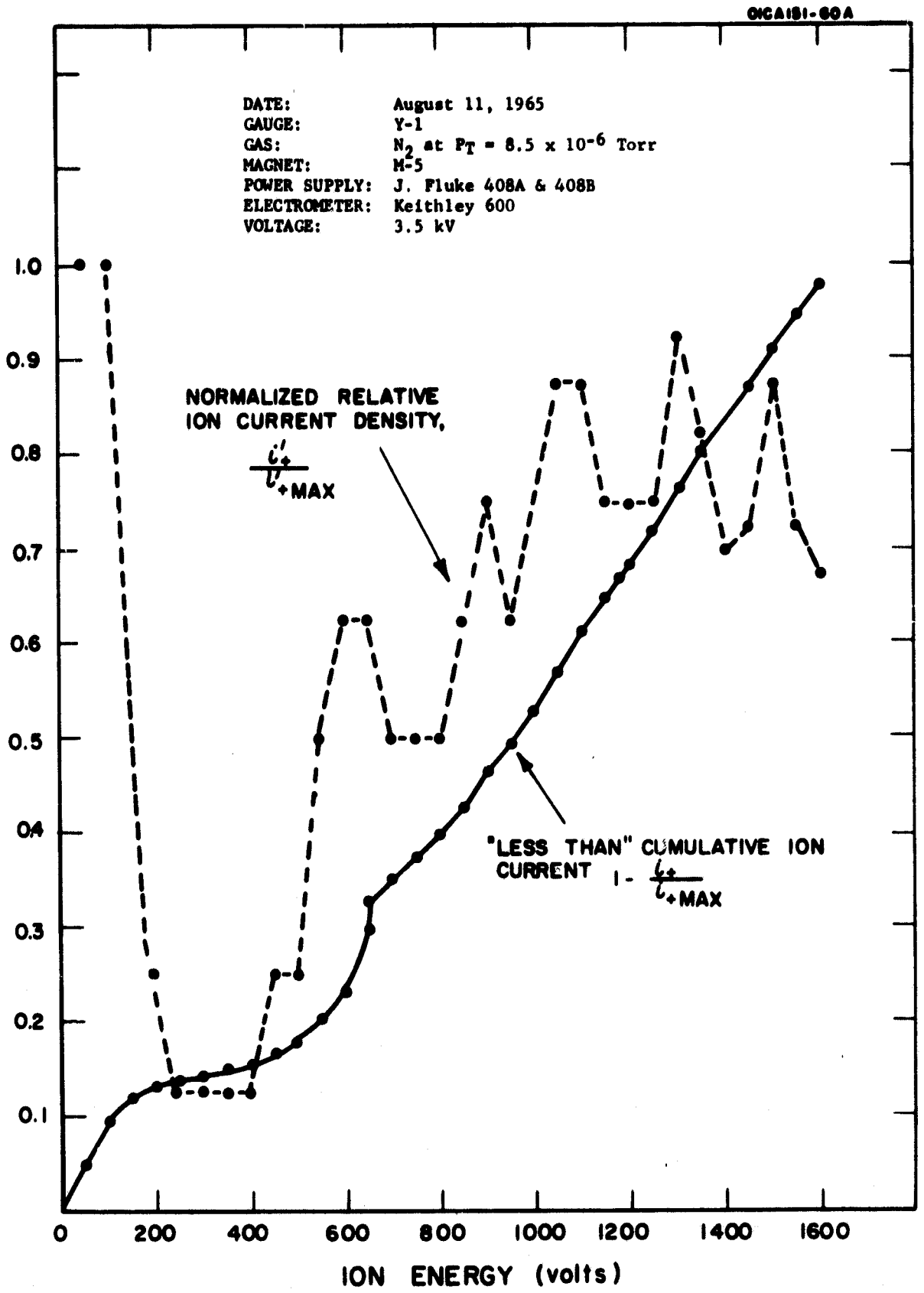

Figure 9. Fractional cumulative ion probe current and relative ion current density at 3.5 kV for nitrogen gas at 8.5 x 10^{-6} torr.

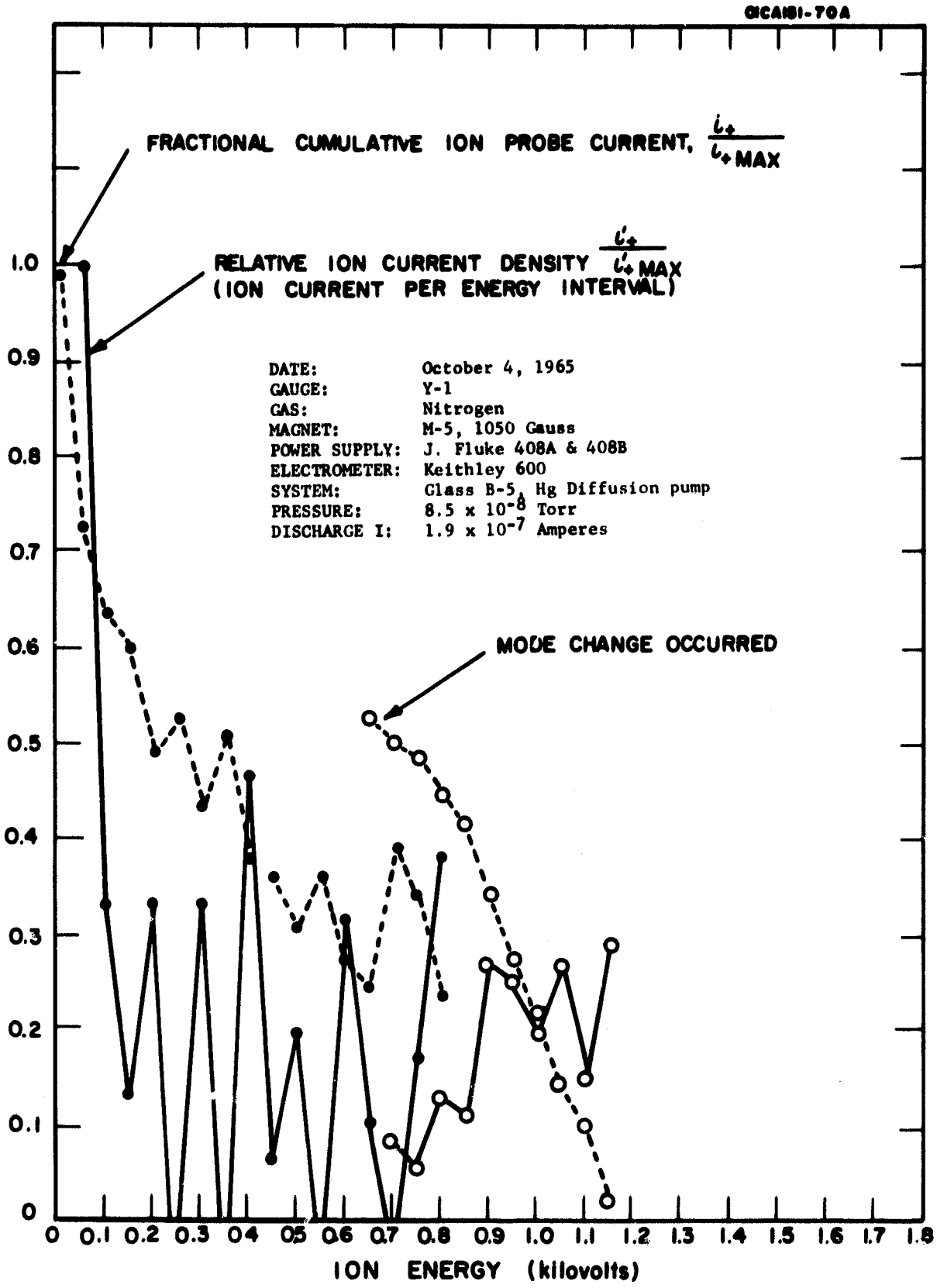

Figure 10. Fractional cumulative ion probe current and relative ion current density at 3.0 kV for nitrogen gas at 8.5×10^{-8} torr.

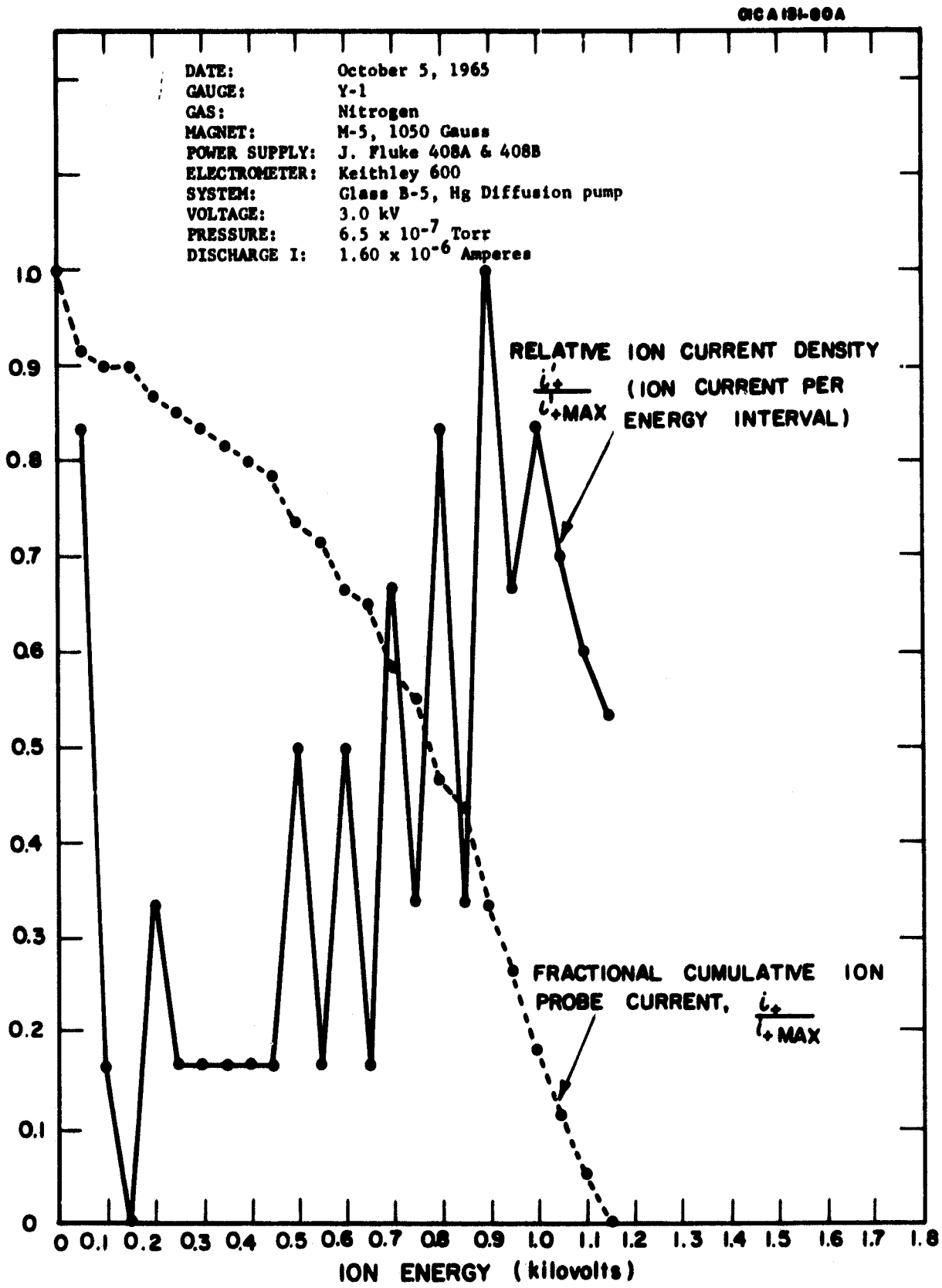

Figure 11. Fractional cumulative ion probe current and relative ion current density at 3.0 kV for nitrogen gas at 6.5×10^{-8} torr.

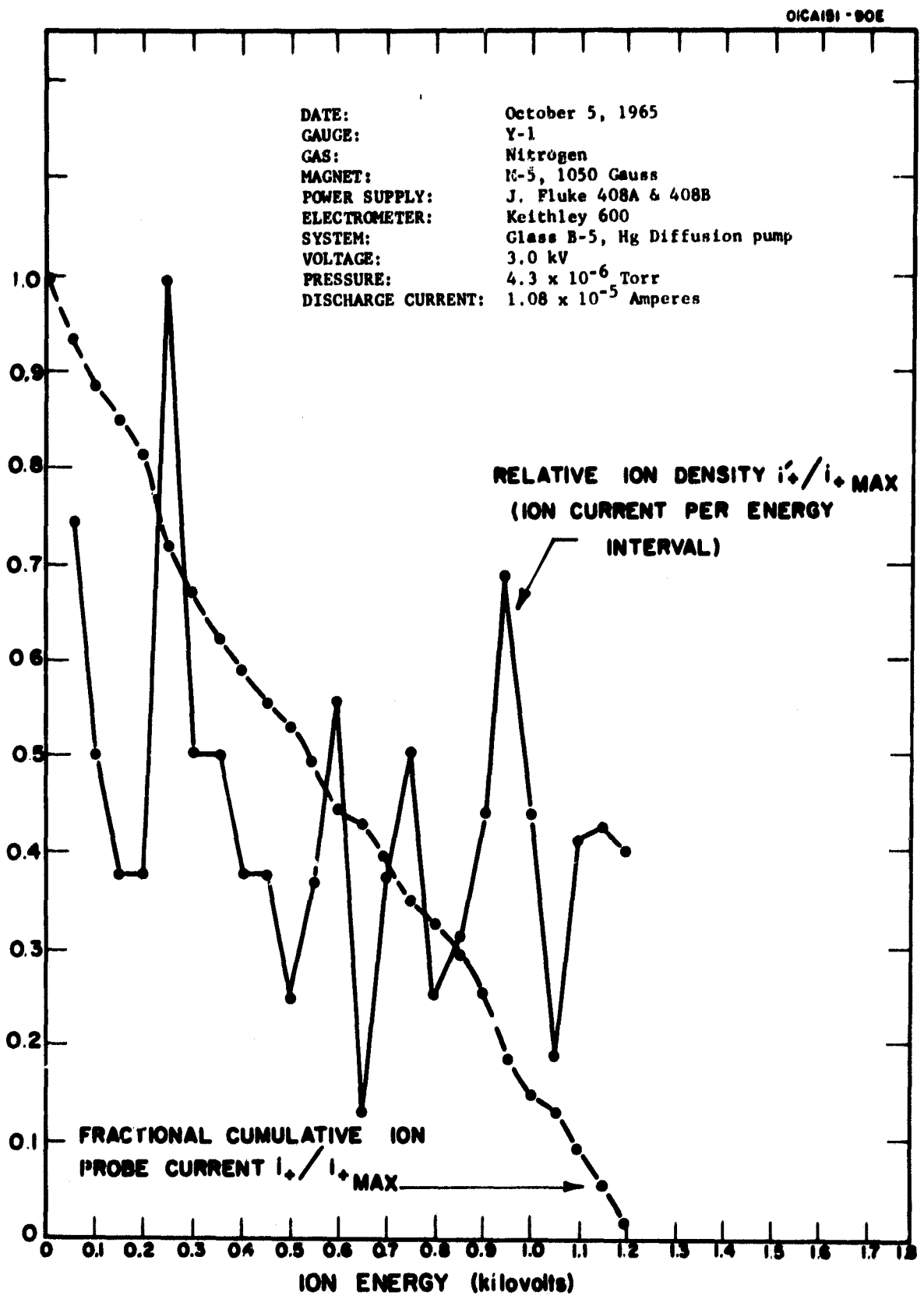

Figure 12. Fractional cumulative ion probe current and relative ion current density at 3.0 kV for nitrogen gas at 4.3×10^{-6} torr.

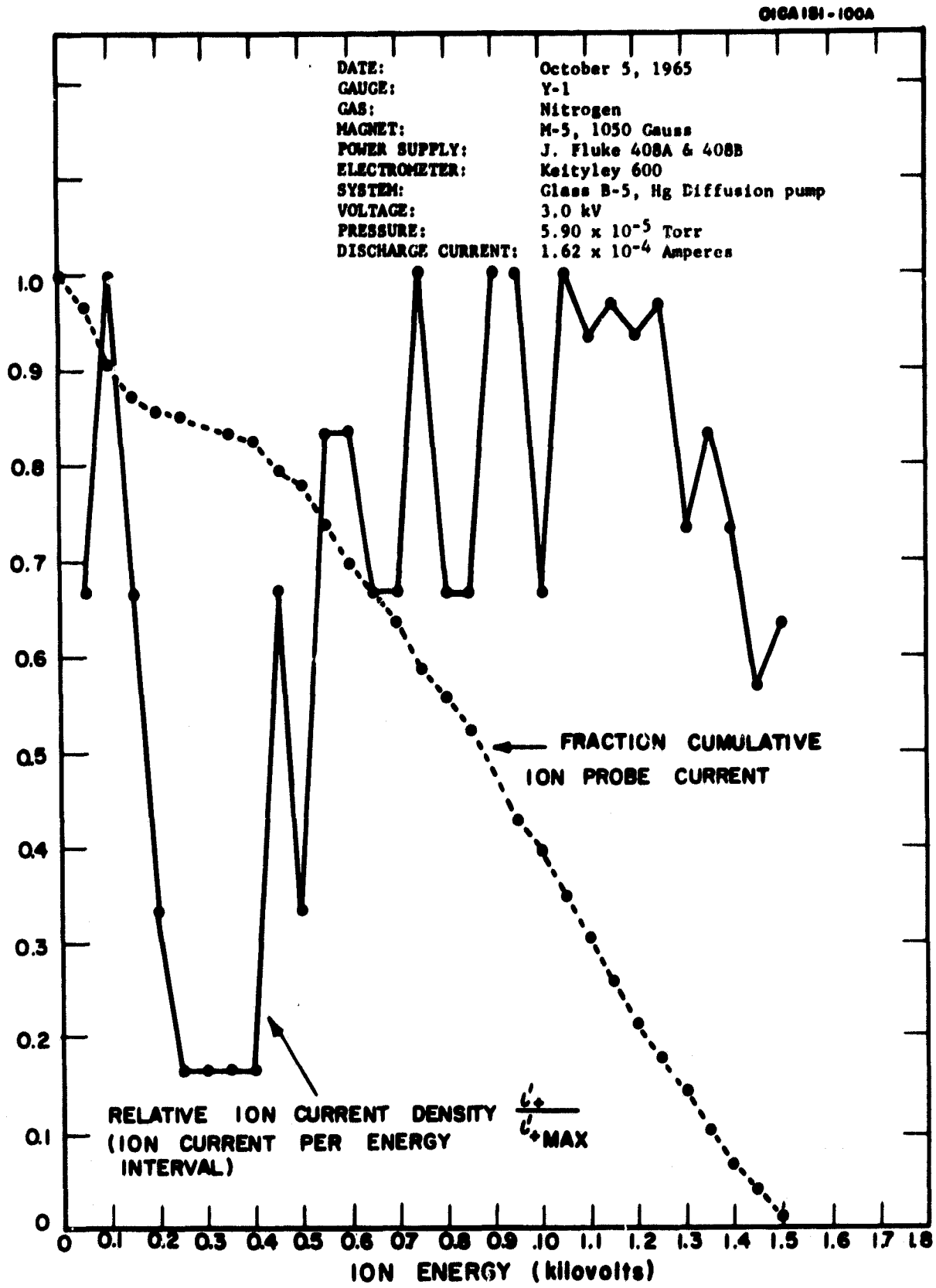

Figure 13. Fractional cumulative ion probe current and relative ion current density at 3.0 kV for nitrogen gas at 5.90×10^{-5} torr.

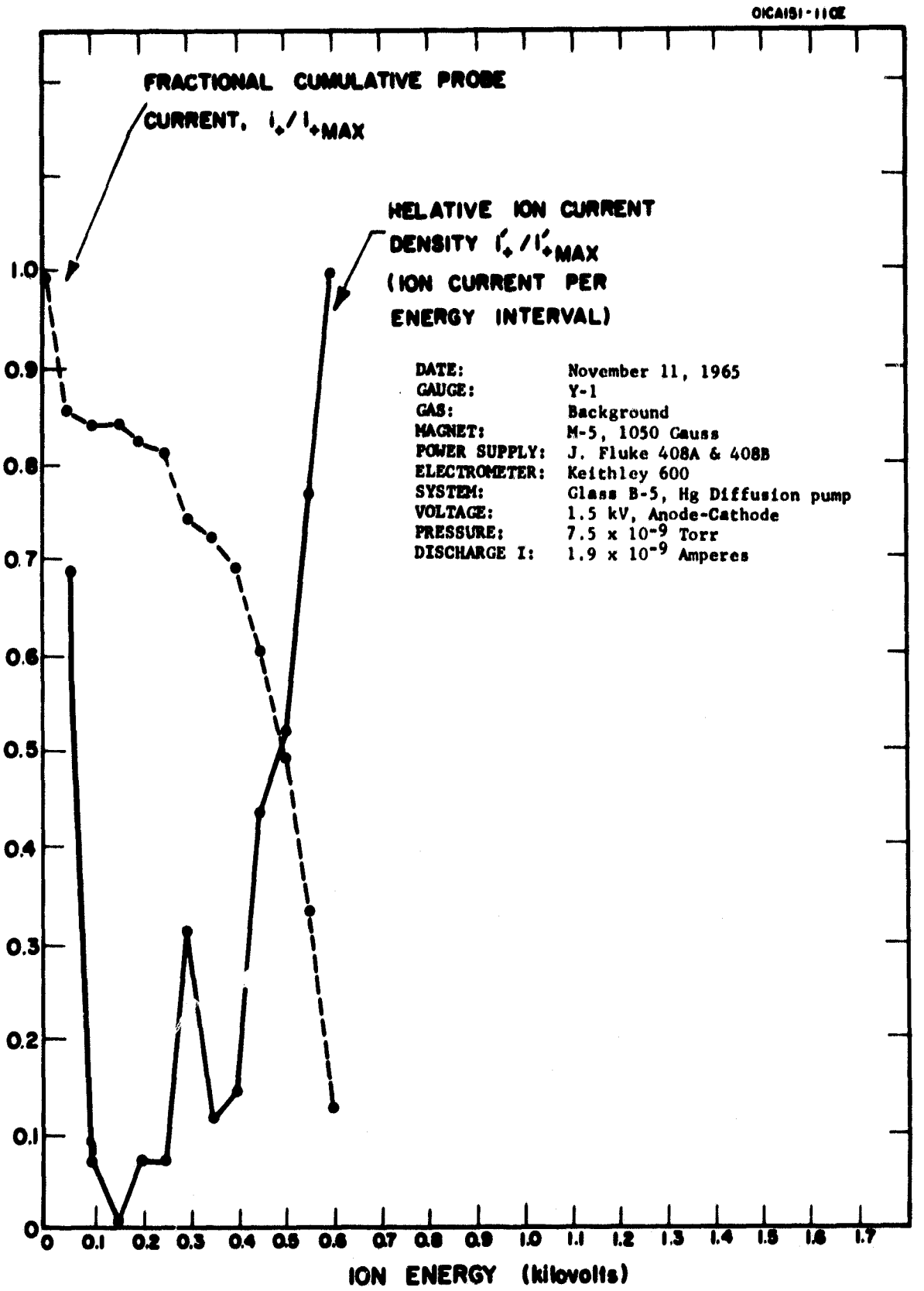

Figure 14. Fractional cumulative ion probe current and relative ion current density at 1.5 kV for background gas at 7.5 x 10^{-9} torr.

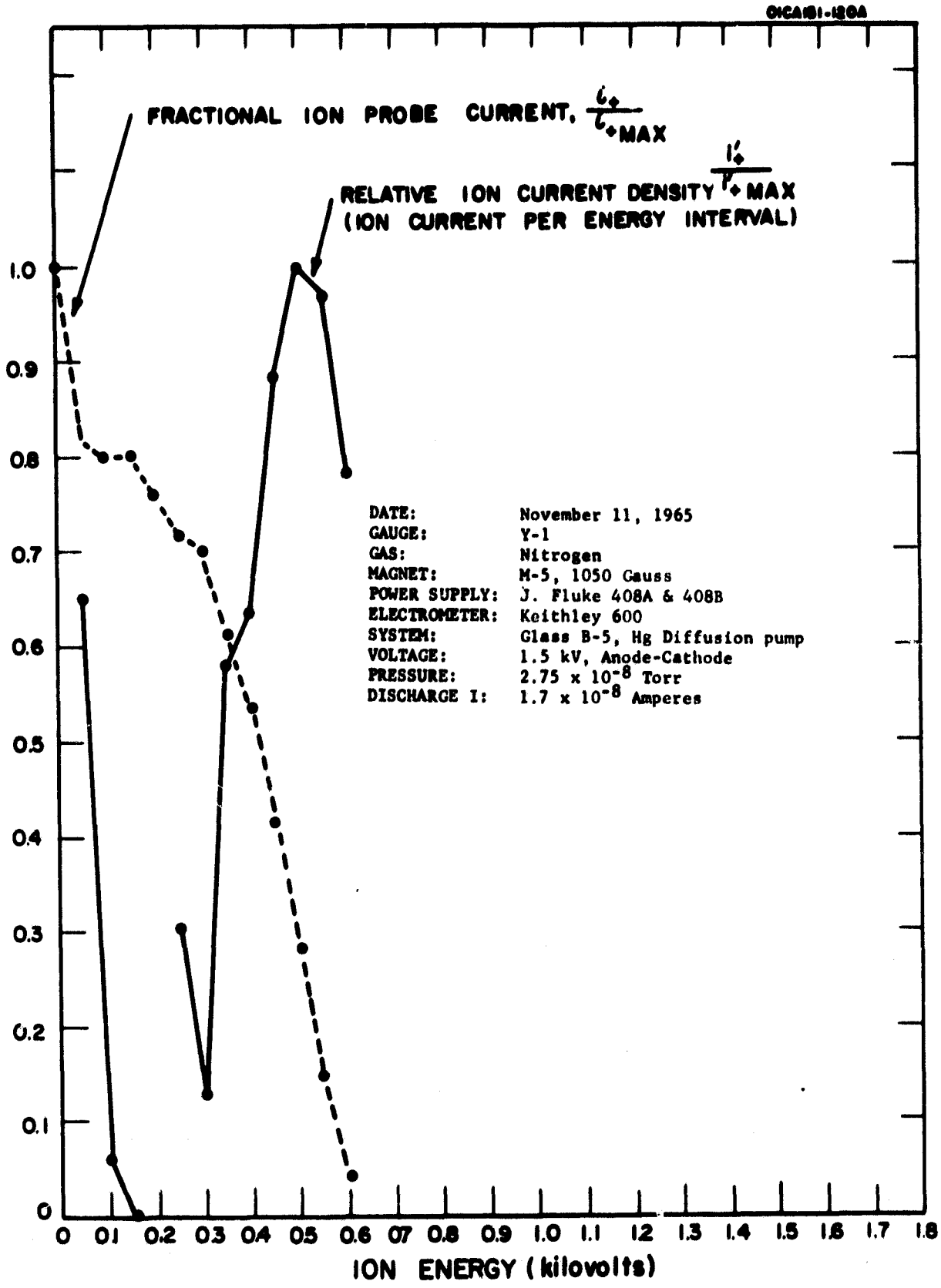

Figure 15. Fractional cumulative ion probe current and relative ion current density at 1.5 kV for nitrogen gas at 2.75 x 10^{-8} torr.

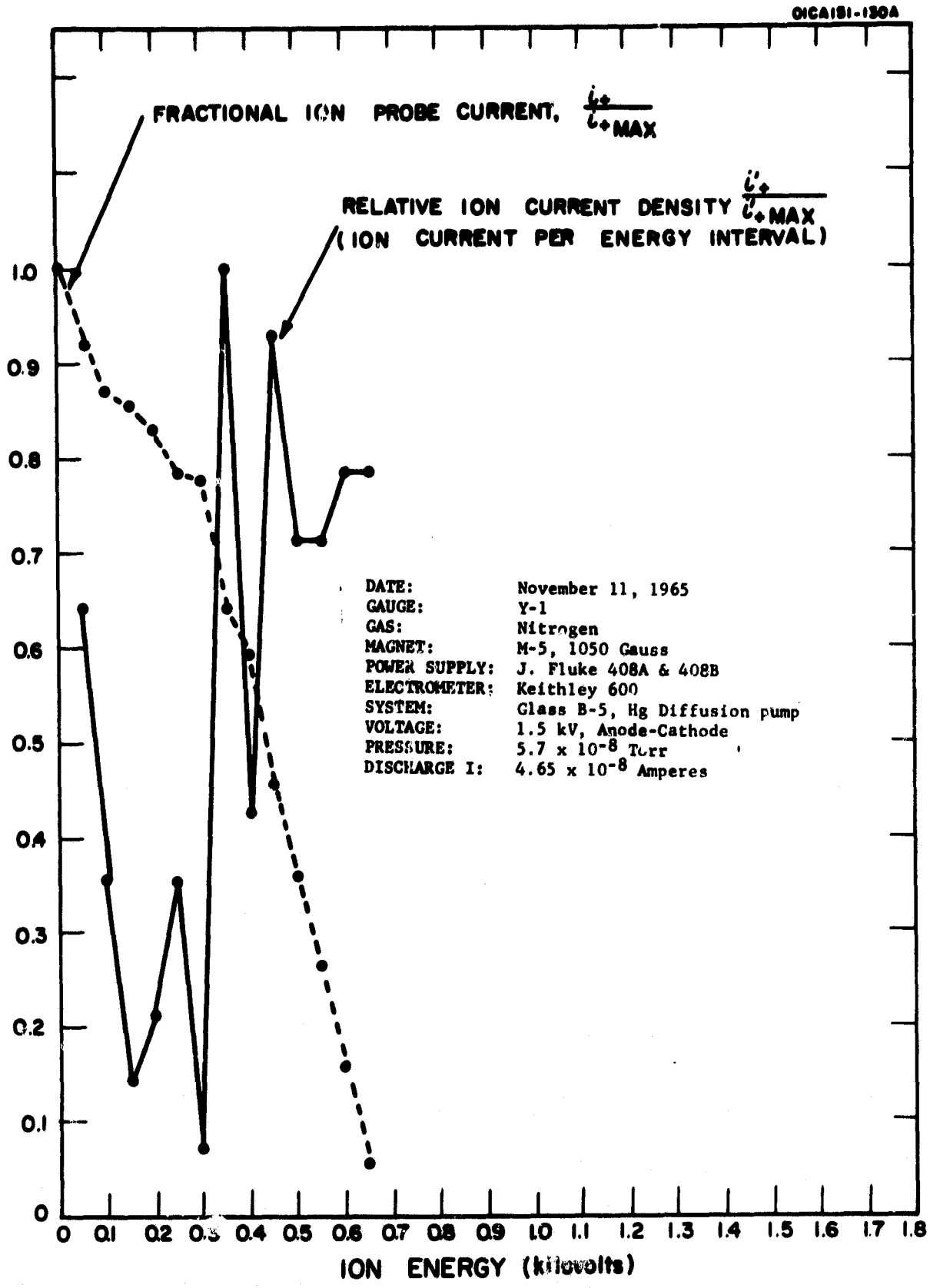

Figure 16. Fractional cumulative ion probe current and relative ion current density at 1.5 kV for nitrogen gas at 5.7×10^{-8} torr.

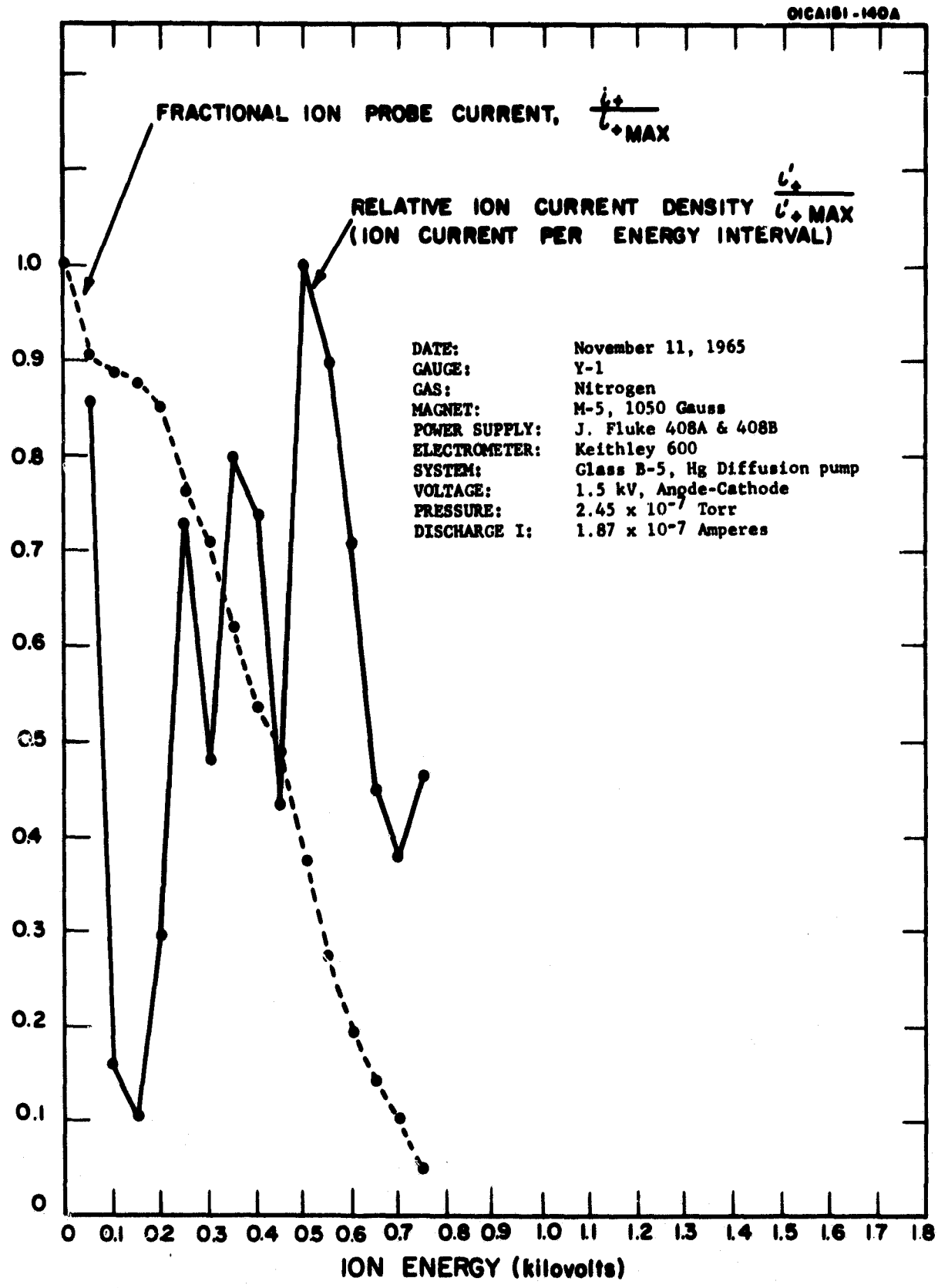

Figure 17. Fractional cumulative ion probe current and relative ion current density at 1.5 kV for nigrogen gas at 2.45×10^{-7} torr.

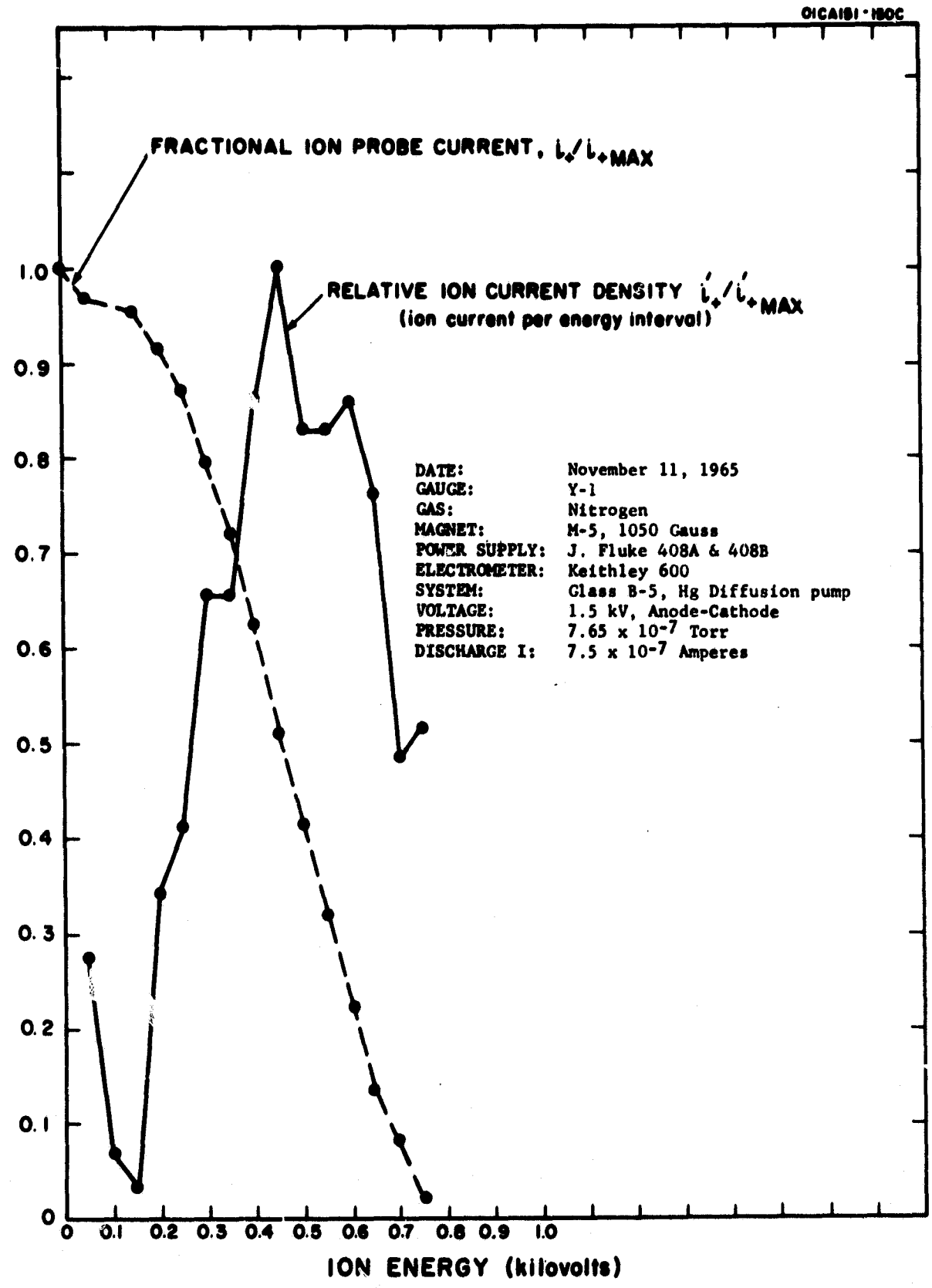

Figure 18. Fractional cumulative ion probe current and relative ion current density at 1.5 kV for nitrogen gas at 7.65 x 10^{-7} torr.

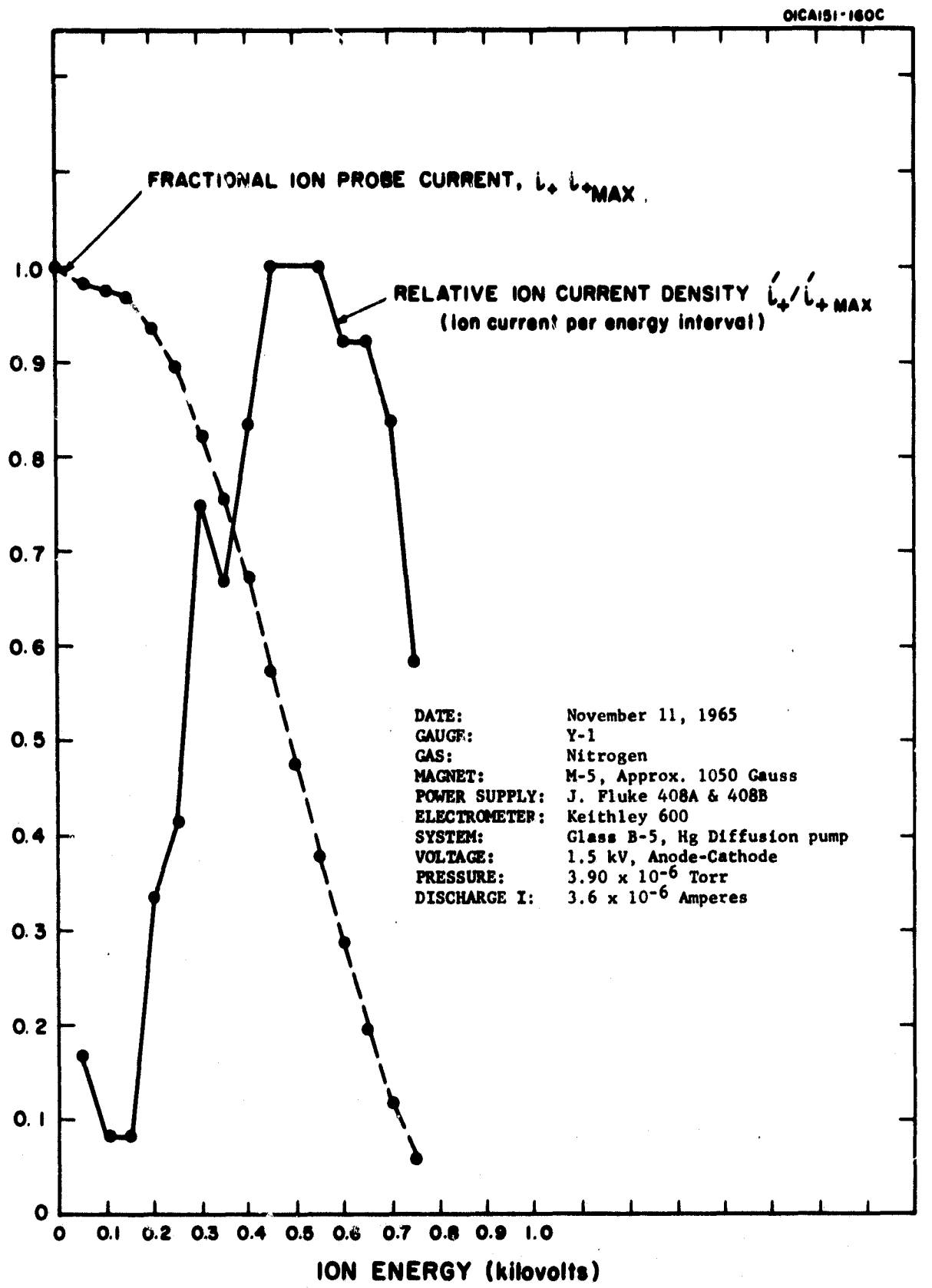

Figure 19. Fractional cumulative ion probe current and relative ion current density at 1.5 kV for nitrogen gas at 3.90 x 10^{-6} torr.

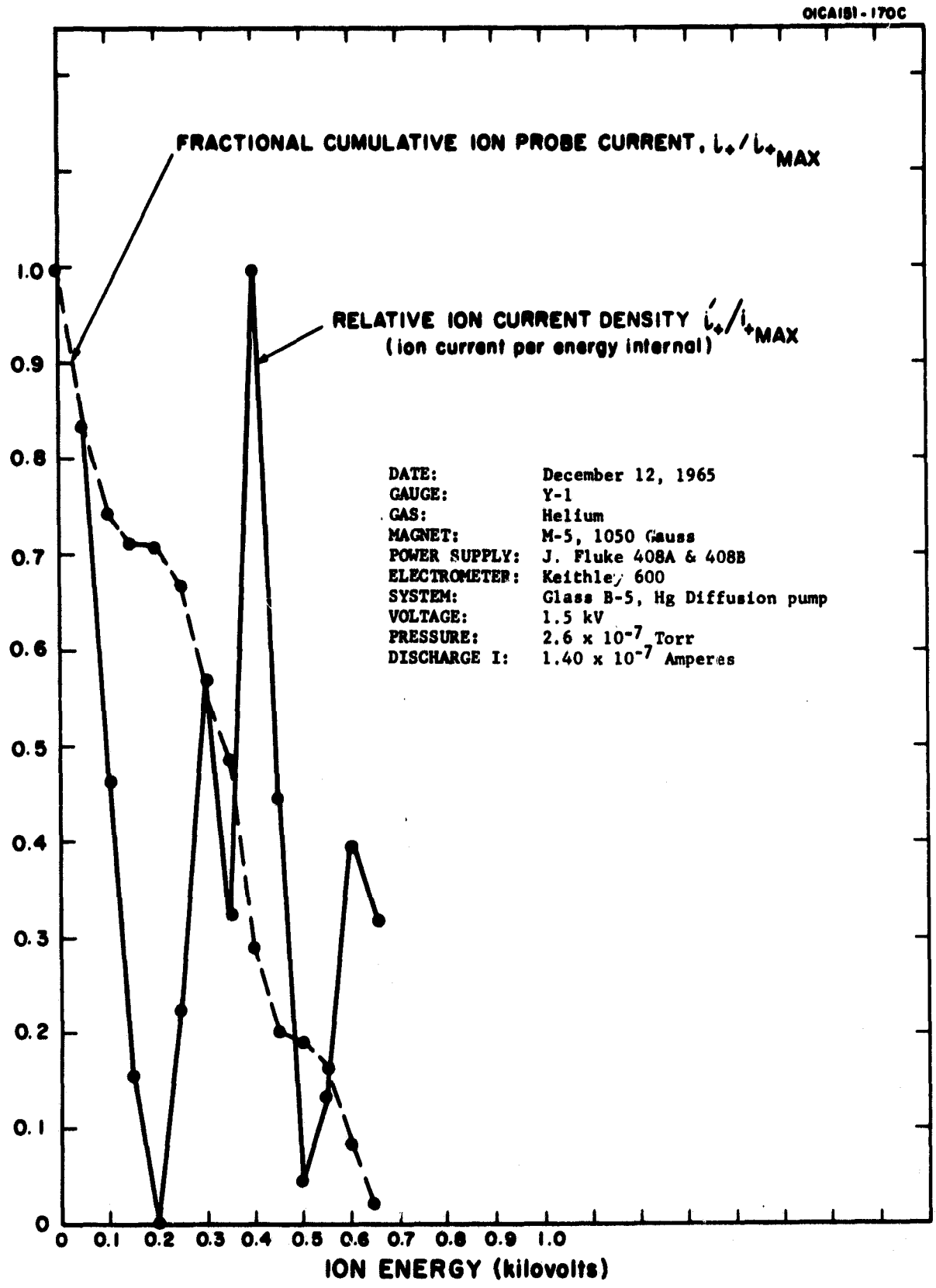

Figure 20. Fractional cumulative ion probe current and relative ion current density at 1.5 kV for helium gas at 2.6 x 10^{-7} torr.

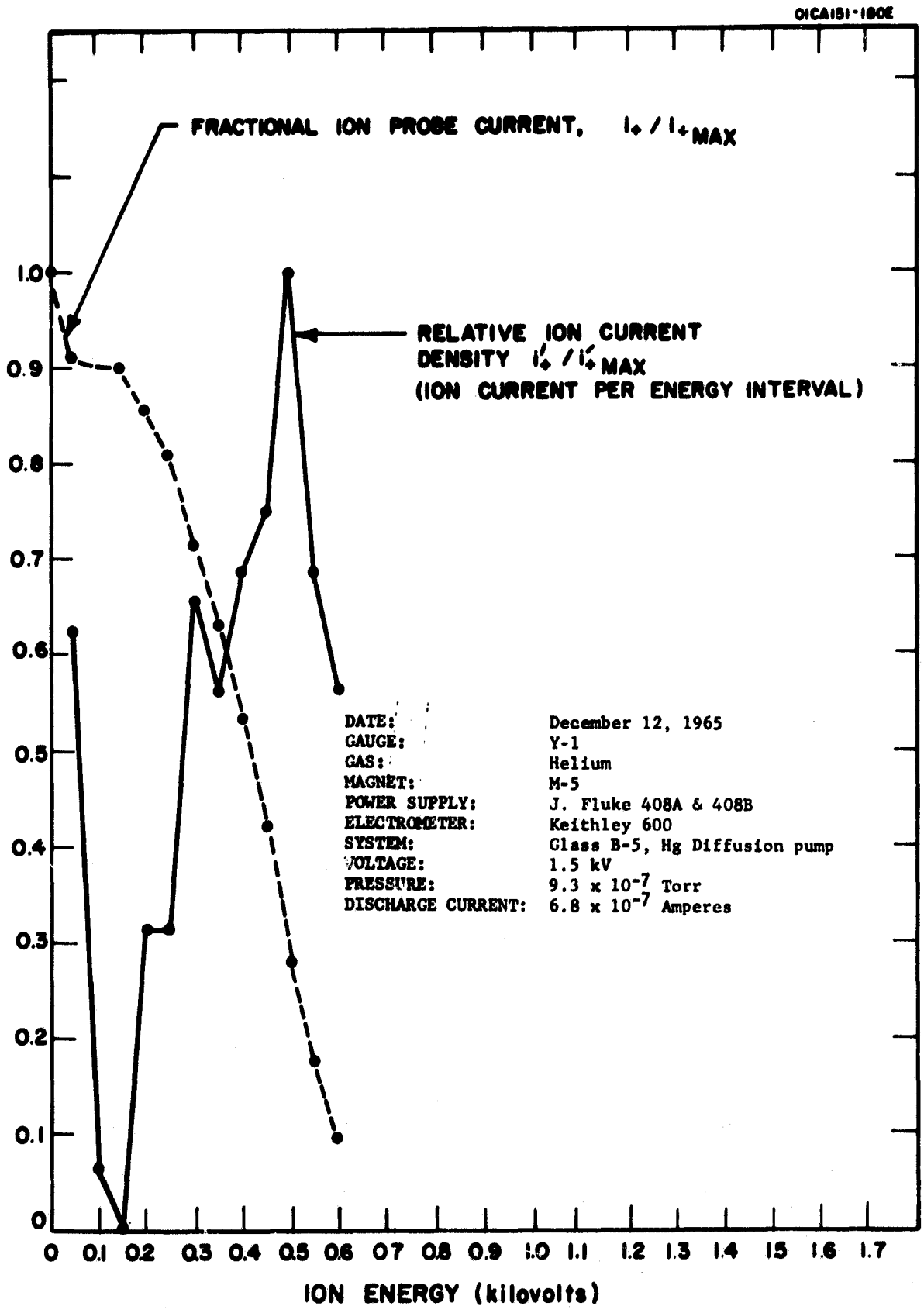

Figure 21. Fractional cumulative ion probe current and relative ion current density at 1.5 kV for helium gas at 9.3×10^{-7} torr.

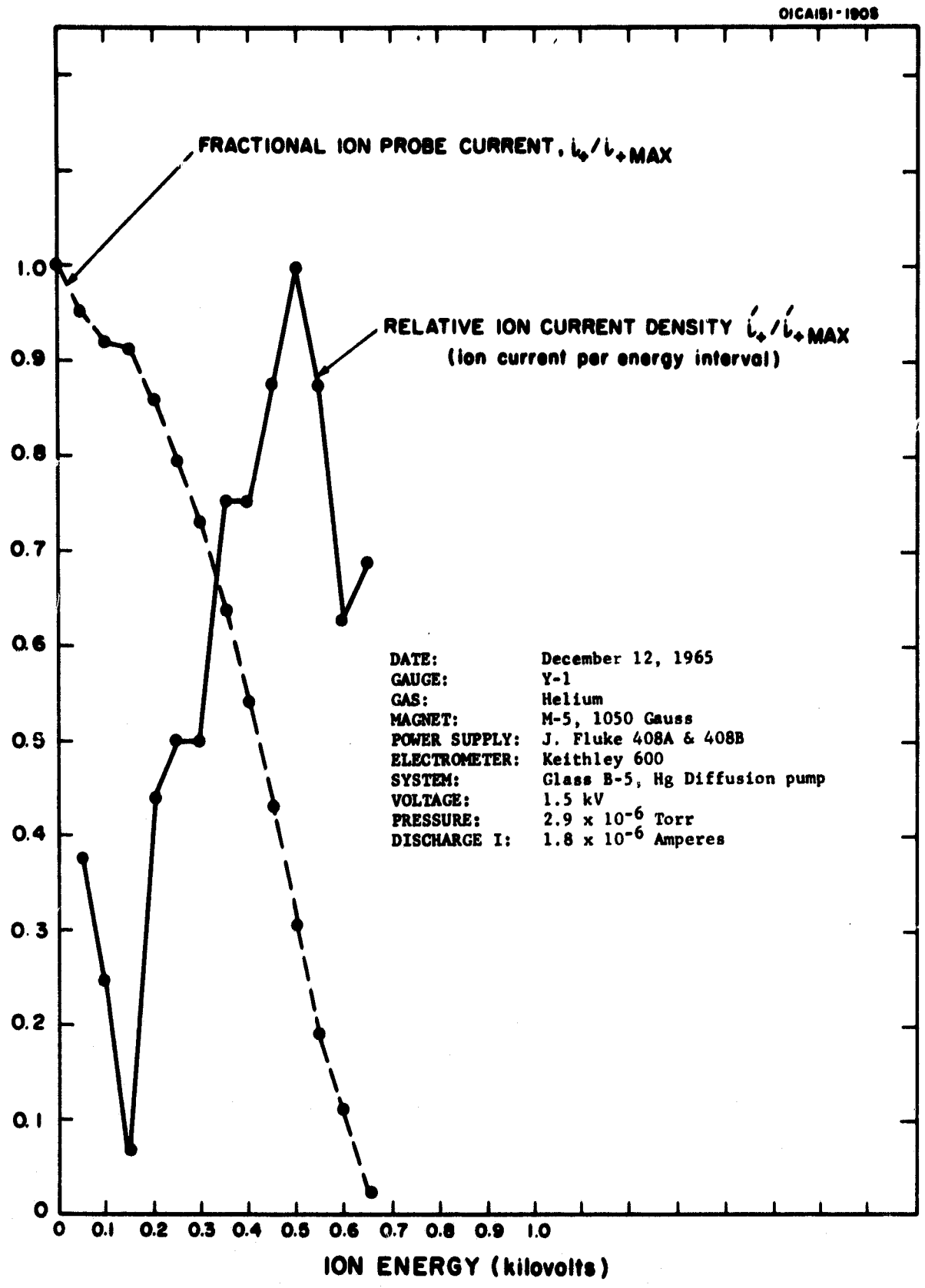

Figure 22. Fractional cumulative ion probe current and relative ion current density at 1.5 kV for helium gas at 2.9×10^{-6} torr.

The same appears to be true for helium gas, but the data for helium is more limited. For all pressures, there is a second energy band that extends from 150 volts to 300 or 350 volts. Additional energy bands appear out to the maximum ion energies present. For an anode-to-cathode voltages of 3.0 kV, up to ten energy bands are evident. The number of energy bands increases with increasing anode voltages. As the gas pressure increases, the energy bands tend to widen and merge into a single continuous distribution.

It is also observed from the data that at very low pressures, the energy bands tend to be isolated from one another. In one case, at least, a mode change occurred at a pressure of 2.75×10^{-8} torr nitrogen with 1.5 kV on the Y-1 gauge anode. There was no change in the initial energy band, but the second energy band changed from having a maximum at 300 volts (at a background gas pressure of 7.5×10^{-9} torr), to having a minimum at 300 volts. In addition, the mode of the ion energy distribution shifted strongly to lower voltages contrary to the general behavior. The relative ion current density decreased to zero at 150 volts for the pressure at which the mode change occurred.

It can be seen from the data that the percentage of positive ions with higher energies increases as the pressure increases. Another way of putting this is to state that the average ion has a higher energy at higher pressures. Also, in agreement with this trend, the percentage of positive ions in the first energy band (0 to 150 volts) decreases as the pressure increases. And, finally, it is observed that as the gas pressure decreases, not only is there a larger percentage of positive ions in the first energy band, but the remainder of the ions tend to group into the highest energy band, thus leaving a near absence of positive ions between these two energy bands. The ion current density tends toward a bimodal, "inverted normal" type distribution. It is a though the positive ions become restricted to two regions at low pressures - the initial or first energy band near the cathode and a high energy band perhaps near the anode. Certainly, the valley in the ion current density between these two bands widens as the pressure decreases.

According to the data obtained, about 95 percent of all positive ions have energies that are less than one half the anode-to-cathode voltage. About 15 to 20 percent of the positive ions at low pressures have energies less than 150 volts.

In all the data presented thus far, the ion probe currents were measured at energy intervals of 50 volts. Two additional experiments were carried out in which the ion probe currents were measured at 10-volt intervals for retarding potentials between 0 and 200 volts. Nitrogen gas was used in these measurements with 1.5 kV on the gauge anode. Figures 23 and 24 show the results of these detailed low energy measurements.

In both low energy measurements, the positive ions appear to be grouped in narrow energy bands that vary in width from about 20 to 35 volts. At the lower pressure of 5×10^{-8} torr, the 20-volt energy bands are just separated.

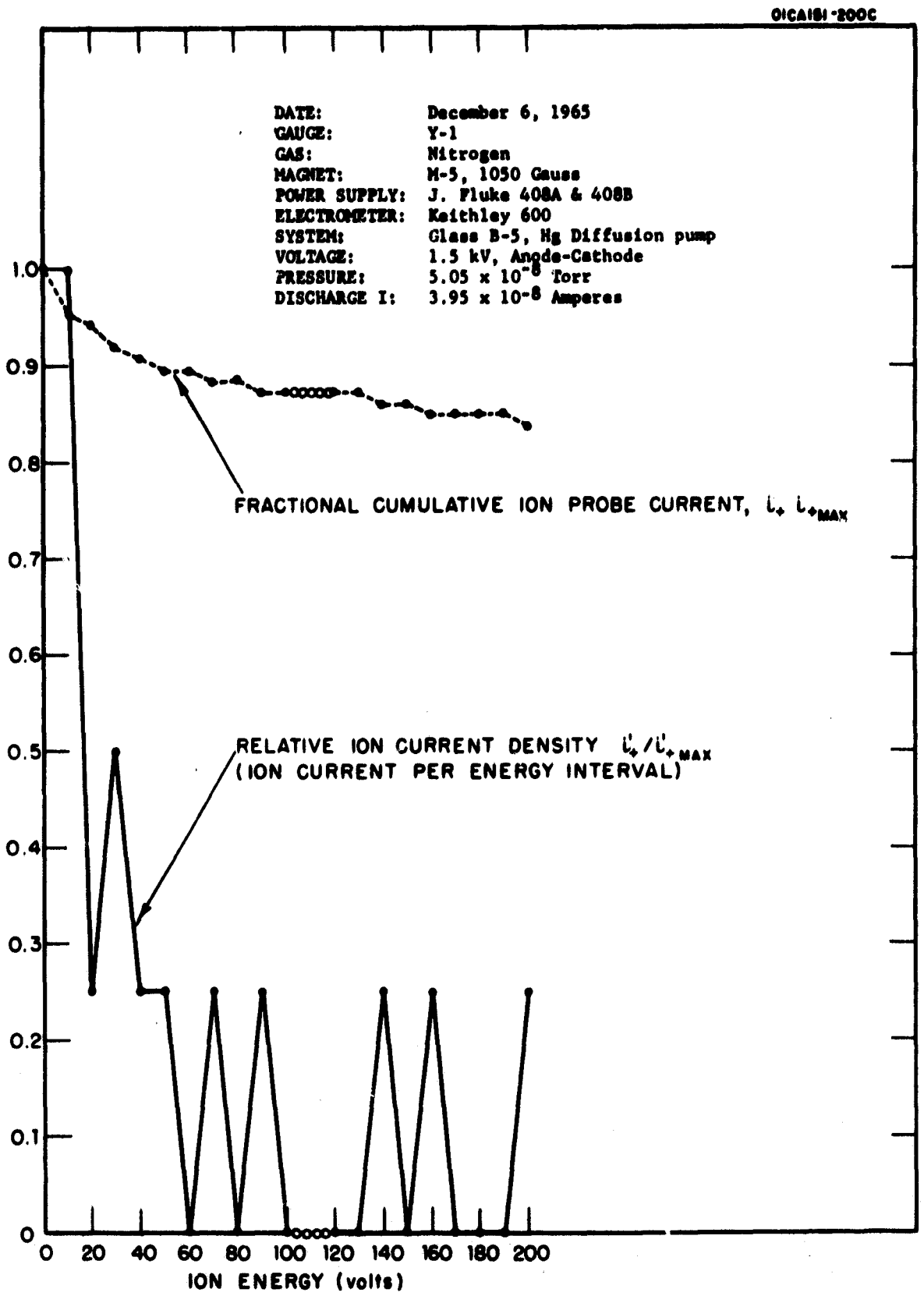

Figure 23. Low energy fractional cumulative ion probe current and relative ion current density at 1.5 kV for nitrogen gas at 5.05×10^{-8} torr.

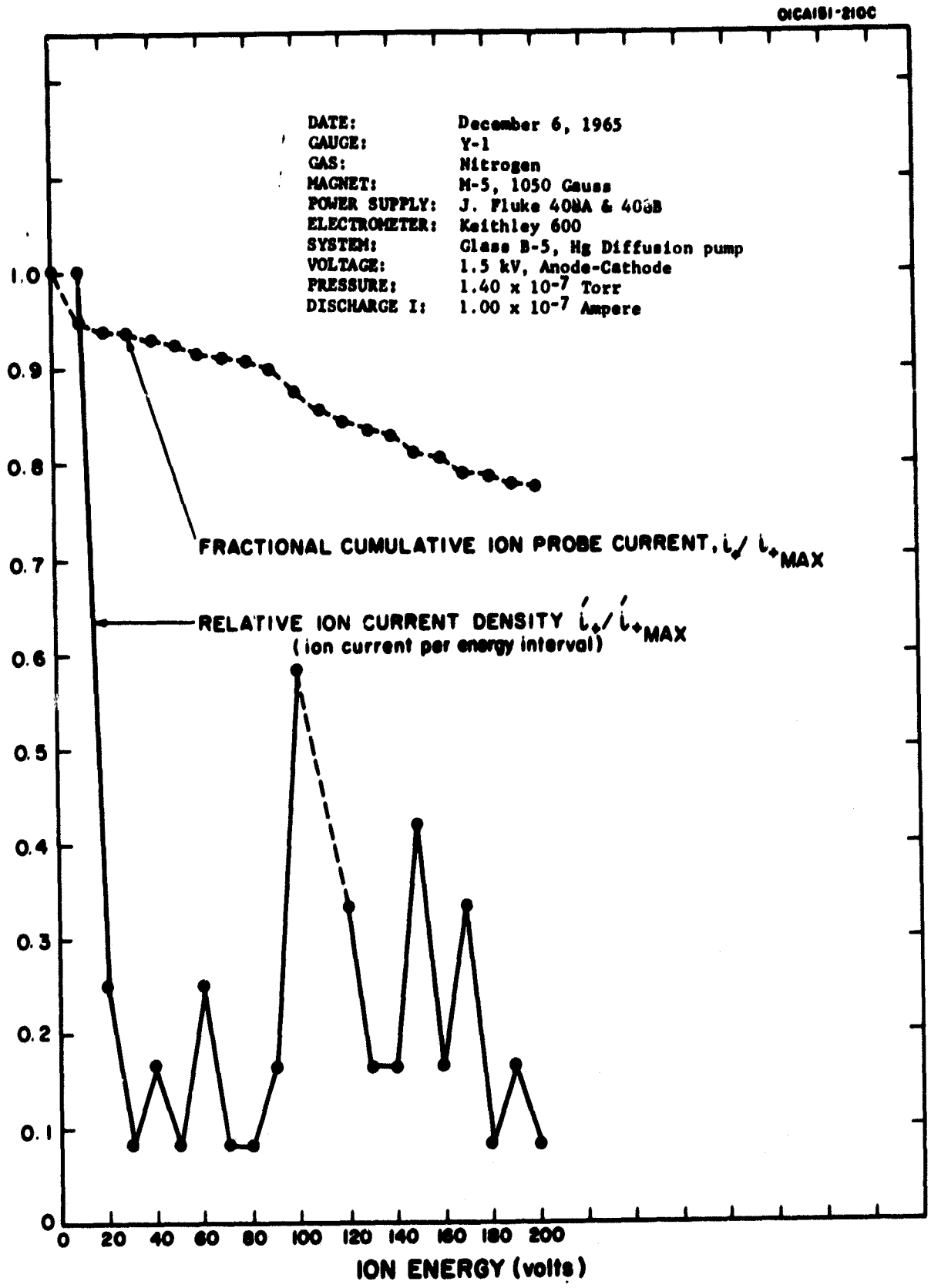

Figure 24. Low energy fractional cumulative ion probe current and relative ion current density at 1.5 kV for nitrogen gas at 1.40×10^{-7} torr.

At the higher pressure of 1.4×10^{-7} torr, there is an overlapping of energy bands that are 30 to 35 volts wide. In addition to the detailed small scale energy bands, most of the narrow bands in Figure 24 appear to form a single larger energy band that extends from 30 to 200 volts. In both experiments, it can be seen that 5 percent of the total number of positive ions have energies less than 10 volts.

It is believed that the ion energy data obtained to date represents a a first necessary step in understanding the nature of a cold cathode gauge discharge. Further additional measurements of positive ion energies will be necessary to verify any detailed theory of gauge operation. The new measurements should be made for various magnetic field strengths as well as for different anode-to-cathode voltages and different pressures of each of several gases.

Electronic Space Charge Measurements. The Y-2 experimental gauge was sealed to the test chamber of the glass vacuum test system and was connected electrically as shown in Figure 25. A J. Fluke model 408A high voltage regulated power supply was used to furnish high voltage to the gauge anode. The gauge cathode was connected to ground through a Keithley model 600 electrometer while the movable probe wire was connected to a bias battery and a second Keithley model 600 electrometer to ground. The bias battery voltage was adjustable up to a value of 300 volts. This battery was mounted on a teflon block to minimize leakage currents to ground. An NRC model number 46756 permanent magnet was used to supply a magnetic field of 1000 gauss.

The Y-2 gauge seemed to start and operate normally for anode voltages between 0.5 and 4.0 kV and a gas pressure of about 1×10^{-8} torr. The probe was biased positively at successive values of +22.5, + 45 and +300 volts to attempt to draw electrons out of the discharge through the small holes in the cathode end plate. There was a small net electron flow to the probe, but there was no evidence of a periodic current pickup as expected through the holes of the cathode end plate.

In another experiment, the Y-2 gauge was operated with the anode at ground potential and the cathode at -900 volts. The probe was operated at ground potential and did exhibit a net electron flow. The net electron flow did increase as the probe was moved radially inward, but it is believed that the current increase may have been caused by the approach of the probe connecting wire to the anode-cathode gap.

The third experiment performed with the Y-2 gauge, with its anode at + 4.0 kV and its cathode grounded, was to bias the probe negative by 45 volts so that it would collect a net positive current and then move the probe radially inward in .005 inch steps. It was reasoned that only the relative changes in probe current as a function of radial distance were of importance independent of the absolute magnitude and sign of the current. The results of the measurement are shown in Figure 26.

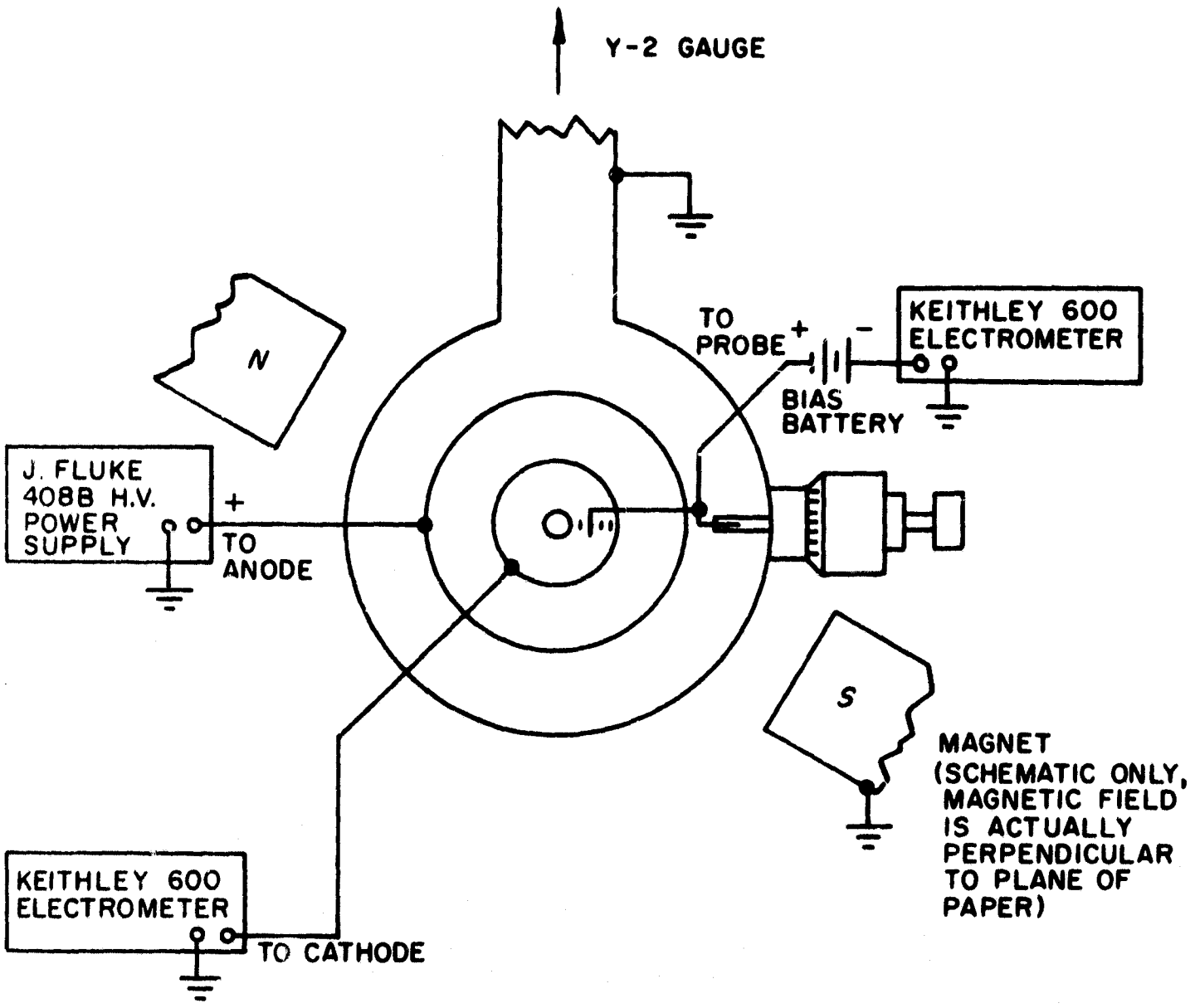

Figure 25. Electrical connections used to measure the relative radial electronic space charge distribution in the Y-2 experimental gauge.

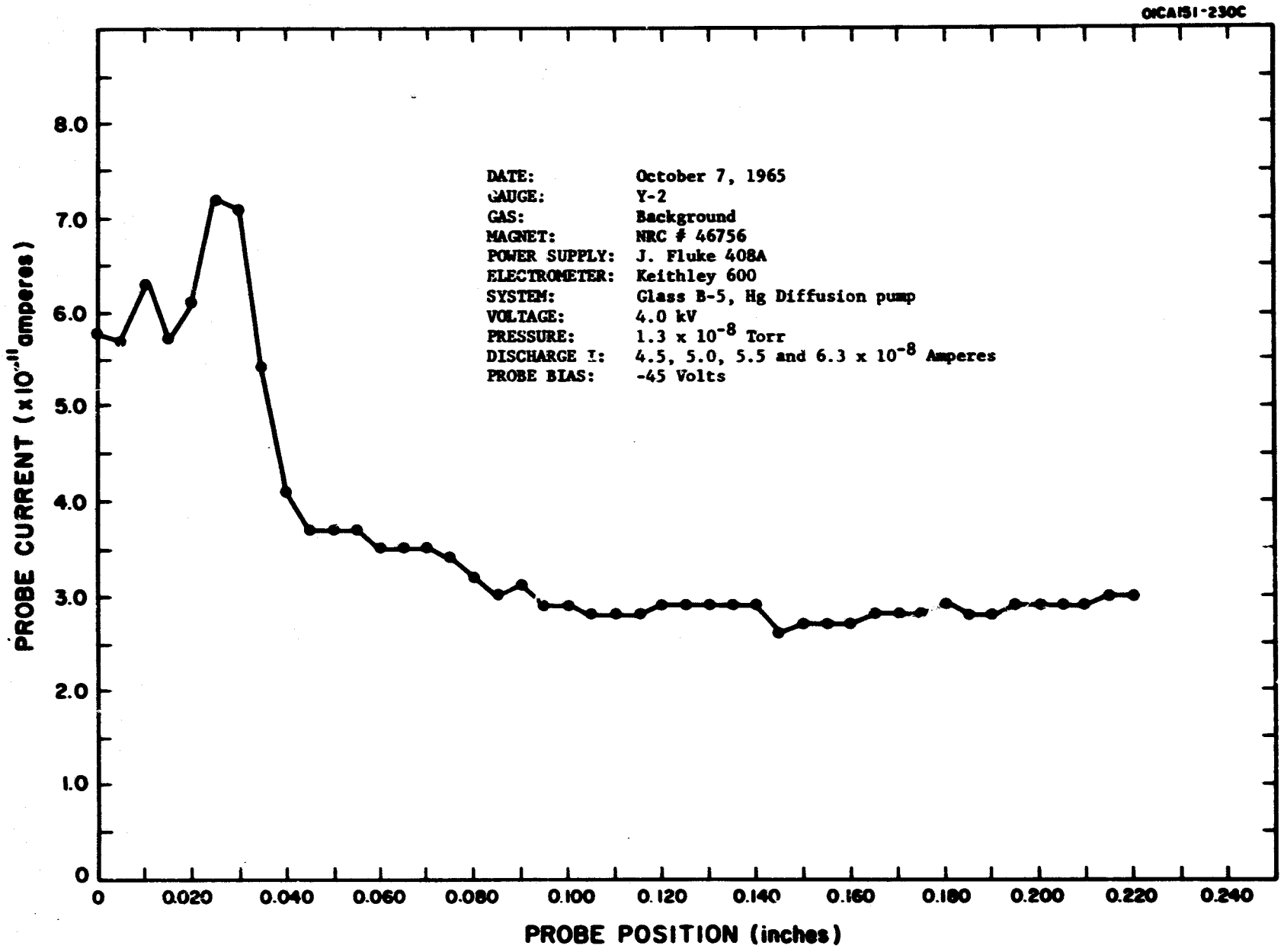

Figure 26. Positive probe current in the Y-2 experimental gauge.

As can be seen in the figure, the positive ion current to the probe was a maximum with the probe located near the edge of the cathode end plate. As the probe was moved radially inward, the net positive current to the probe decreased. This is equivalent to an increase in electronic current to the probe. However, there was not sign of periodic decreases in the positive current as would occur if high energy electrons moved from the discharge through the holes in the cathode end plate. It must be concluded that little or no electrons are being drawn out of the discharge in the axial direction (same direction as the magnetic field) in the Y-2 gauge. During this experiment, the discharge current had a total of four modes of operation, with the current changing by only a small percentage between modes.

The conclusion drawn from measurements made with the Y-2 gauge is that the electronic space charge current does not have any strong axial components. The electronic space charge current must be almost purely circumferential. On the other hand, there is a leakage of both electrons and positive ions in the region between the anode and the outer edges of the cathode end plates.

III. POSITIVE ION TRAJECTORIES IN A MAGNETRON-TYPE COLD CATHODE IONIZATION GAUGE

Design andConstruction of the Model X-1 Experimental Gauge

The model X-1 gauge was designed and constructed for an earlier experimental program [1]. This gauge was built to permit several different kinds of measurements to be made. For one thing, the gauge contained a radially-divided anode to facilitate measurements of radio frequency that might be generated during its operation. Another feature of this gauge was the placement of a small fixed probe adjacent to, but electrically isolated from, one of the two slits in the gauge anode. Positive ions or electrons might then be drawn out of the discharge to the fixed probe. The third feature of the gauge design, the feature utilized in the current research, was the placement of a movable, central ion probe within the hollow cathode of the gauge. A small aperture in the center of the cylindrical wall of the gauge hollow cathode formed a beam of positive ions which could be detected by the central probe. The curvature and spread of the positive ion beam for ions of a single species (mass) would depend on the origin and energy of these ions within the discharge region and on the strength of the magnetic field. If the energies of the various ions that entered the hollow cathode could be ascertained, then the positions at which the ions were detected by the movable probe would be a function of the origin of the ions. A knowledge of the energy (potential) of each positive ion and its origin (point of ionization within the discharge) would yield the gauge potential as a function of radial distance. From the potential distribution, one can easily find the electric field distribution and the space charge distribution. It can be seen that successful operation of the X-1 gauge could lead to a fairly complete measurement of cold cathode ionization gauge discharge properties.

The model X-1 gauge, shown in Figure 27, was built with a radially-divided anode and a movable, 0.010-inch diameter, tungsten central wire probe located inside the hollow cathode. A bellows-sealed, micrometer-type motion feedthrough was used to move the central probe. This feedthrough is very similar to that shown earlier in Figure 5. A hole 1/8-inch in diameter was drilled through the center of the cylindrical portion of the cathode. This hole was then covered with a sheet of thin wall stainless steel in which a 0.010-inch diameter aperture hole had been drilled. This latter hole served as an aperture to permit positive ions from the discharge to enter the interior of the cathode. The positive ions that entered the cathode were collected by the movable 0.010-inch diameter tungsten probe.

Experimental Results and Trajectory Analysis for Helium Gas

The Model X-1 Gauge Data. A number of experiments were performed with the Model X-1 gauge, but only three of these will be discussed in this chapter. The X-1 gauge was mounted on the test chamber of the all-glass vacuum test system. A 1030 gauss, 1-1/4-inch gap length permanent magnet (the model M-5

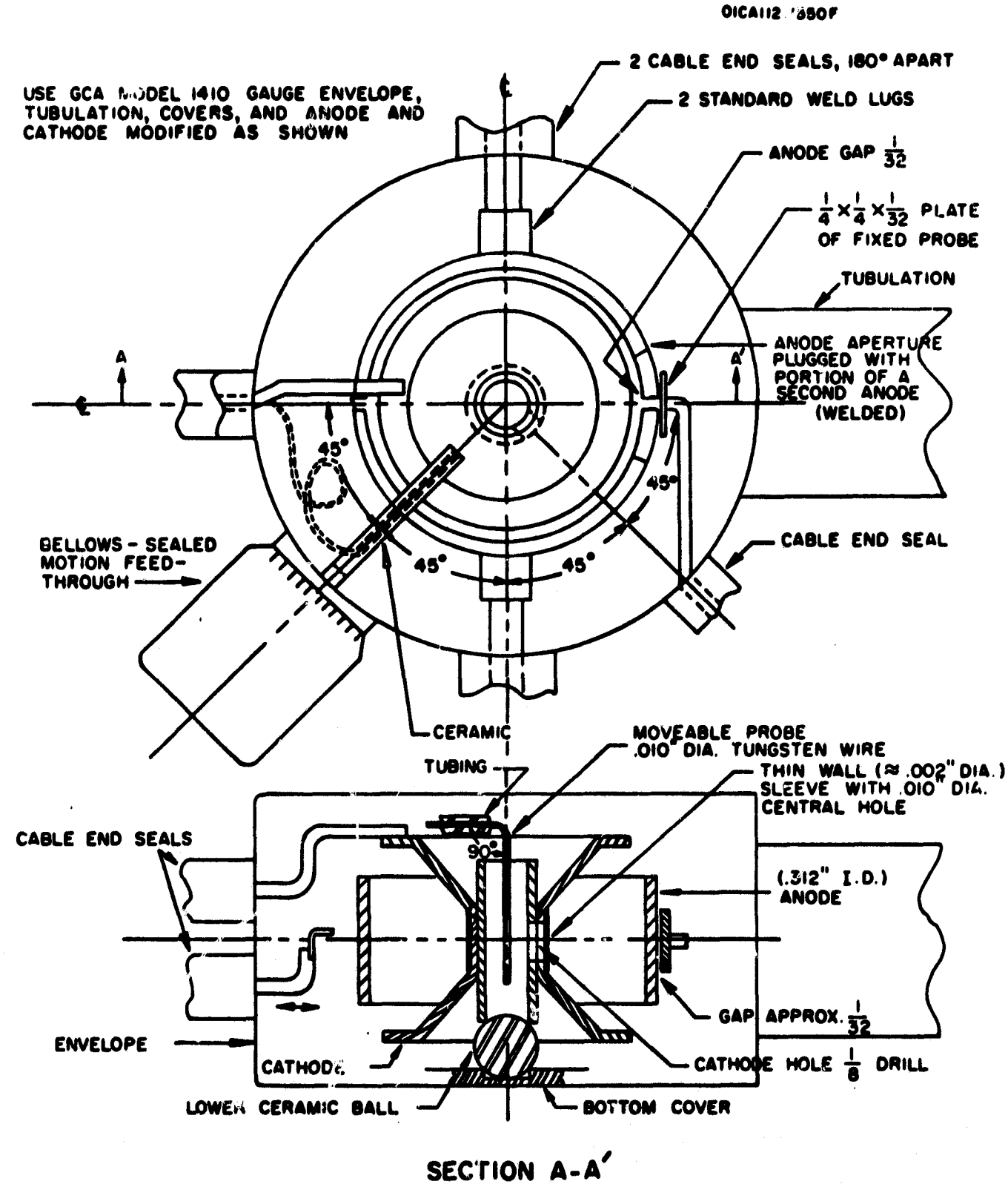

Figure 27. Model X-1 experimental cold cathode gauge.

magnet) was used to supply the magnetic field. An anode voltage of 4.0 kV was furnished by a GCA laboratory type unregulated but well-filtered high voltage power supply. Keithley Model 600 electrometers were used to measure the cathode current and the central ion probe current. The system had been baked out mildly several days prior to the experiments. The background pressure in the system with the spherical cold trap filled with liquid nitrogen was about 1×10^{-8} torr (Veeco RG-75 gauge at 10 mA emission).

After the desired pressure of a particular gas had been established in the system in the usual way, the central ion collector probe was moved radially from a position 0.050-inch off-center to the center of the cathode (and gauge) and then moved 0.050-inch off-center in the opposite radial direction. The positive ion current to the probe was observed at 0.005-inch intervals of probe position. One experiment was conducted with a nitrogen pressure of $3\ 8 \times 10^{-7}$ torr in the test chamber. The results of this experiment are shown in Figure 28. As can be seen, the positive ion current to the central probe formed a beam having dimensions that were determined primarily by the width of the cathode aperture (0.010-inch) and the probe diameter (also 0.010-inch). The probe-to-aperture spacing of 0.156 inch (dimension Z) is an important parameter in the analysis of the data. The maximum beam current for nitrogen was about 7-1/2 times greater than the background current to the ion probe.

The second experiment was conducted with helium gas at a pressure of 7.2×10^{-6} torr. The gauge anode voltage was 4.0 kV and the magnetic field at the center of the gauge was 1030 gauss. The cathode (discharge) current was 1.2×10^{-5} amperes during the experiment, over 100 times greater than the gackground gas discharge current of 7.0×10^{-8} amperes. The results of this experiment are plotted in Figure 29. Notice the displacement of the beam of light helium ions with respect to the center of the gauge cathode. The peak current of the helium ion beam was only about 3-1/2 times greater than the ion background current within the cathode, indicating greater scattering and reflection of the ions within the cathode. The helium beam was only about 0.035-inch wide. The position of the ion probe with respect to the center of the gauge cathode is only an estimate that was obtained by visual alignment when the gauge was constructed. Later experimental evidence indicated that this alignment could be off by approximately ± 0.010-inch. Notice that the probe ion current was roughly a normal type distribution. The values of probe current were taken in steps of 0.005 inch. As can be seen from the graph, this position interval was too large to yeild a detailed distribution curve. An interval no longer than 0.0025 inch should have been used.

The Cycloidal Ion Trajectory Approximation. In order to make use of the model X-1 gauge data, it is necessary to relate the ultimate position of a positive ion within the X-1 gauge cathode with its initial starting point within the discharge. Since the X-1 gauge cathode is at zero potential and the central ion probe is also at zero potential, there is no electric field within the hollow cathode. A positive ion that enters the cathode through the aperture will move in a short segment of a circular arc due to the action of the magnetic field. The radius of the circular arc may be easily expressed in terms of the ion potential (V abvolts), the ion charge-to-mass ratio, $\eta \equiv e/m$ emu/gram and the magnetic field strength (B gauss). If the magnetic force Vev is equated

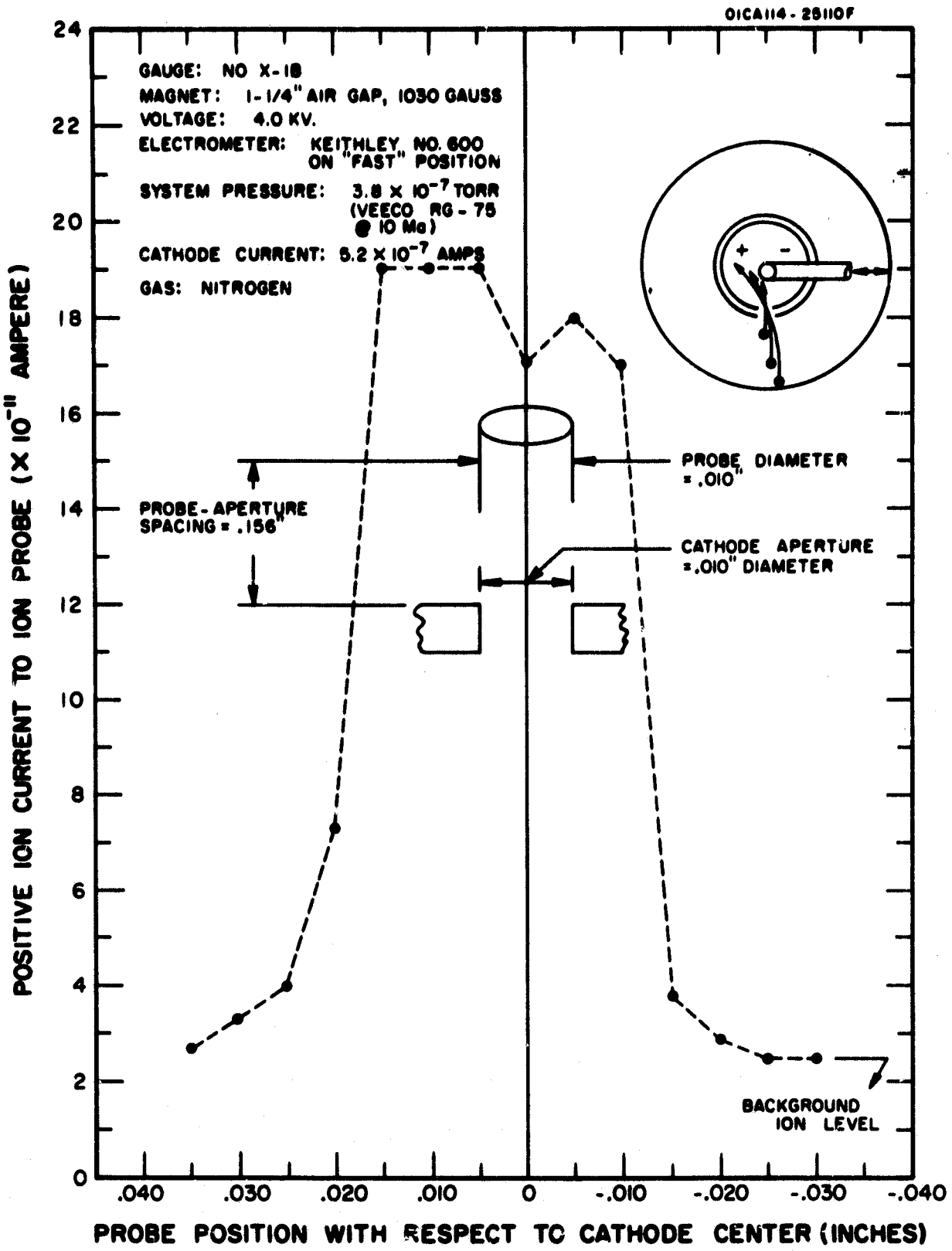

Figure 28. Central ion probe current-position characteristic for nitrogen gas in the X-1 gauge.

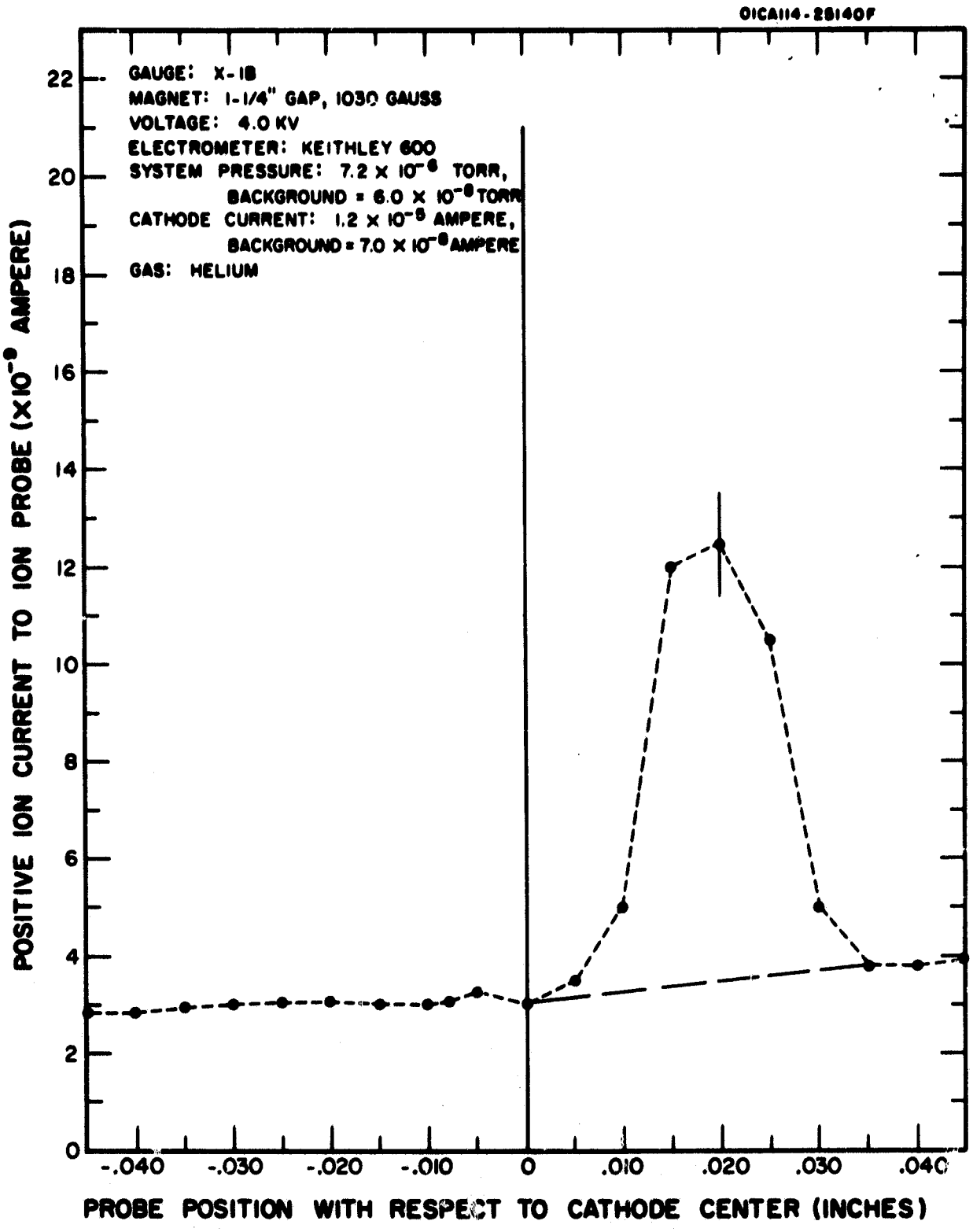

Figure 29. Central ion probe current-position characteristic for helium gas in the X-1 gauge.

to the balancing centrifugal force mv^2/R where v is the ion velocity and can be expressed in terms of the ion potential, mass and charge as $v = (2\ eV/m)^{1/2}$, the resulting expression for the radius R is:

$$R = (1/B)\sqrt{2\ V/\eta} \qquad (1)$$

Now, in addition to knowing the radius of curvature of the ion trajectory within the cathode, it is necessary to know the angle β at which the positive ion entered the cathode. Once the entrance angle β of the ion is related to the starting position of the ion, the probe data can be used to determine the starting positions of ions of various potentials.

One approximate methode of relating the ion entrance angle β to the ion origin is to assume that the ion trajectories within the discharge region between the anode and cathode are portions of a cycloidal arc. It is assumed that the spatially varying electric field in the discharge region can be replaced with an "effective constant electric field" E volts/cm, and that the motion of an ion in the combined crossed electric and magnetic fields is cycloidal.

Figure 30 shows the manner in which a positive ion may be assumed to move in a cycloidal trajectory from its point of origin to the cathode aperture and then continue on into the hollow cathode until it strikes the central ion probe.

The slope of a cycloidal arc, as given by the derivative dy/dx in rectangular coordinates, is:

$$\left.\frac{dy}{dx}\right|_{y=y_o} = \tan\alpha = \sqrt{(D/y_o) - 1} \qquad (2)$$

where α is the slope angle, the complement of the entrance angle β (the angle between the direction of the ion beam and the normal to the aperture), D is the cycloid diameter (cycloid height D = 2a where "a" is the radius of gyration, the radius of the cycloid generating circle), and y_o is the value of the y coordinate at the point where the slope is being determined. The cycloid diameter D is given by the well-known expression:

$$D = \frac{2 \times 10^8\ E}{\eta\ B^2} \qquad (3)$$

where E is the electric field in volts/cm, η is the ion charge-to-mass ratio in emn/gm and B is the magnetic field in gauss.

Equations (2) and (3) relate the angle α to the distancy y_o. In this model, the distance y_o is used as an approximation to the radial distance r_o between the gauge cathode and the point of ion origin. All that remains is to determine the angle α from the geometry of the gauge and the position S along the line of probe motion at which the ion is detected.

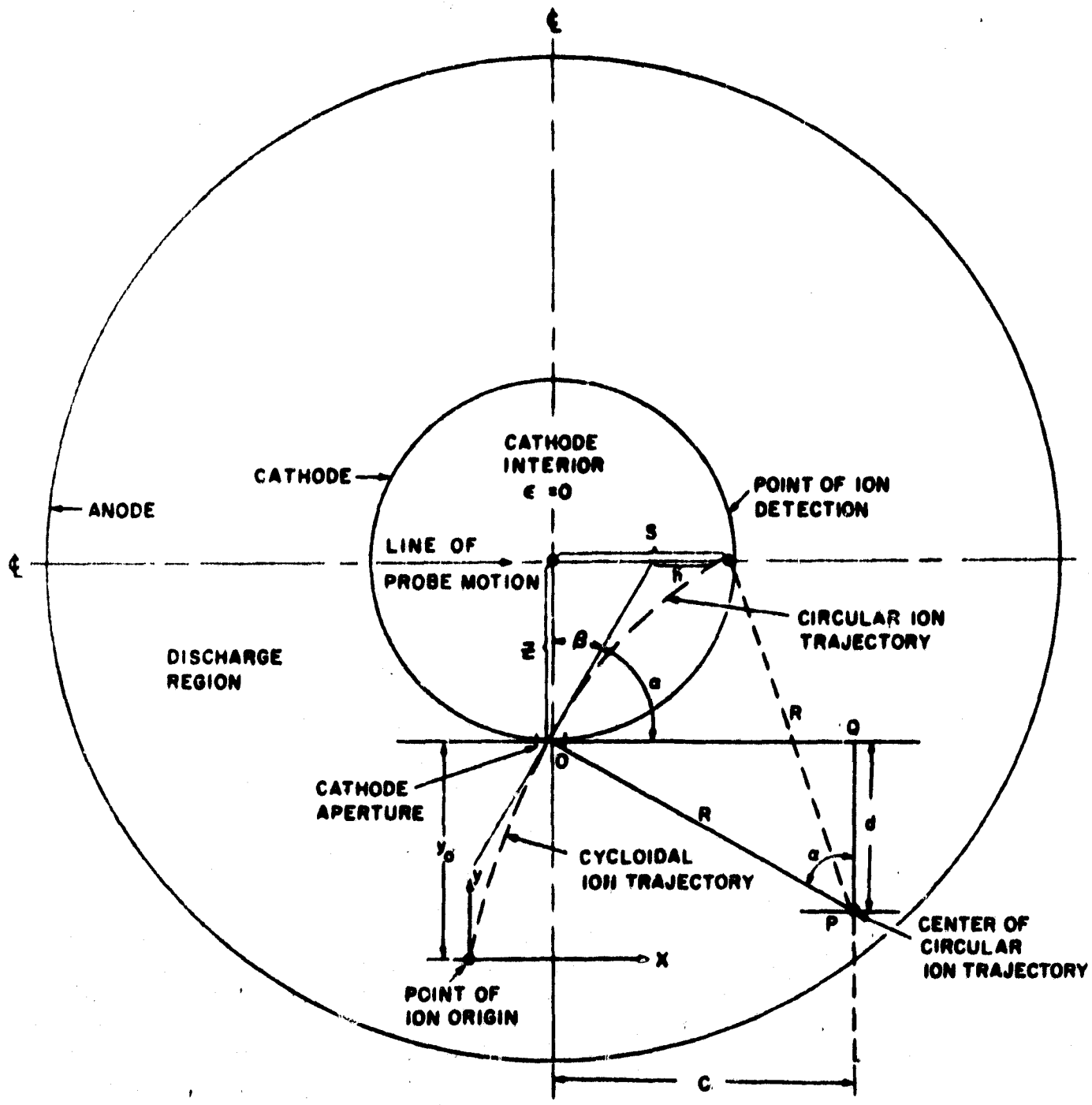

Figure 30. Approximate cycloidal trajectory of a positive ion in the X-1 gauge.

If one writes the equation for the circular ion trajectory within the hollow cathode and then demands that this circular arc passes through the point of ion detection, one obtains an expression for the coordinates C and d which locate the center of the circular arc in terms of the parameters R, S and Z. The expression for d is:

$$d = \frac{1}{2}\left[- Z + S \sqrt{\frac{4 R^2}{S^2 + Z^2} - 1} \right] \qquad (4)$$

From Figure 30, it is evident that

$$\cos \alpha = d/R = \sin \beta \qquad (5)$$

where R may be calculated from equation (1). Equations (1), (4) and (5) are used to determine the value of the angle α in terms of the gauge constants, the potential of the ion, and the probe position or point of ion detection.

In performing ion trajectory analysis with the above model, there are two arbitrary elements. First of all, it is necessary to assign a value of potential V to the ions which are detected at a particular probe position S. It will be shown in later sections that it is possible to remove the arbitrary nature of this selection. The second arbitrary element is the selection of the electric field E. Here we have a fundamental difficulty inherent in the model. About all that can be done is to select a value of E that will be consistent with the value of V and the solution value y_o. Since E represents an <u>average</u> electric field over the cycloidal trajectory, its value should be of the order of V/y_o.

In order to test the cycloidal trajectory theoretical model and also gain some insight into the positive ion motions, a number of calculations were made to find the point of origin for ions detected at three points of the helium ion probe current-position characteristic of Figure 29. In this figure, the probe position of +0.005-inch was labeled point A, the probe position of +0.020-inch was labeled point B, and the probe position of +0.035-inch labeled point C. It would appear that according to equation (1), low energy ions would have a small radius of curvature R within the hollow cathode and would be detected at points farthest from the center of the cathode. Thus, the point C at a probe position of 0.035-inch would be associated with low energy ions. In the same way, high energy ions should be deflected least within the cathode and would be associated with the point A. The point of highest frequency in the distribution curve of Figure 29, the point B, would most naturally be associated with the ion energies of maximum frequency. From the previous ion energy measurements, one can make use of the following rule of thumb, vis., the mode of an ion energy distribution taken at a gas pressure of about 10^{-6} torr occurs at roughly one-third the maximum anode to cathode potential.

Dycloidal trajectory calculations that were made for the points A, B and C of the ion probe current position characteristic are summarized in Table 1. The value of the potential V selected for point A was the full anode-cathode voltage of 4,000 volts (4000×10^8 abvolts). For an assumed electric field of

TABLE 1

SUMMARY OF HELIUM ION ORIGINS AND ENTRANCE ANGLES CALCULATED IN ACCORDANCE WITH THE CYCLOIDAL MODEL

Data Point	Voltage, V (abvolts)	Electric Field, E (volts/cm)	Ion Origin, Y_o (cm)	Entrance Angle, β (Degrees)	Probe Position, S (cm)	Magnetic Deflection, h (cm)
A	$4{,}000 \times 10^8$	4,000	0.157	$1^\circ\ 12'$	0.0127	0.0044
		22,220	0.873			
		25,450	1.000			
B	$1{,}333 \times 10^8$	630	0.655	$6^\circ\ 11'$	0.0508	0.0079
		680	0.707			
		721	0.750			
		840	0.873			
		962	1.000			
		1,333	1.386			
C	15×10^8	1,249	0.100	$1^\circ\ 50'$	0.0889	0.0762
		2,000	0.160			
		12,490	1.000			
	25×10^8	227	0.100	$4^\circ\ 18'$	0.0889	0.0591
		2,000	0.879			
	150×10^8	50	0.100	$9^\circ\ 15'$	0.0889	0.0244
		198	0.400			
		2,000	4.042			

4×10^3 volts/cm, the value of the distance y_o turned out to be small, only 0.157 cm compared with the anode-to-cathode distance of 0.873 cm. In order to place the origin of 4,000 volt ions at the anode in this model, it was necessary to assume an average electric field equal to 2.22×10^4 volts/cm. The angle α calculated for point A was 88 degrees 49 minutes, equivalent to an entrance angle β of 1 degree 12 minutes. Most of the ion deflection (value of the parameter S) of 0.005 inch or 0.0127 cm was due to the entrance angle rather than to the bending within the cathode by the magnetic field. This is ascertained by computing the distance h, as shown in Figure 30, and comparing the values of h and S.

The value of the potential selected for point B was one-third the anode-to-cathode voltage of 4,000 volts. Here, calculations were made for several different electric fields. As can be seen from Table 1, increasing values of the electric field E yielded increasing values of the distance y_o. Average electric fields of about 600 to 800 volts/cm give reasonable values for the points of ion origin. Notice that the entrance angle for these most abundant ions has increased to about 6 degrees. The magnetic deflection of these ions within the cathode is only about one-sixth of the total deflection as given by the probe position S.

Three values of potential V were used to describe the low energy data point C. Several values of electric field were assumed for each of the three potentials. Very low 15-volt energy ions were associated with relatively large electric fields of the order of 1,000 to 2,000 volts/cm and a small entrance angle of β equal to about 2 degrees. Twenty-five volt positive ions were associated with much smaller electric fields of the order of 200 to 400 volts/cm and an entrance angle β of about 4 degrees. One hundred and fifty volt positive ions were associated with very small electric fields of the order of 50 to 100 volts/cm and an entrance angle β of about 9 degrees.

The results obtained with the cycloidal model for helium gas, although not definitive, are not unreasonable, and they show the expected increase in the electric field as one moves from the gauge cathode to the gauge anode. The possible inversion of the beam entrance angle β as the ion energy increases from the lowest to the highest values is also evident. The entrance angles, moreover, are calculated from the probe position data and depend on ion potential only. These angles will be the same regardless of the theoretical model used to determine the origin of the ions. The cycloidal model has served to confirm the identification of the high and low energy portions of the X-1 gauge probe current distribution, although a little study and manipulation of equations (1) and (4) will show that there is a minimum potential for ions below which ions can no longer reach the probe. This minimum potential is:

$$V_{min} = \frac{(S^2 + Z^2)^2 \eta B^2}{8 S^2} \qquad (6)$$

Since Z^2 is much greater than S^2, the minimum potential decreases as the probe distance S increases. By substituting the appropriate numbers into equation (6) for values of S at each end of the probe current distribution, it becomes evident that only one end of the distribution can correspond to low energy ions.

The greatest shortcoming of the cycloidal trajectory model is the arbitrary manner in which the electric field must be selected. In addition, however, it can be seen from Figure 30 that this model requires that the ion start its trajectory parallel to the aperture normal (that is, in the r direction). In truth, the ion trajectory must really start radially, in the direction of the electric field. Such a change in the initial direction of the ion can cause a significant change in the ion trajectory.

In the next section, an exact expression for the point of ion origin will be developed. The new theory will be applied to some recent experimental data taken with the X-1 gauge for nitrogen gas. A method of reducing the X-1 gauge data and correcting it for several systematic errors will be presented. The corrected probe position data will then be correlated with positive ion energy data to obtain a correspondence between the probe position of detected ions and their energy (potential). The new positive ion trajectory theory involves no arbitrary assumptions about electric fields. Values of the ion entrance angle β and the ion potential V lead directly to values of the ion origin radius r_o.

Experimental Results and Trajectory Analysis for Nitrogen Gas

The Model X-1 Gauge Data and Its Correction for Aperture Width and Probe Width. The third experiment that was performed with the Model X-1 gauge was a refinement of the experiments described earlier. The experiment was performed with the X-1 gauge attached to the test chamber of the all-glass test system. The test system had been pumping for about 1 week and had been baked with heating tapes. The background pressure in the system was 3×10^{-8} torr as measured with a Veeco RG-75 Bayard-Alpert gauge.

The X-1 gauge was connected in the usual way with just one innovation that will be described shortly. A J.Fluke model 408B high voltage power supply was used to furnish +1.5 kV to the gauge anode. Since the anode of this gauge is diveded into two radial half anodes, the two halves were connected together externally. The fixed probe outside the anode was unconnected (floating electrically). Grounding this probe had no effect on the cathode current or the movable central probe current. The magnet used was an M-5 type having a magnetic field of 1035 gauss at the center of its 1-1/4-inch air gap. Special aluminum centering rings were used for the first time to position the magnet relative to the gauge envelope. The centering rings permitted the magnet and its magnetic field to be reversed in direction and still maintain the same position relative to the gauge envelope. The electrical connections to the X-1 gauge are shown schematically in Figure 31.

The experiment was started by first measuring the background beam profile. The test chamber pressure was 4.7×10^{-8} torr and the gauge cathode current was 1.28×10^{-8} amps at 1.5 kV during the measurements. The background probe current was measured in steps of 0.005-inch from -0.040-inch to + 0.040-inch as read by the motion feedthrough micrometer dial. This current was found to vary from a value of 1.2×10^{-11} ampere at a position of - 0.035-inch to a value of 4.5×10^{-12} amperes at a position of + 0.040-inch. This background current will be shown to be small compared with the nitrogen gas probe current.

Nitrogen gas was permitted to enter the test chamber and an equilibrium pressure of 3.70×10^{-6} torr was established. Probe current readings were then taken at 0.0025-inch intervals from - 0.040-inch to + 0.040-inch. Following this procedure, the X-1 gauge was turned off and the permanent magnet was reversed in direction. When the gauge was turned on again, the test chamber pressure was about 5 percent lower. A second set of readings of probe current vs probe position was now taken. The two sets of readings are shown in Figure 32.

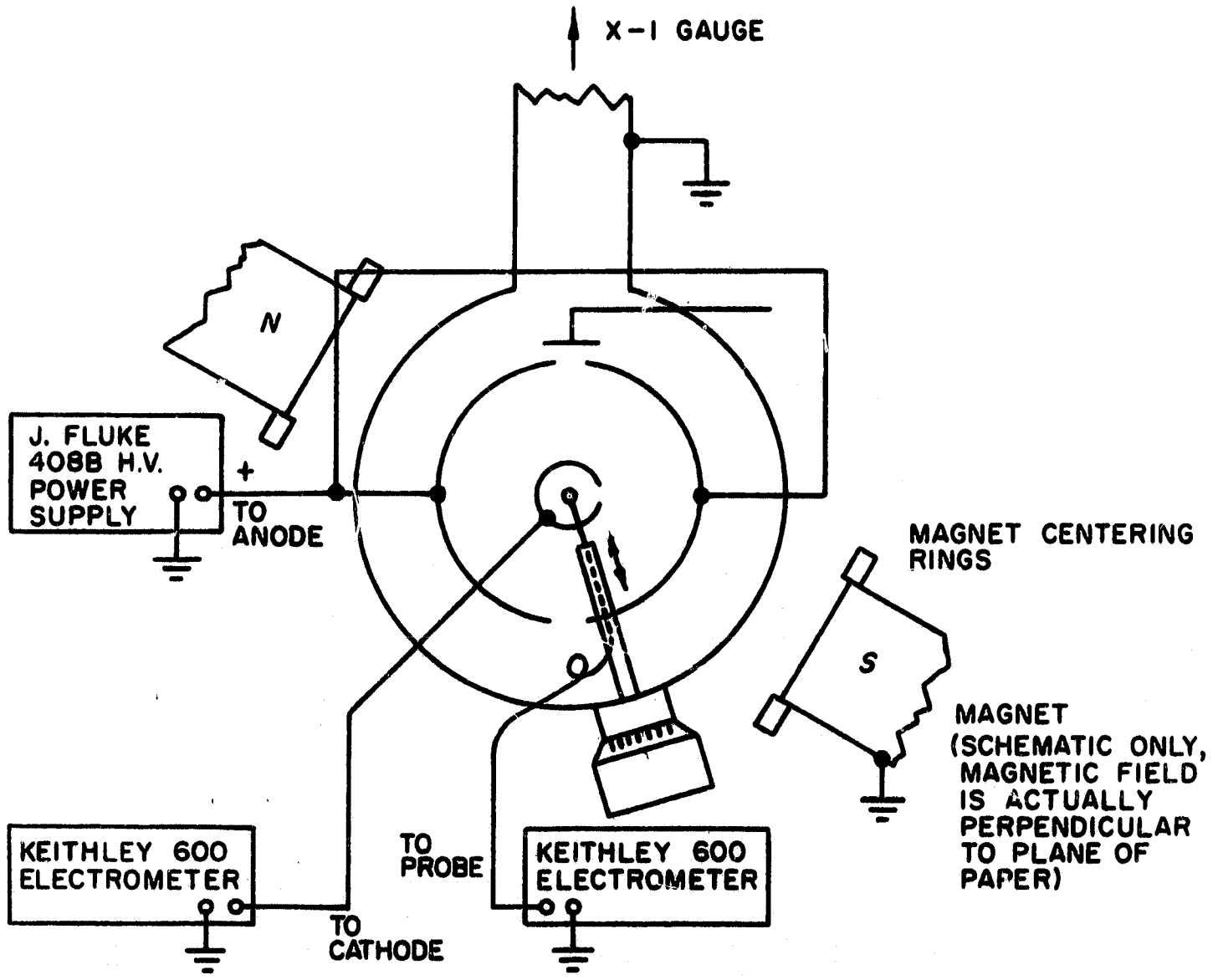

Figure 31. Electrical connections to the X-1 gauge.

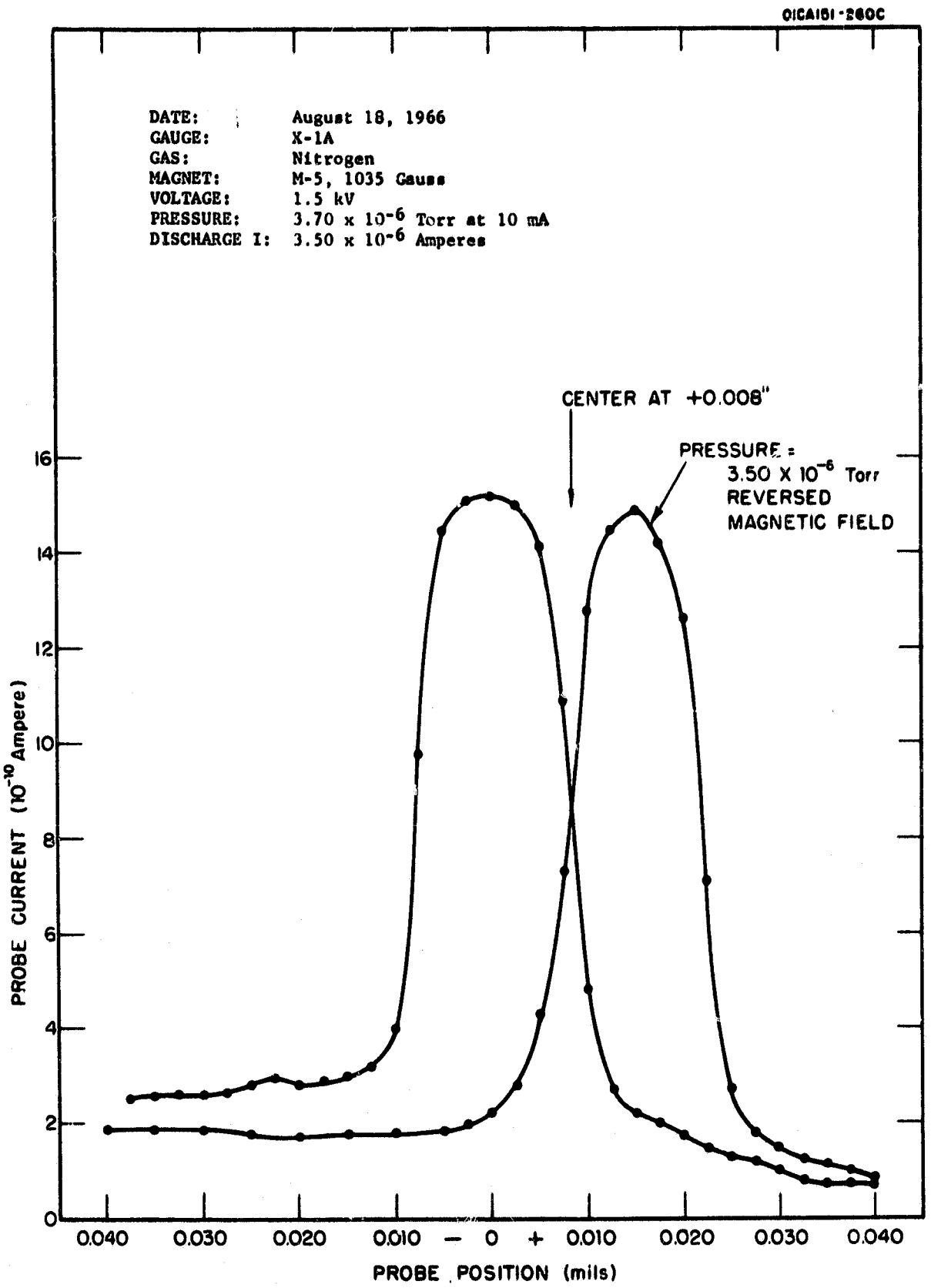

Figure 32. Nitrogen gas probe current vs probe position for 10-mil diameter probe and 10-mil diameter aperture.

The reason for reversing the magnetic field and taking a second set of readings was to provide a method of determining the effective center of the hollow cathode. Since the X-1 gauge was symmetrical, a reversal of the magnetic field should displace the ion beam by an equal amount in the opposite direction from the initial displacement. The data presented in Figure 32 show that the effective center of the gauge cathode was located at a probe position of + 0.008-inch.

It should be recognized that the probe currents that are displayed in Figure 32 represent a considerable integration of positive ions over a rather wide (0.010-inch diameter probe) S interval and an equally wide cathode aperture interval. In order to find the true point distribution of positive ion current within the gauge cathode, one must compute the derivative of the probe current as obtained and displayed in Figure 32. This has been done numerically, using 0.001-inch (1 mil) as the basic probe distance S interval, in order to obtain a corrected current distribution $I_t(S)$. The result of the numerical differentiation is shown in Figure 33. Notice that the normal type distribution of Figure 32 has become a bimodal distribution.

Recognizing that the distribution $I_t(S)$ is also an integration of positive ions from each unit distance (element of area) in the aperture, a second correction must be applied to find the distribution that would result if the aperture were infinitely small. One can consider the distribution $I_t(S)$ to be equal to a finite sum of distributions $I_i(S)$ where each I_i is the distribution due to one small element of area in the aperture. Again, one can use 0.001-inch (1 mil) as the basic i interval in the aperture and numerically add the distributions. Each distribution I_i is identical with the others except that it is shifted in its origin. In this way, the method of finding $I_1(S) = I_2(S + 0.001) = I_3(S + 0.002)$ and so forth, is to use a numerical subtractive process. The extreme value of $I_t(S)$ will derive only from the extreme value of $I_1(S)$. The second point of $I_t(S)$ is due to the second value of $I_1(S)$ plus the first value of $I_2(S + 0.001)$ and so on. The above described numerical subtractive process has been applied to the data points of the $I_t(S)$ distribution that appears in Figure 33. The results of this correction are shown graphically in Figure 34. The new distribution is much narrower than the original distribution of Figure 32, as one would expect. The distribution is really not as detailed as it should be, and the negative-going portions of the curve indicate that the corrections have not been complete and exact. Nevertheless, in spite of all the imperfections, the resulting corrected distribution curve gives a much more accurate picture of how the positive ions move within the hollow cathode than does the original uncorrected distribution.

From the frequency distribution of Figure 34, it is relatively easy to construct a cumulative frequency distribution or "less than" ogive. The percentage cumulative frequency distribution corresponding to the current distribution of Figure 34 is given in Figure 35.

At this point, it may be recalled that ion energy distribution curves for nitrogen gas were obtained earlier in Section II. In fact, one particular ion energy distribution was measured for nitrogen gas at a pressure of 3.90×10^{-6} torr, a value very close to the pressure of 3.70×10^{-6} torr that existed

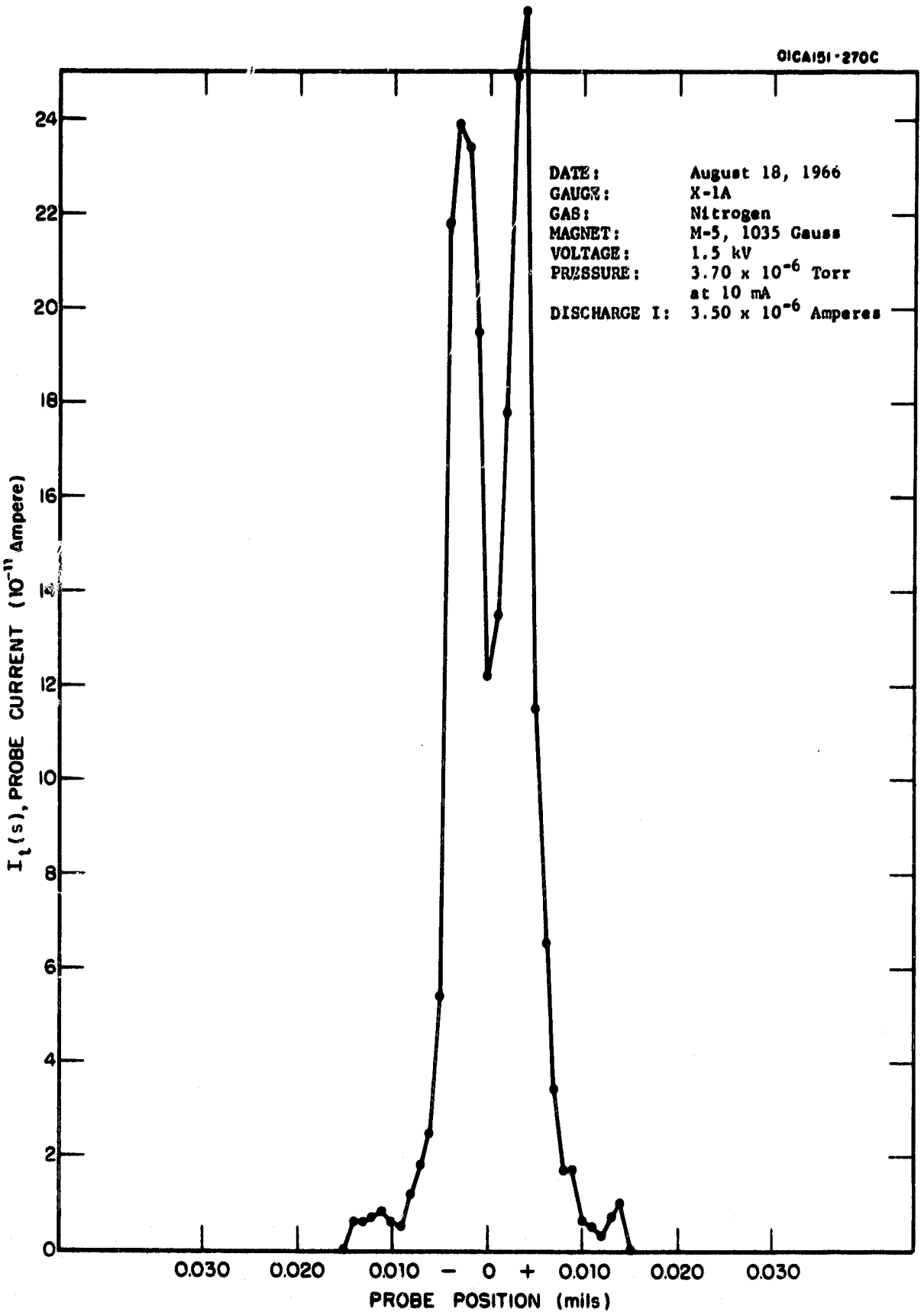

Figure 33. Probe current $I_t(s)$ that would be measured with a 1.0-mil diameter probe.

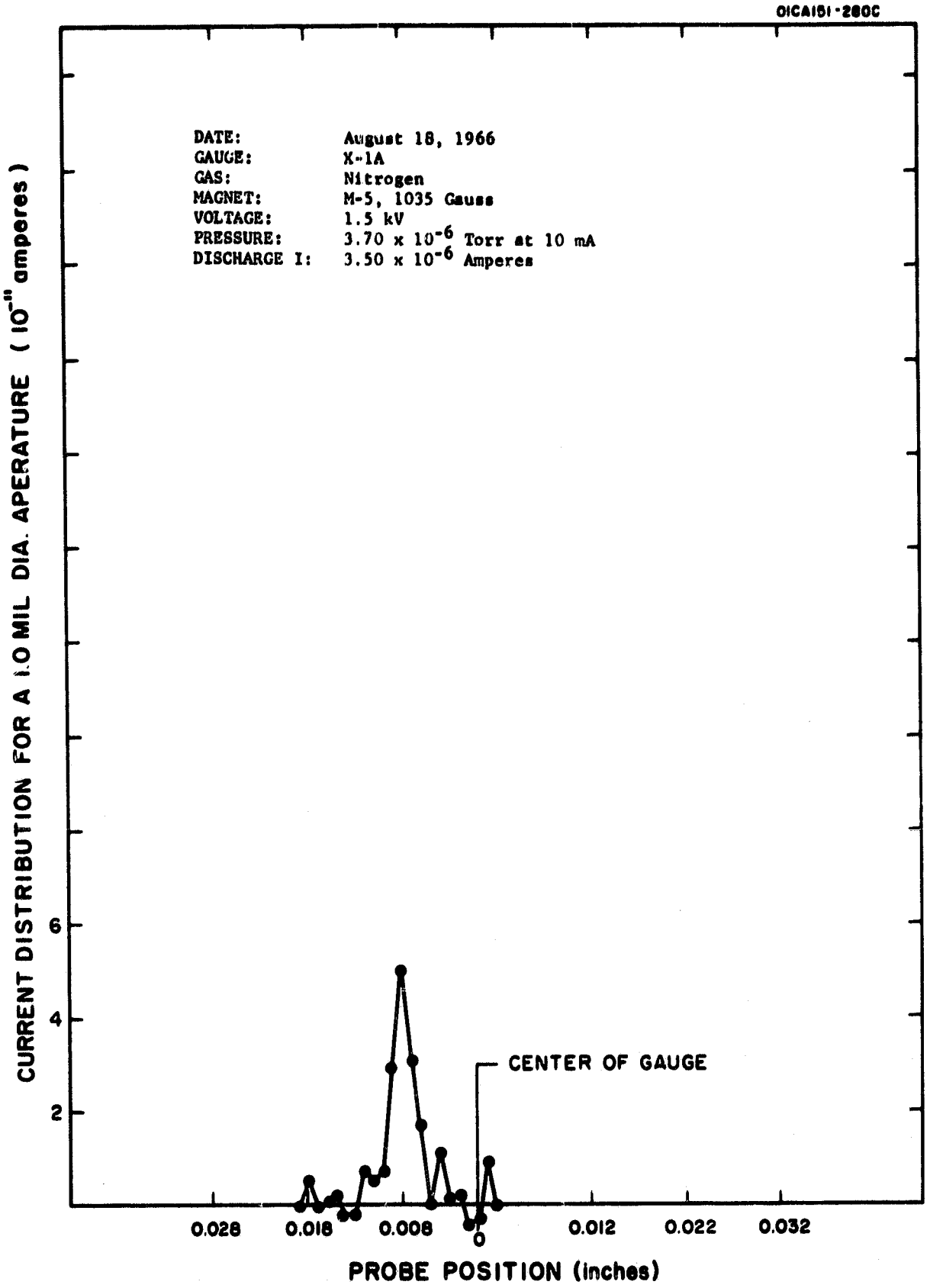

Figure 34. Probe current that would be measured with a 1.0-mil diameter probe if the aperture were 1.0-mil in diameter.

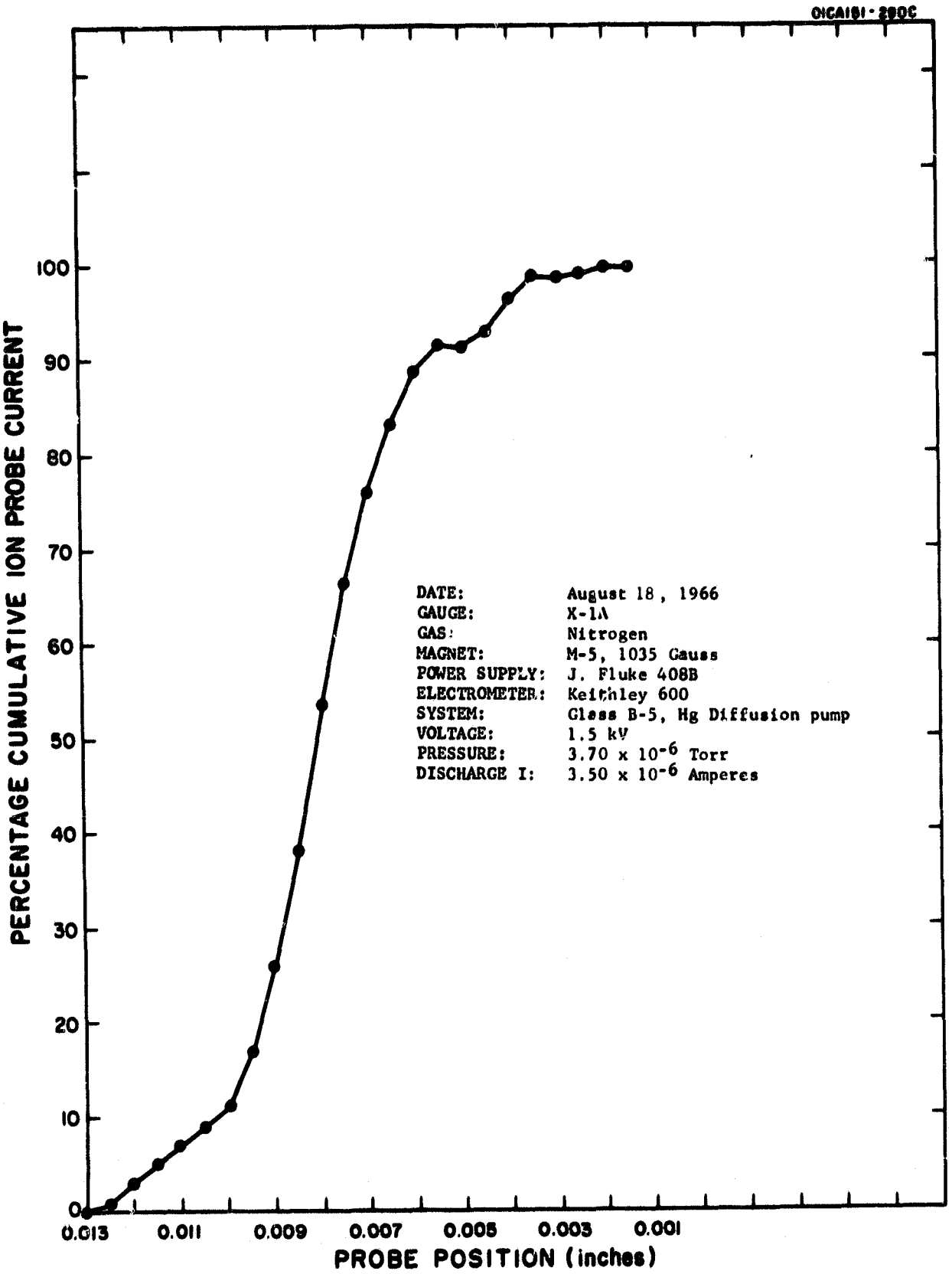

Figure 35. Percentage dumulative ion probe current as a function of probe position for nitrogen gas.

during the nitrogen gas probe current vs. probe position measurements. The percentage cumulative ion probe current as a function of ion energy for this particular ion energy distribution has been plotted in Figure 36.

Comparing the percentage ogive curves of Figures 35 and 36, the method of assigning potentials to various probe positions becomes immediately evident. By matching corresponding percentile values, one can associate a value of potential V with each value of probe position S in a one-to-one fashion. The arbitrary method of assigning potential values to probe positions that was used to reduce the helium gas data has now been eliminated.

Derivation of Equations That Yield Exact Positive Ion Origins. In order to determine the exact origin of a positive ion that moves within a radial electric field in the presence of a transverse magnetic field, it is first necessary to write the basic equations of motion of an ion in such fields. These equations may be derived from first principles or they may be found in any textbook which treats the subject of electron behavior in crossed magnetic and radial electric fields[9]. The differential equations of motion of an electron in such fields is given by:

$$\ddot{r} - r\dot{\theta}^2 = -\frac{e}{m} r\dot{\theta} B_Z + \frac{e}{m} \frac{dV}{dr} \tag{7}$$

$$\frac{1}{r} \frac{d}{dt} (r^2\dot{\theta}) = r\ddot{\theta} + 2 \dot{r} \dot{\theta} = \frac{e}{m} \dot{r} B_Z \tag{8}$$

The dots over the letters indicate differentiation with respect to time, as usual. The quantities r and θ are the standard polar coordinates, e is the electronic charge, m is the electronic mass, B_Z is the axial magnetic field (in the Z direction) and V is the potential. In our application, the signs of the terms containing the electronic charge e must change since we are concerned with positive ions.

Equation (8) may be integrated once with respect to time under the condition that $\dot{\theta} = 0$ at the point of ion origin $r = r_o$ to yield (for positive ions) the expression:

$$r\dot{\theta} = \frac{eB_Z}{2m} \frac{r_o^2 - r^2}{r} \tag{9}$$

The quantity $r\dot{\theta}$ may be recognized as the tangential velocity of an ion. Using the above expression for $r\dot{\theta}$ and substituting into equation (7) with the signs of the two terms containing e changed, one obtains an equation in terms of r and its time derivations alone. This equation can be intergrated once under the condition that $\dot{r} = o$ at $r = r_o$, the point of ion origin, to yield:

$$\dot{r} = \pm \left[\frac{2e}{m} [V9r_o) - V(r)] = \frac{e^2 B_Z^2}{4m^2} [2 r_o^2 - r^2] - \frac{r_o^4}{r^2}^{\circ} \right]^{1/2} \tag{10}$$

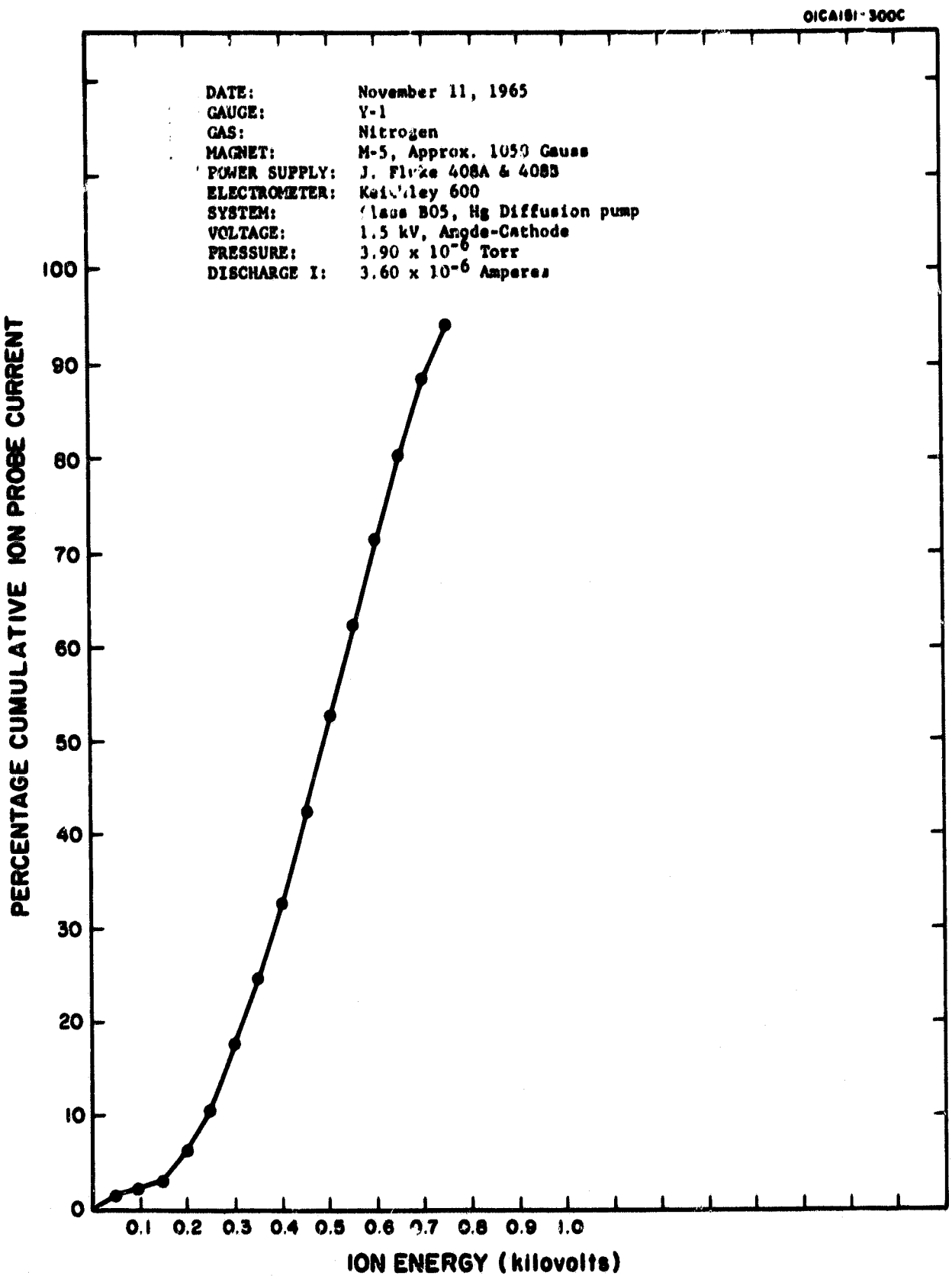

Figure 36. Percentage cumulative ion probe current as a function of ion energy for nitrogen gas.

Since positive ions will move radially inward in our application, $\dot{r}$ is actually negative. However, in the derivations that follow, we shall only be interested in the absolute values of both the radial velocity $\dot{r}$ and the tangential velocity $r\dot{\theta}$.

Now, when a positive ion reaches the aperture of the gauge cathode, it has a definite radial velocity and a definite tangential velocity. The angle at which the ion enters the aperture is given by the expression:

$$|\tan \beta| = \left| \frac{r\dot{\theta}}{\dot{r}} \right|_{r = Z} \tag{11}$$

where Z is the value of the radius r at the cathode aperture. At the cathode aperture, we shall assume that the potential V is zero. Under these conditions, one may write:

$$|r\dot{\theta}|_{r = Z} = \frac{eB}{2mZ} (r_o^2 - Z^2) \tag{12}$$

and

$$|\dot{r}|_{r = Z} = \left[\frac{2e\ V(r_o)}{m} - \frac{e^2 B^2}{4m^2 Z^2} (r_o^2 - Z^2)^2 \right]^{1/2} \tag{13}$$

The next step in the solution is to solve equations (11), (12) and (13) for r_o in terms of the quantities β, e, B, m, V and Z. The result is:

$$r_o = \left[\frac{Z}{B} \quad \frac{8m}{e} V(r_o) \quad \sin \beta + Z^2 \right]^{1/2} \tag{14}$$

Equation (14) is the exact solution for the radius of the ion origin r_o.

Application of the Exact Equations. Having worked out the mathematical relationship between the origin of an ion, its entrance angle, the potential at the point of origin, the charge-to-mass ratio of the ion, the magnetic field strength and the radius at the cathode aperture, the final phase of the program was to apply this theory to the X-1 and Y-1 gauge nitrogen gas data.

From the graphs of Figures 35 and 36, values of the potential V for values of probe positions S corresponding to fairly evenly spaced percentile intervals on the two ogive curves were recorded. Equations (1), (4) and (5) were then used to determine the values of sin β. Finally, equation (14) was used to find the corresponding values of the ion origin r_o. The data and results of the calculations are given in Table 2 and Figure 37.

As can be seen, the potential as a function of radial distance appears to be reasonable for points near the gauge cathode. The electric field at the cathode is of the order of 150 volts/cm and this field increases continually for radial positions further from the cathode. At a radial position 0.37 cm from the cathode, the electric field increases considerably to a practically constant value of 4.2×10^3 volts/cm. The potential drop in this region of constant electric field is about 400 volts.

TABLE 2

INITIAL DATA AND RESULTS OF ION ORIGIN CALCULATIONS
FOR NITROGEN GAS

Percentage Cumulative Ion Probe Current	Ion Potential V (volts)	Probe Position S (Inches)	Probe Position S (cm)	Magnetic Deflection h (cm)	Entrance Angle β (Deg + Min)	Radius of Ion Origin r_o (cm)
2	75	0.0122	0.0310	0.0124	$2^o41'$	0.634
5	178	0.0115	0.0292	0.00810	$3^o3'$	0.766
10	240	0.0103	0.0262	0.00690	$2^o47'$	0.782
20	315	0.00932	0.0237	0.00602	$2^o33'$	0.796
30	385	0.00882	0.0224	0.00545	$2^o27'$	0.815
40	440	0.00843	0.0214	0.00515	$2^o21'$	0.823
50	490	0.00810	0.0206	0.00489	$2^o16'$	0.828
60	540	0.00774	0.0197	0.00454	$2^o11'$	0.832
70	595	0.00730	0.0185	0.00436	$2^o3'$	0.827
80	650	0.00670	0.0170	0.00422	$1^o51'$	0.809
90	715	0.00572	0.0145	0.00399	$1^o31'$	0.765
94	750	0.00435	0.0110	0.00390	$1^o2'$	0.675

Parameter Values

β = 1035 Gauss

$h = \frac{e}{m} = 3.445 \times 10^2$ emu/gm nitrogen

Z = 0.39624 cm

V_a = 1.5 kV (Anode Voltage)

$p = 3.70 \times 10^{-6}$ Torr

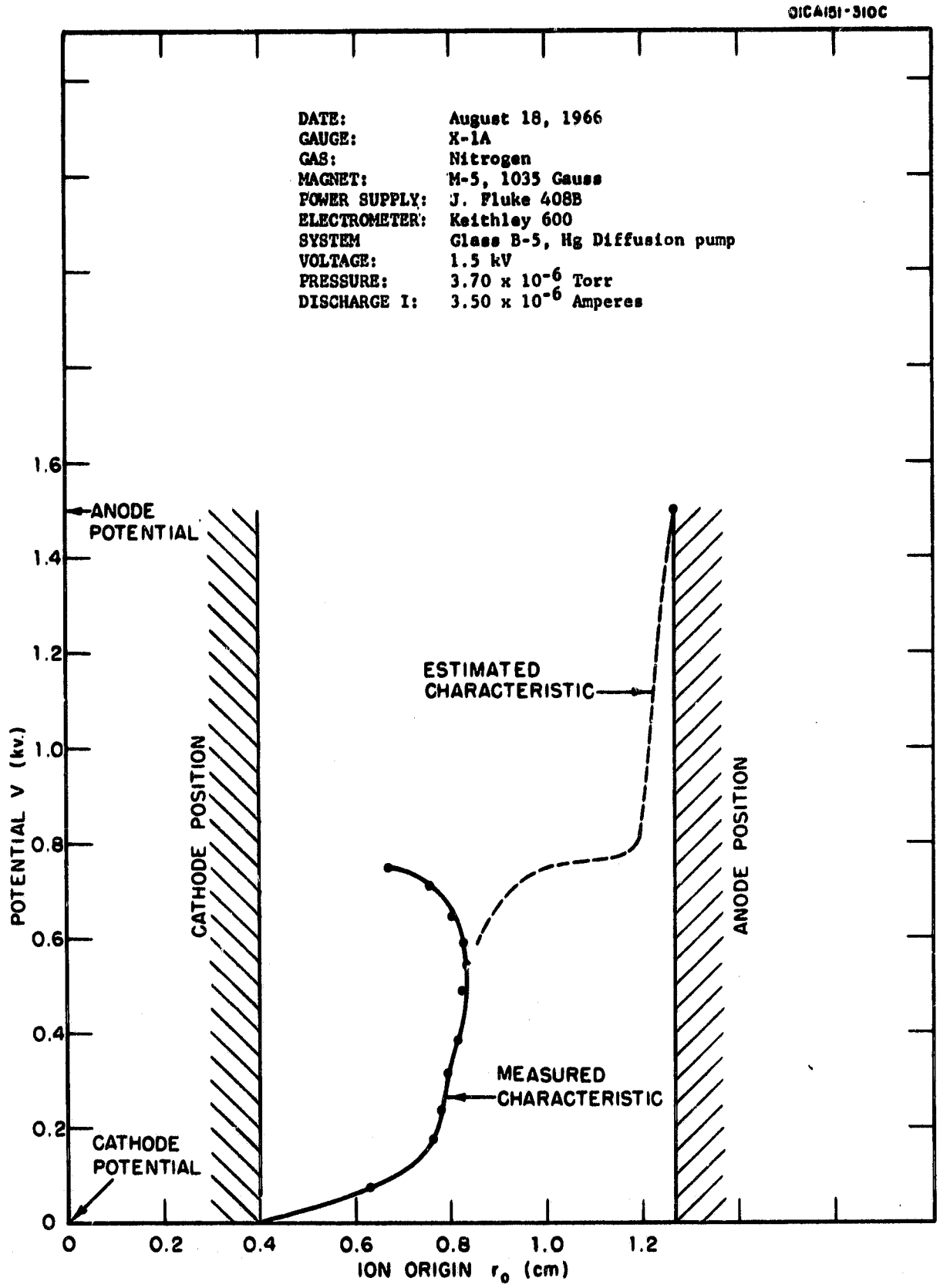

Figure 37. Potential as a function of radial distance in the X-1 gauge for nitrogen gas.

It is most significant to notice that the potential appears to vary quadratically with radial distance from the cathode in the region from 0 to about 175 volts. This region constitutes 0.37 cm/0.873 cm = 42.5 percent of the total distance between cathode and anode. In the region from 175 to 575 volts, the potential varies linearly with the radial distance.

The potential vs. radial distance curve appears to reverse itself for values of potential greater than 575 volts. The reason for this reversal is not known at the present time. The potential inversion may not be a real effect and is possibly the result of inaccurate data obtained with the X-1 gauge. We are somewhat handicapped in interpreting the curve of Figure 37 due to the absence of ion energy data for voltages above 750 volts. It would seem at first appearance that if there were very few ions with energies above 750 volts, then there could be very little space charge in the region near the anode so that the potential curve is this region must have its space-charge-free value. Yet electrons must eventually be captured by the anode, and so there must be space charge near the anode. A reasonable explanation of the conditions within the gauge for higher values of potential is as follows: For values of potential between approximately 575 volts and 750 volts, the electric field gradually decreases from a value of 4.2×10^3 volts/cm to a value less than 1×10^3 volts/cm. For values of potential above 750 volts, the electric field remains less than 1×10^3 volts/cm until the region of the anode is approached. Near the anode, the electric field starts to increase very rapidly such that the field at the anode is very high and there is a large potential drop of the order of 700 volts at the anode. Positive ions can be created close to the anode, but very few ions will be formed due to the relatively short lifetime of most electrons in this region and their high energy. There would appear to be a considerable space charge near the anode which is not effective in creating positive ions, if this explanation is correct. The region of effective space charge appears to be centered about midway between the cathode and the anode.

IV. DESIGN OF A MAGNETRON-TYPE COLD CATHODE GAUGE LAW RESOLUTION MASS SPECTROMETER

Experiments that were performed with the model X-1 gauge, in which there is a moveable probe located inside the hollow gauge cathode, showed that a beam of positive ions was formed by a pinhole in the center of the cathode side wall. The construction and operation of the X-1 gauge have been described in the preceding chapter, where it was shown how the origin of a positive ion could be found in terms of the probe position S at which the ion was detected. In this chapter, our attention will focus on the ion trajectories within the hollow cathode and the manner in which these trajectories are affected by various parameters, particularly the mass of the ion. The object of this investigation will be to design a gauge similar to the X-1 gauge that can be used to separate ions of various masses. It is believed that a study of the behavior of the X-1 gauge together with a study of the fundamental equations of the ion trajectories is the first step in the design of a magnetron type cold cathode gauge mass spectrometer.

For the X-1 gauge with its 0.010-inch diameter cathode aperture and its 0.010 inch wide ion probe, the ion beams have an apparent width of about 0.015 inch at their half-amplitude position. In the last chapter it was shown how the width of this beam (the ion probe current vs probe position) would be narrowed by using a 0.001-inch diameter aperture and a 0.001 inch wide ion probe. From the calculations and Figure 34, it appears that for this case the beam would have a width of about 0.003 inch at the half-amplitude position. For two gases such as helium and oxygen, the spacing between beams may be of the order of 0.008 inch [1]. Under these circumstances, the two ion beams would be completely separated or resolved. In the pages that follow, it will be shown that higher resolutions than this can be achieved, so that such an instrument may be able to separate hydrogen and helium from all heavier gases and many of the heavier gases may be separated from one another.

Equation (14) of the previous chapter relates the radius position of the ion origin r_o with the entrance angle β of the ion at the cathode aperture. This equation may be easily inverted to express the angle β in terms of the ion origin radius, the ion mass and the other parameters of the gauge. The result is:

$$\sin \beta = \frac{\sqrt{e}\ B\ (r_o^2 - Z^2)}{\sqrt{8m}\ Z\ \sqrt{V(r_o)}} \qquad (15)$$

It can be seen that the sine of the entrance angle (approximately equal to β in radians for the small angles that are involved here) is inversely proportional to the square root of the ion mass.

Using equations (4) and (5) of the previous chapter and neglecting the terms -1 and S^2 in the radical of equation (4), one obtains the approximate expression:

$$S \cong \frac{2R \sin \beta + Z}{2R} \tag{16}$$

If now, the value of sin β from equation (15) and the value of R from equation (1) are substituted into equation (16), one obtains the basic expression for the probe distance S as a function of the various parameters:

$$S \cong \frac{r_o^2 \quad B \sqrt{e}}{2Z \sqrt{2V} \sqrt{m}} \tag{17}$$

Equation (17) shows that the deflection S of a positive ion along the center line of the hollow cathode of a magnetron gauge mass spectrometer is inversely proportional to the square root of the ion mass.

Aside from any geometrical spreading of an ion beam due to aperture and probe widths, there is an inherent spread in each beam of ions of the same mass due to a spread in values of the ion origin radius r_o and the ion potential $V(r_o)$. The exact manner in which these parameters affect the displacement or deflection spread is given by equation (17). Notice that variations in r_o and V tend to cancel since it is the ratio of the two quantities that is involved and they tend to increase and decrease together.

From equation (17), one can easily derive the expression for the fractional change in the beam deflection S as a result of changes in the ion potential and radial position:

$$\frac{dS}{S} = \frac{2 \, dr_o}{r_o} - \frac{1}{2} \frac{dV}{V} \tag{18}$$

In a similar manner, one can derive the expression for the change in mass per unit mass, an expression which immediately yields the mass resolution as follows:

$$m = \frac{r_o \, V}{r_o \, dV - 4V \, dr_o} \tag{19}$$

Equations (18) and (19) show quite clearly the cancellation possibilities for position spread (dr_o) and energy spread (dV). If the potential V were known as a function of r_o, one could compute the beam spread and resolution from equations (17), (18) and (19). It is of interest to note in passing that there is one simple relationship between V and r_o for which the inherent beam spread will be zero. If $V = Kr_o^4$ where K is a constant, the beam deflection spread vanishes and the instrument resolution becomes infinite. When V varies with r to the nth power, with n less than 4, the position spread dr_o dominates and the beam spreads in the direction of decreasing mass. With the exponent n greater than 4, the energy spread dV dominates and the beam spreads in the direction of increasing mass. It has been shown in the previous chapter that $V \alpha r^2$ for low energy ions and $V \alpha r$ for most of the remainder of the ions. One would then expect ion position spread to dominate. Theoretically, if the gauge potential varied with the fourth power of the radius over a limited region of the discharge (most likely near the gauge anode) and if it were possible to

select out only those ions from this region, one would obtain very high resolutions.

One practical way to reduce the spread of all ion beams is to use a retarding electrode just inside the hollow cathode that will stop all ions having less than a specified energy. In this way, not only is the energy spread of the ions reduced, but the radial position spread will also be reduced. Of course the sensitivity will be decreased too, but this is not a major consideration. As an example, in the case of the nitrogen gas ion beams formed in the X-1 gauge at an anode voltage of 1.5 kV, as described in the preceding chapters, placing the retarding electrode at a potential of +500 volts would remove about half of the total number of ions, but it would also cut the beam spread approximately in half.

The retarding electrode that is used to reduce the beam spread can also be used to electrically deflect the ion beam within the hollow cathode. For example, two electrically isolated plates can be used to make up the retarding electrode. The potentials of the two plates can be varied to yield a transverse electric field that deflects the beam. Another method would be to place a single axial conductor at the enter of the hollow cathode and then vary the positive potential of this conductor. The effect in this case however, would be to simultaneously change the beam spread and the beam deflection.

Greater separation of ion beams will be achieved if the beam detector is located not at the center line of the hollow cathode, but at a point that is further from the aperture. Such a location would be on the inner wall of the cathode opposite the aperture. The separation between ion beams would then be more than twice the separation available on the cathode center line.

As can be seen from equation (17), increasing the magnetic field would increase the ion beam deflection, assuming that the potential distribution as a function of the radius is not drastically changed.

All the elements of a workable device are now at hand. A sketch of a prototype low resolution mass spectrometer is presented in Figure 38. Notice that the circular aperture of the X-1 experimental gauge has been replaced with a narrow axial slit. Since the areas of a 0.010-inch diameter aperture and a 0.001 inch by 0.080 inch rectangular slit are about equal, there should be no change in sensitivity. The combination ion beam retarding and deflecting electrodes are mounted inside the cathode on either side of the entrance slit. Both electrodes are at a positive potential. They are biased so that their average potential remains constant but the potential between them varies to change the beam deflection (Vo + V and V_o-V). A dual, mechanically coupled potentiometer could be used to provide a positively increasing voltage to one of these electrodes simultaneous with a positively decreasing voltage to the other electrode. Such an arrangement would be used to manually sweep for various mass peaks. Positive going and negative going electronically generated sweep voltages could be provided to make the operation automatic. Any strip chart recorder could then be used to display and record the output of the ion detector electrometer.

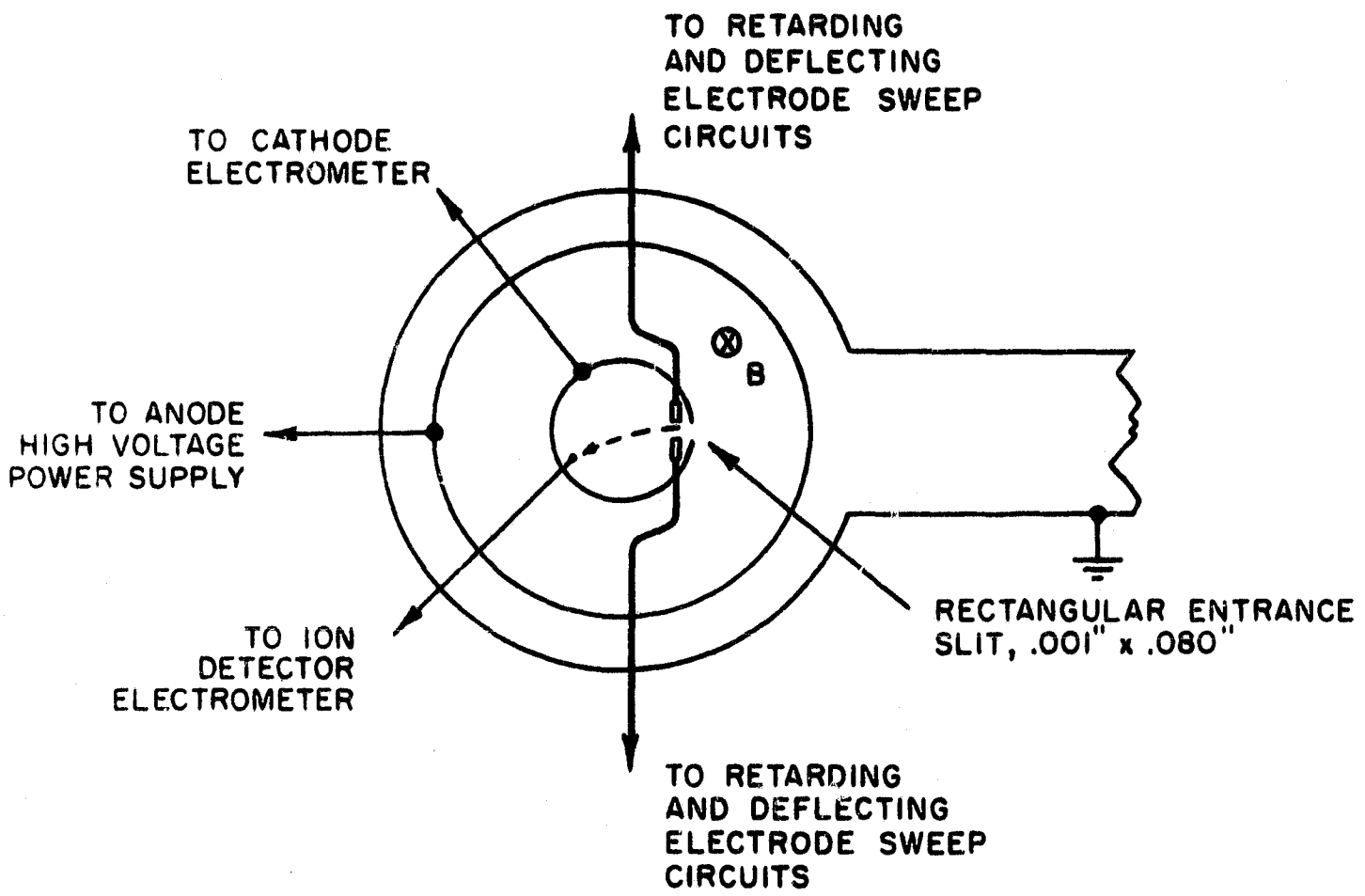

Figure 38. Simplified schematic diagram of a magnetron-type cold cathode gauge low-resolution mass spectrometer.

V. COLD CATHODE GAUGE PUMPING AND RE-EMISSION STUDIES

Equipment

The test system that was used to study gauge pumping and re-emission could be pumped with either getter-ion pumps or a liquid helium cryopump. The cryopump-ion pump system, as shown in the block diagram of Figure 39 and the photograph of Figure 40, was an all-metal test system that was quite different from the all-glass test system described earlier. The ultra high vacuum part of this system consisted of four basic components: (1) a liquid helium cryopump; (2) a Vacion type getter-ion pump; (3) a test chamber; and (4) a 1-1/2 inch bakeable UHV valve. The UHV components were mounted on an insulated oven base and positioned so that they could be baked out by a roll-on type oven.

Connected to the test chamber, but not shown in the drawing of Figure 39, were the following additional pieces of equipment: (1) a Varian nude Bayard-Alpert ionization gauge; (2) a UHV 1-1/2 inch "Tee" type valve; (3) a G.E. model 22PT110 partial pressure analyzer (PPA); and (4) a GCA model R-5 flight type cold cathode ionization gauge whose pumping and re-emission characteristics were being studied. The G.E. PPA and the GCA model R-5 gauge were connected to the two arms of the UHV "Tee" valve so that they could both be valved off from the test chamber, but they could not be valved off from each other.

The fore-vacuum components used with this vacuum system consisted of a Varian VacSorb zeolite sorption pump, a Varian 8ℓ/sec Vacion sputter-ion pump, a fore-vacuum valve, a glass Bayard-Alpert ionization gauge, an adjustable UHV type leak valve and a 1 liter bottle of pure nitrogen gas.

In addition to the above componants, some auxiliary equipment was available for use during the system bakeout period. This extra equipment included a rotary mechanical vacuum pump, a zeolite-charged fore-vacuum trap, two glass vacuum cold traps in series, and a rubber connection to the VacSorb pump. The rubber connection to the VacSorb pump was disconnected and the auxiliary equipment was not used during the pumping and re-emission experiments.

The entire system was constructed to fit both above and below a standard laboratory table 30 inches by 84 inches by 34 inches high. The additional table length served to support the roll-on oven when it was not in use, as shown in Figure 40. A standard electronics rack housed the control units for the ion pumps and ionization gauges.

The liquid helium cryopump, which mounted directly on top of the test chamber via a 6 inches O.D. ConFlat flange, was not used during the pumping and re-emission experiments. The UHV 8ℓ/sec Vacion pump was connected to one of the four side tabulations of the test chamber. There was adequate clearance for mounting the ion pump magnet. The weight of the magnet was carried by the pump and test chamber. The UHV right angle valve that isolated the test chamber from the forevacuum part of the system was a Varian 1-1/2 inch bellows sealed valve.

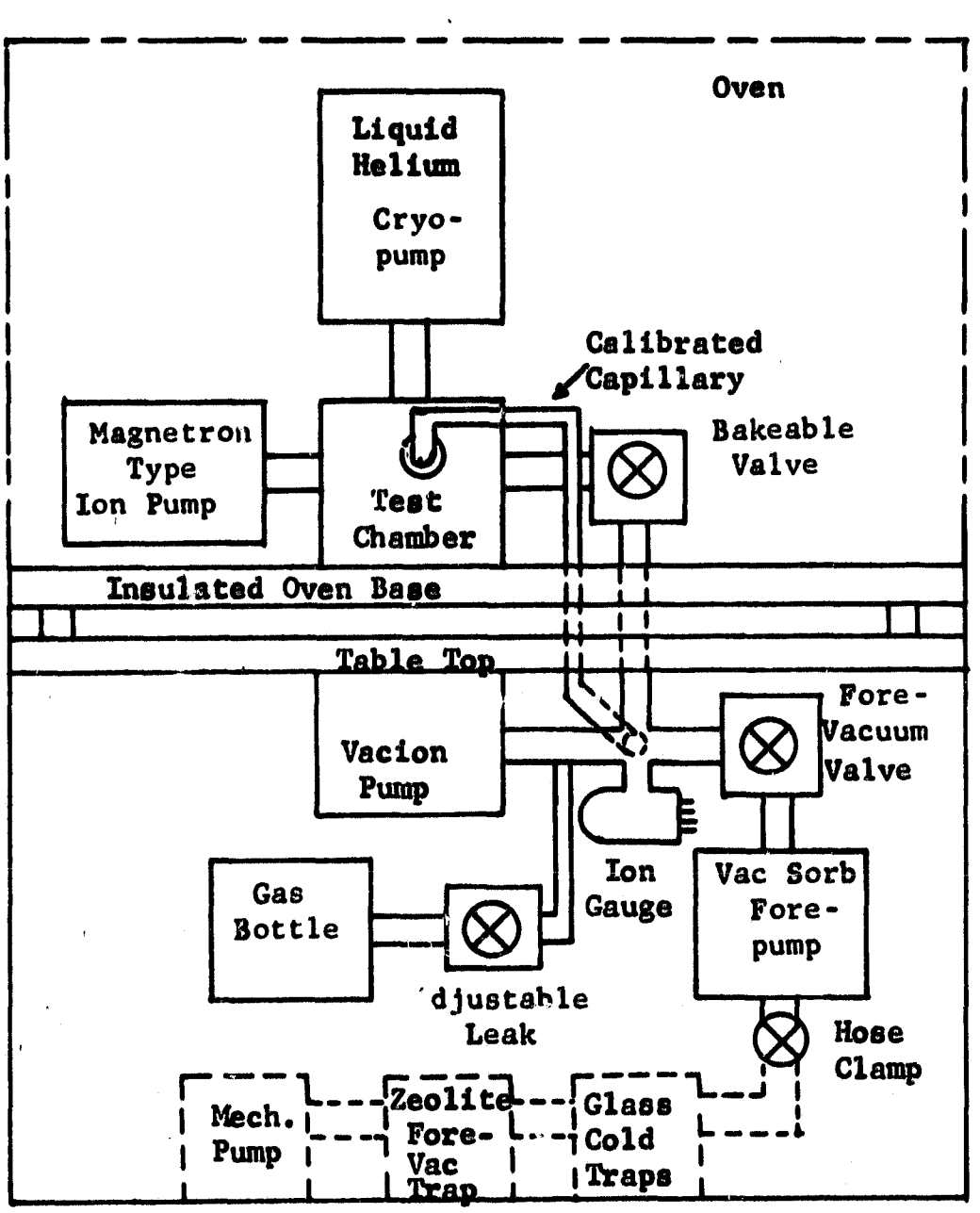

Figure 39. Block diagram of cryopump-ion pump system.

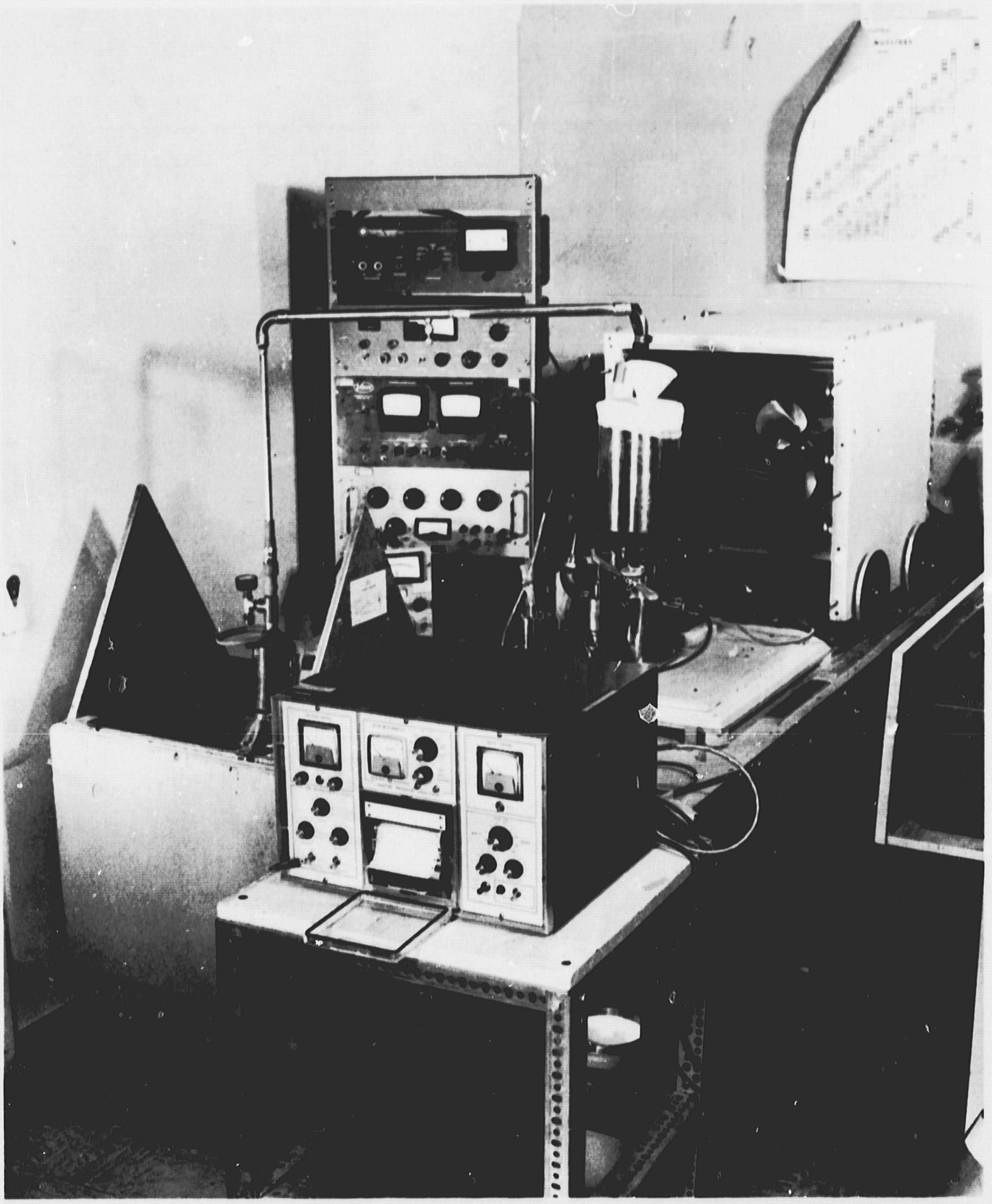

Figure 40. Photograph of cryopump-ion pump system.

It was mounted on the test chamber side tabulation directly opposite the UHV "Tee" type valve, which was also a Varian 1-1/2 inch bellows sealed valve. The fourth side tabulation of the test chamber contained a Varian UHV-14 nude, hot filament B.A. type ionization gauge.

The UHV right angle valve that isolated the test chamber from the fore-vacuum part of the system was connected via 1-1/2 inch O.D. tubing to one port of a stainless steel ConFlat-flanged Tee fitting located just below the table top. The forevacuum ion pump and a second Varian right angle 1-1/2 inch bakeable valve (the fore-vacuum valve) were connected to the remaining two ports of the Tee fitting. A glass Veeco RG-75 hot filament ionization gauge and a glass tubulation to the Granville Phillips type C UHV gas bottle leak valve were attached to the Tee fitting via Kovar-Pyrex graded seals. The Varian VacSorb forepump was flanged directly to the fore-vacuum valve.

The VacSorb pump, after activating it by baking, was used to evacuate the entire system from atmospheric pressure to the 10^{-3} or 10^{-4} torr level. At this time, the forevacuum ion pump was started and the VacSorb pump was valved off. When the system pressure had decreased by several decades, the upper ultra high vacuum part of the system above the table top could be baked. At the end of the bakeout period, the isolation UHV valve above the oven base was closed and the UHV 8ℓ/sec ion pump was turned on to pump down the test chamber and keep it under vacuum.

Pure nitrogen gas was admitted to the test chamber in the following way: The Granville Phillips type C adjustable leak valve was opened to allow gas from the gas bottle to flow into the Tee fitting. The pressure that was established in the Tee fitting chamber was determined by the leak valve setting and the effective pumping speed of the forevacuum ion pump. This pressure was measured with the Veeco ionization gauge. Pure gas from the Tee fitting chamber was admitted to the test chamber by opening the UHV isolation valve.

Detailed descriptions of some of the unusual components of this all-metal test system have been presented in a recent NASA Contractor Report [10].

Experimental Procedures

At the time that the pumping and re-emission tests were started, the best procedure for making these measurements was not known. In order to determine the best methods to use, and at the same time, see if changes in procedures would lead to different results, it was decided to carry out pumping and re-emission measurements under different conditions. Three separate pumping and re-emission measurements were made for nitrogen gas for the same GCA model R-5 cold cathode ionization gauge. The three measurements were made at approximately one month intervals of time. The conditions under which the measurements were made and the procedures that were used are listed below.

The first experiment was performed on October 12, 1965. The cryopump-ion pump system had been pumped down from atmospheric pressure about two days earlier.

Once the system pressure had gone below 1 x 10^{-3} torr, only the fore-vacuum ion pump was used to pump out the entire system. The system had not been baked. At the time the experiment was started, the test chamber background pressure, as read by the Varian nude B.A. gauge, was 6.1 x 10^{-7} torr. All of the system gauges including the model R-5 cold cathode gauge and the G.E. partial pressure analyzer (PPA) had been operating for at least 284 hours. The PPA background nitrogen peak was 1.1 x 10^{-9} Ampere as measured with a 10-second sweep and an emission current of 1.0 mA at 70 volts. There were many other peaks in the mass spectrum. In all three experiments, a nitrogen gas pressure was established in the test chamber by opening and adjusting the nitrogen gas bottle leak valve and allowing this gas to be pumped by the forevacuum ion pump. In the first experiment, the R-5 cold cathode gauge was turned off but the Varian nude gauge and the G.E. PPA were allowed to stay on while nitrogen in the test chamber equilibrium pressure. The test chamber background pressure had decreased to 3.20 x 10^{-7} torr and the PPA background nitrogen gas peak was 0.22 x 10^{-9} Ampere. The nitrogen peak was the largest in the mass spectrum. The model R-5 gauge and the PPA were turned off before nitrogen gas was admitted to the test chamber in the usual way. An equilibrium pressure of 7.20 x 10^{-6} torr was established in the test chamber. The nitrogen gas pump-down phase was started by closing the UHV Tee valve and turning on the R-5 gauge at about the same time. After 5 minutes of pumping, a small mode change in the gauge current occurred. After 9 minutes of gauge pumping, the PPA was turned on. The pressure in the closed R-5 gauge and PPA volume (0.500 liter) increased by about a factor of 3 as indicated by the R-5 gauge readings. After 10-1/2 minutes of R-5 gauge pumping, the R-5 gauge was turned off the the re-emission phase started. The PPA was kept operating with a 10-second sweep and an emission of 1.0 mA at 70 volts as before. It was discovered that the G E. PPA 10^{-8} and 10^{-9} electrometer scales did not give the same readings. The re-emission of nitrogen was recorded for 40 minutes. After this, a calibration of both the PPA for nitrogen and the model R-5 gauge for nitrogen was performed by turning on the R-5 gauge and opening the UHV Tee valve. The test chamber pressure had decreased somewhat to a value of 6.7 x 10^{-6} torr at that time with pure nitrogen flowing into the system from the gas bottle and being pumped by the forevacuum ion pump. The readings of the R-5 gauge and the PPA were compared with the Varian nude gauge reading.

The third and last experiment was performed on December 15, 1965 after the system had been vented and then placed in operation again. The system was put through a four-day bakeout cycle a few days before the experiment was performed. The ultra high vacuum portions of the system above the table top gas was admitted to the test chamber, the R-5 gauge and the PPA (The UHV "Tee Valve" was open). A pressure of 1.45 x 10^{-5} torr, as read by the nude gauge, was established in the test chamber. The nitrogen gas pump-down phase was started by turning off the PPA, closing the UHV Tee valve, and, 5 minutes latter, turning on the R-5 cold cathode gauge. Readings of the R-5 gauge were taken every minute. After 10 minutes of gauge pumping, the PPA was turned on. Three minutes later, after 13 minutes of gauge pumping, the R-5 gauge was turned off and the re-emission phase started. The PPA was kept operating with a short 10-second sweep covering the region of the nitrogen n/e 28 peak. The nitrogen peak was recorded for both increasing and decreasing accelerating voltage of the PPA. Re-emission in this experiment was monitored for 17 minutes. After about 2 hours of re-emission,

the UHV Tee valve was opened. The R-5 gauge was not turned on the only the PPA readings for the nitrogen peak were compared with the reading of the Varian nude gauge to yield a calibration for the PPA nitrogen peak. It was assumed that the Varian nude gauge gave an accurate reading of the pressure in the test chamber.

The second experiment was performed on November 12, 1965. The cryopump-ion pump system had been operating continuously since the first experiment with the forevacuum ion pump doing the pumping. It still had not been baked. One of the objectives of the second experiment was to see if continued, long ion pumping without bakeout would affect pumping and re-emission measurements. All of the system gauges and the PPA were operated before the experiment was performed.

The PPA would outgas when it was initially turned on. It increased the test chamber pressure by about 20 percent initially and caused an increase of 10 percent were baked for about 3 days at temperatures as high as 360°C. The Varian nude test chamber gauge and the G.E. PPA filament were outgassed for about 30 minutes. The UHV isolation valve that joins the test chamber with the forevacuum was closed and the test chamber 8 liter/sec ion pump was turned on. The model R-5 gauge, the PPA and the Varian nude gauge were all operated for several hours prior to the experiment. The background pressure in the test chamber was 2.5×10^{-8} torr. The PPA nitrogen peak background reading was 0.13×10^{-9} ampere. Before admitting nitrogen gas to the test chamber in the usual way, the R-5 gauge, the PPA and the test chamber ion pump were turned off. The forevacuum ion pump was on continuously and the flow of nitrogen gas was adjusted with the UHV leak until the pressure in the test chamber was 4.9×10^{-6} torr. The nitrogen gas pump-down phase was now started uniquely by first turning on the PPA. The Varian nude gauge pressure indication increased to 5.1×10^{-6} torr, a 4 percent increase. About 2-1/2 minutes after the PPA was turned on in the presence of the high pressure nitrogen, the UHV Tee valve was closed and the R-5 gauge was started immediately afterward. After 5-1/2 minutes of pumping, during which period the R-5 gauge reading was recorded every half minute, the R-5 gauge was turned off and the re-emission phase started. The PPA nitrogen mass peak was recorded with the 10-second sweep as usual with the emission at 1.0 mA and 70 volts. All of the re-emission data were taken on a single scale, the 10^{-9} Ampere scale of the PPA. The nitrogen gas peak was monitored for 76 minutes. The calibration of the R-5 gauge and the PPA was performed in a somewhat different manner than in the first two experiments. First, the nitrogen gas bottle UHV leak valve was closed. Since the forevacuum ion pump remained on, the system and test chamber pressure decreased. After about 30 minutes, the test chamber pressure was 2.8×10^{-8} torr. At this time, the UHV Tee valve was opened and a nitrogen pressure was re-established in the test chamber by adjusting the UHV leak valve until the test chamber pressure had increased to a valve of 2.20×10^{-7} torr. At this time, the readings of the R-5 gauge and the PPA were compared with the reading of the Varian nude gauge, the pressure standard for these experiments.

Results

Pumping Speed Measurements. The results of pumping a closed volume (0.500 liter volume) of nitrogen gas with the model R-5 gauge in the three experiments that were performed are presented in Figures 41, 42 and 43. It should be observed that in all three cases, the pump-down proceeded in three separate steps or phases. The first pumping phase was one of maximum pumping speed, and a maximum amount of gas was pumped during this phase in the three experiments. The second step was one of intermediate pumping speed, while the third step was one of minimum pumping speed, and a minimum amount of gas was pumped during this phase in all three experiments. The three separate pumping phases are labelled as regions I, II and III in the figures. The three-step pumping process is not understood at this time, but several explanations are possible. For example, the first high speed pumping stage may be due to sputter gettering or activated adsorption at various gauge surfaces, but primarily the gauge anode. The second intermediate pumping speed stage may be due to true ion pumping at central regions of the gauge cathode. The third low pumping speed stage may be the result of ion pumping at fringe regions of the cathode after the small central region of the cathode has been saturated. Additional light will be shed on this subject by performing pump-down experiments with other gases. It is of interest to note that the pumping speed was constant during each phase of the pump down. This is to be contrasted with the continuously changing pumping speed (as a function of pressure) of getter-ion type pumps.

In two of the three experiments, there was a mode change at the end of the second pumping phase. There may be a connection between the type of pumping responsible for the second phase of the pump-down and the basic physics of mode changing.

The actual pumping speeds and the amounts of gas pumped in each phase of the three phase pump-downs are listed in Table 3. A number of interesting observations can be made on the basis of this table and the pump-down graphs. From the graphs, for example, it can be seen that phase I pumping lasted longer (3 minutes) for the first experiment than for the second (2 minutes) and third (1/2 minute) experiments. The initial nitrogen gas pressure (1.45×10^{-5} torr) for the first experiment was greater than that for the second experiment (7.20×10^{-6} torr) and that for the third experiment (5.1×10^{-6} torr). Similarly, the R-5 gauge was less well outgassed for the first experiment than for the following experiments. Phase I pumping terminated at the highest pressure in the first experiment and the lowest pressure in the third experiment. The foregoing conditions are consistent with the successively higher pumping speeds measured for the first to the third experiments. The cleaner the gauge, the higher the pumping speed and the shorter the phase I pump-down period. The higher the initial nitrogen pressure, the more the gas that was pumped during this phase and the other two phases as well. One interesting observation about phase II pumping is that the pumping time remained constant at 2 minutes. The low value of the phase II pumping speed for the second experiment is not understood, but it serves to imply a different method of pumping for phase II than phase I. The phase III pumping speed for the second experiment was also unusually low, indicating that the phase II and phase III pumping are similar.

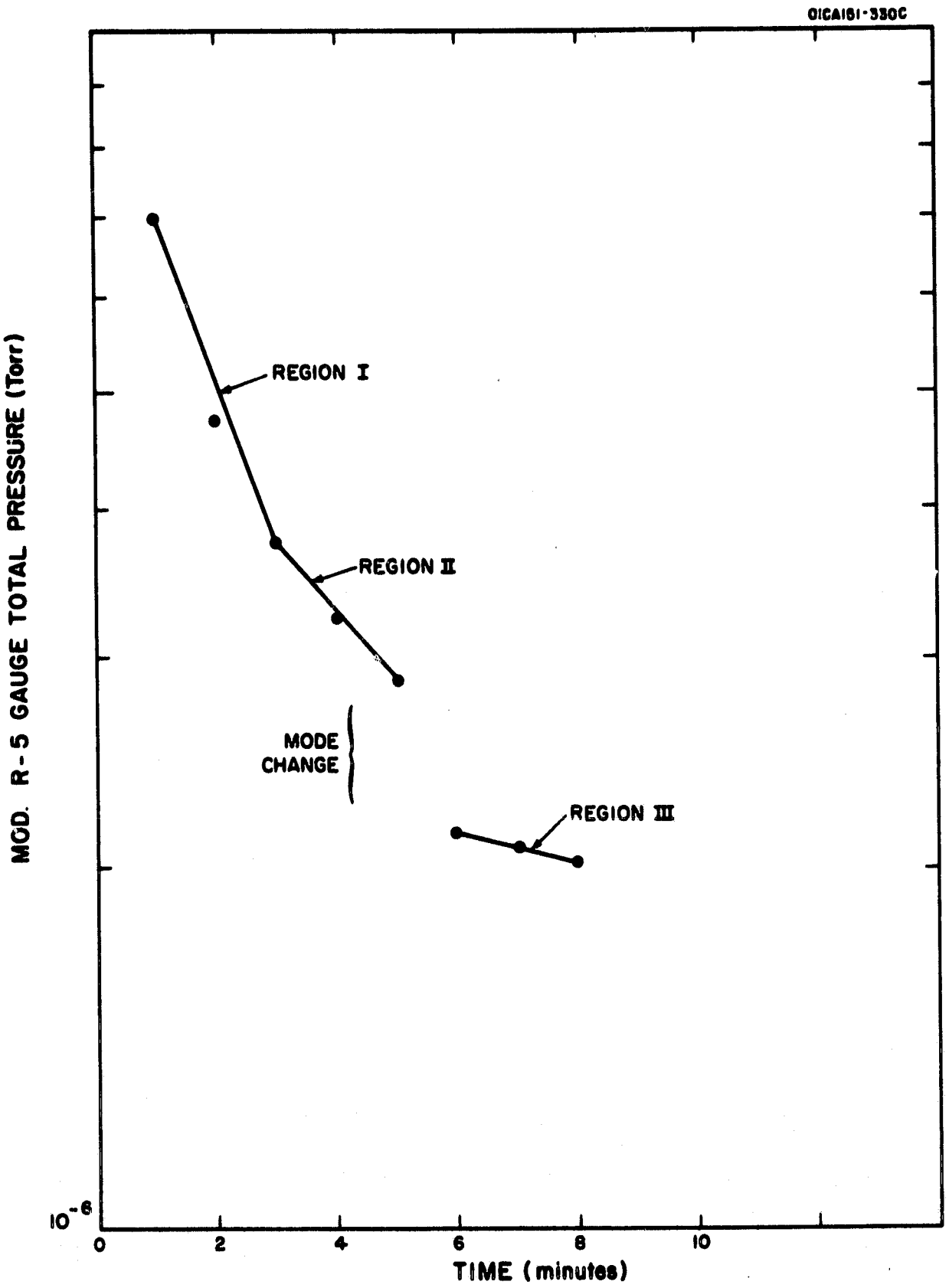

Figure 41. Pumping action of an unbaked GCA .1 R-5 cold cathode gauge for nitrogen gas, starting at an initial pressure of 1.45×10^{-5} torr.

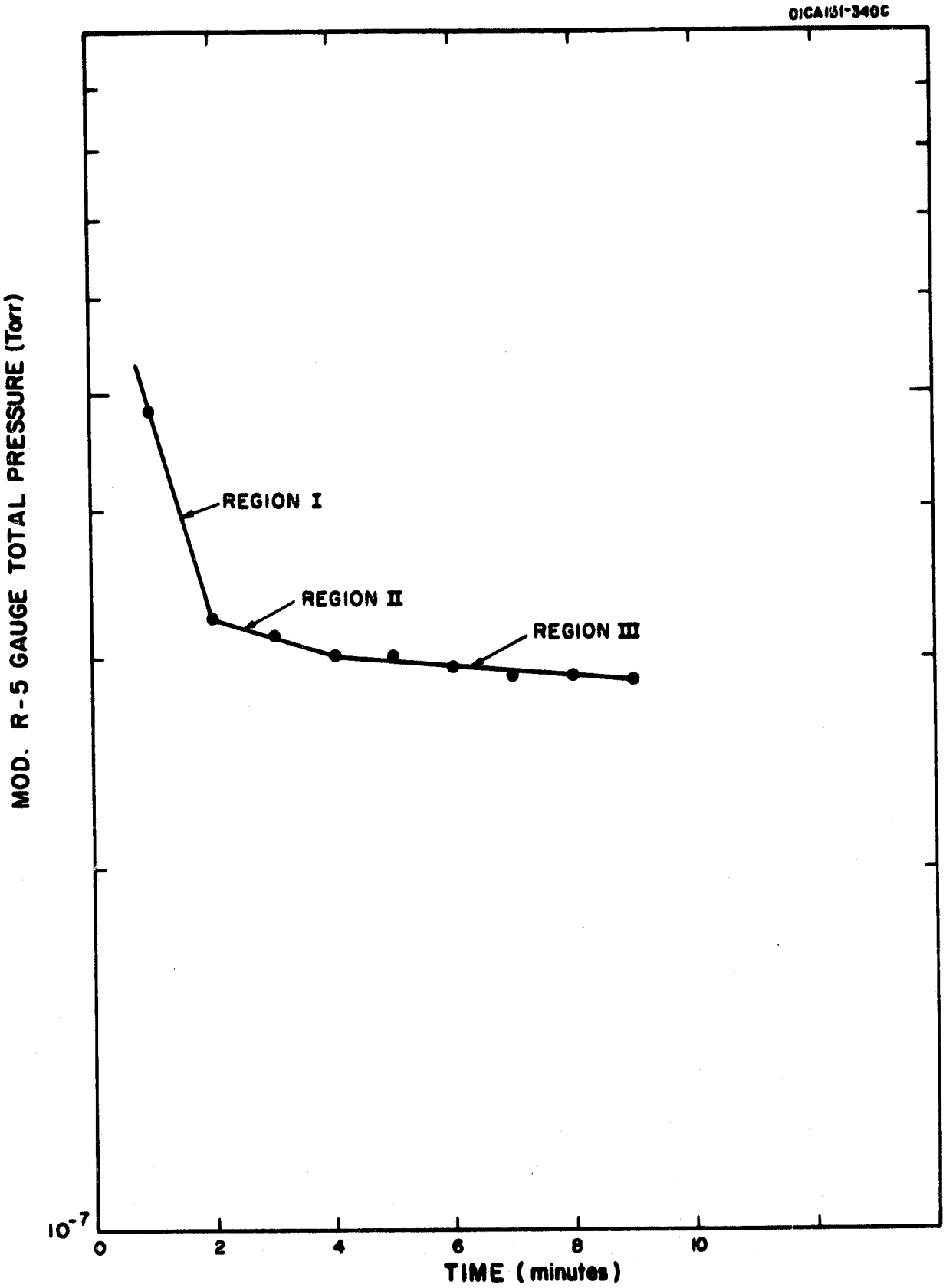

Figure 42. Pumping action of an unbaked but well-pumped GCA model R-5 cold cathode gauge for nitrogen gas, starting at an initial pressure of 7.20×10^{-6} torr.

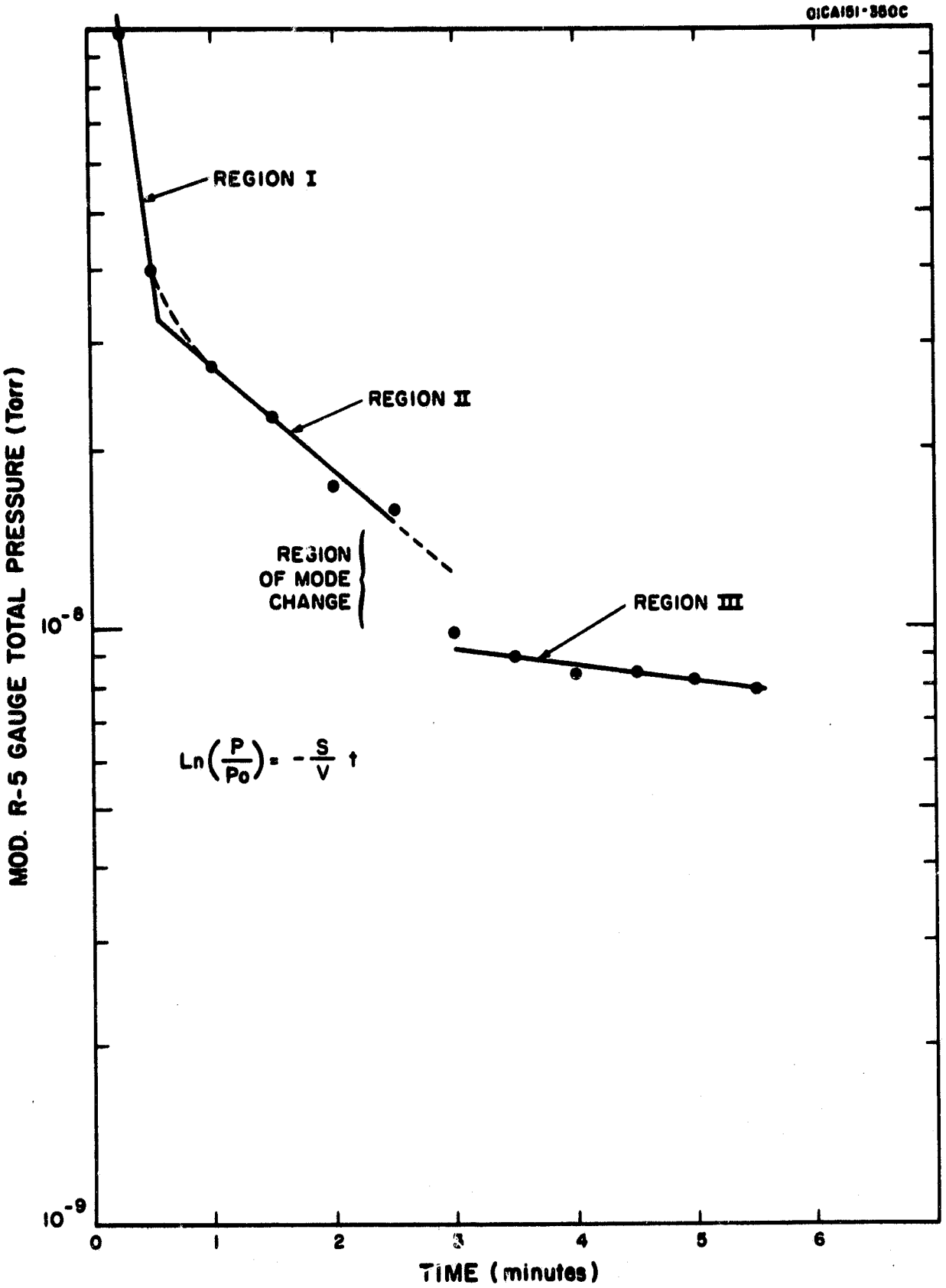

Figure 43. Pumping action of a well-baked GCA Model R-5 cold cathode gauge for nitrogen gas, starting at an initial pressure of 5.1×10^{-6} torr.

TABLE 3

MEASURED PUMPING SPEEDS AND THE AMOUNTS OF NITROGEN GAS PUMPED BY A GCA MODEL R-5 COLD CATHODE IONIZATION GAUGE

Pumping Phase	Pumping Speeds (liters/sec)			Total Nitrogen Pumped (torr liters)		
	First Experiment	Second Experiment	Third Experiment	First Experiment	Second Experiment	Third Experiment
I	2.60×10^{-3}	3.35×10^{-3}	3.08×10^{-2}	5.37×10^{-6}	3.44×10^{-6}	2.53×10^{-6}
II	1.09×10^{-3}	3.07×10^{-4}	3.36×10^{-3}	0.43×10^{-6}	0.011×10^{-6}	0.010×10^{-6}
III	2.58×10^{-4}	7.85×10^{-5}	4.85×10^{-4}	0.065×10^{-6}	0.007×10^{-6}	0.0006×10^{-6}

Some additional comments pertaining to the gauge pumping experiments are in order. In the second and third experiments, the pressures in the R-5 gauge at the end of the phase I pumping periods were very close to the background pressures of the test chamber. It appears that practically all of the nitrogen gas introduced into the 0.500 liter closed volume was pumped by the gauge during the phase I pumping. During phase II pumping, the closed volume pressure decreased below the original background pressure, indicating that some background gas was being pumped during this period. The lower pumping speed of phase II could be attributed partially to a change in the gas composition. It could also be attributed to a partial saturation of pumping sites by the nitrogen pumped during phase I. Finally, the lower pumping speed could also be affected by the ion energy distribution change at lower pressures. The same factors mentioned above may also be involved in the transition from phase II to phase III pumping.

Pumping speed calculations are based on the well-known equation:

$$S = -\frac{V}{t}\ell n(p/p_o) = -2.303\frac{V}{t}\log(p/p_o) \qquad (20)$$

where S is the pumping speed in liters/sec (assumed to be constant), V is the volume of the closed system in liters, t is the time in seconds, p_o is the initial pressure in torr and p is the final pressure in torr. The semi-logarithmic plots of pressure as a function of time, as presented in Figures 41, 42 and 43, are very convenient since periods of constant pumping speed appear as straight lines with the actual pumping speeds being proportional to the negative slopes of these lines.

Re-emission Measurements. The re-emission results obtained for the model R-5 gauge for each of the three experiments performed are shown in Figures 44, 45, 46 and 47. The first three of these figures are plotted on logarithmic paper to show the very general power low relationship between the re-emitted gas and the time. It is immediately obvious from these graphs that the re-emission of nitrogen gas was different for each of the three experiments.

A brief study of Figure 44 shows that the nitrogen partial pressure in the closed 0.500 liter volume increased linearly with time (since the slope of the curve, when averaged, was unity on the log-log plot) on the average for the re-emission of the first experiment. A linearly increasing pressure in a closed volume can only be caused by a constant flow of gas (re-emission). Thus, in this case, for a re-emission period of about 13 minutes, the average re-emission was constant at a value of 1.54×10^{-8} torr liters/sec. For the re-emission period from 13 to 17 minutes, the graph shows a trend towards declining re-emission. During the re-emission period, it can be seen that the re-emission function had a number of clearly delineated values that approximately averaged to a constant re-emission rate. For example, the re-emission rate increased with time for the periods from 1 to 2 minutes and from 6 to 9 minutes. On the other hand, the re-emission rates decreased with time for the periods from 2 to 6 minutes and from 9 to 17 minutes. During the latter period, the slope of the graph on the logarithmic plot was 0.54, a value which appeared in the third experiment and which will be discussed shortly.

In order to better understand the re-emission data presented in the graphs, a brief mathematical description of re-emission will be presented. Workers in this field have found that spontaneous thermal re-emission of pumped gas appears to vary with time according to an inverse power relationship. That is,

$$R(t) = R_o\, t^n, \quad n \leq 0 \tag{21}$$

where R(t) is the rate at which previously pumped gas molecules are emitted in units of torr liters/sec, R_o is the re-emission coefficient, t is the time in seconds, and n is a negative number or zero depending on the type of re-emission.

The rate of increase of pressure P(torr) in a closed volume V(liters) due solely to the re-emission rate R(t) is:

$$V \frac{dP}{dt} = R(t) = R_o\, t^n \tag{22}$$

If the above differential equation is integrated subject to the initial condition that the pressure in the volume V is p_o at time $t = 0$, the result is

$$p - p_o = \frac{R_o}{V} \frac{t^{n+1}}{(n+1)} \tag{23}$$

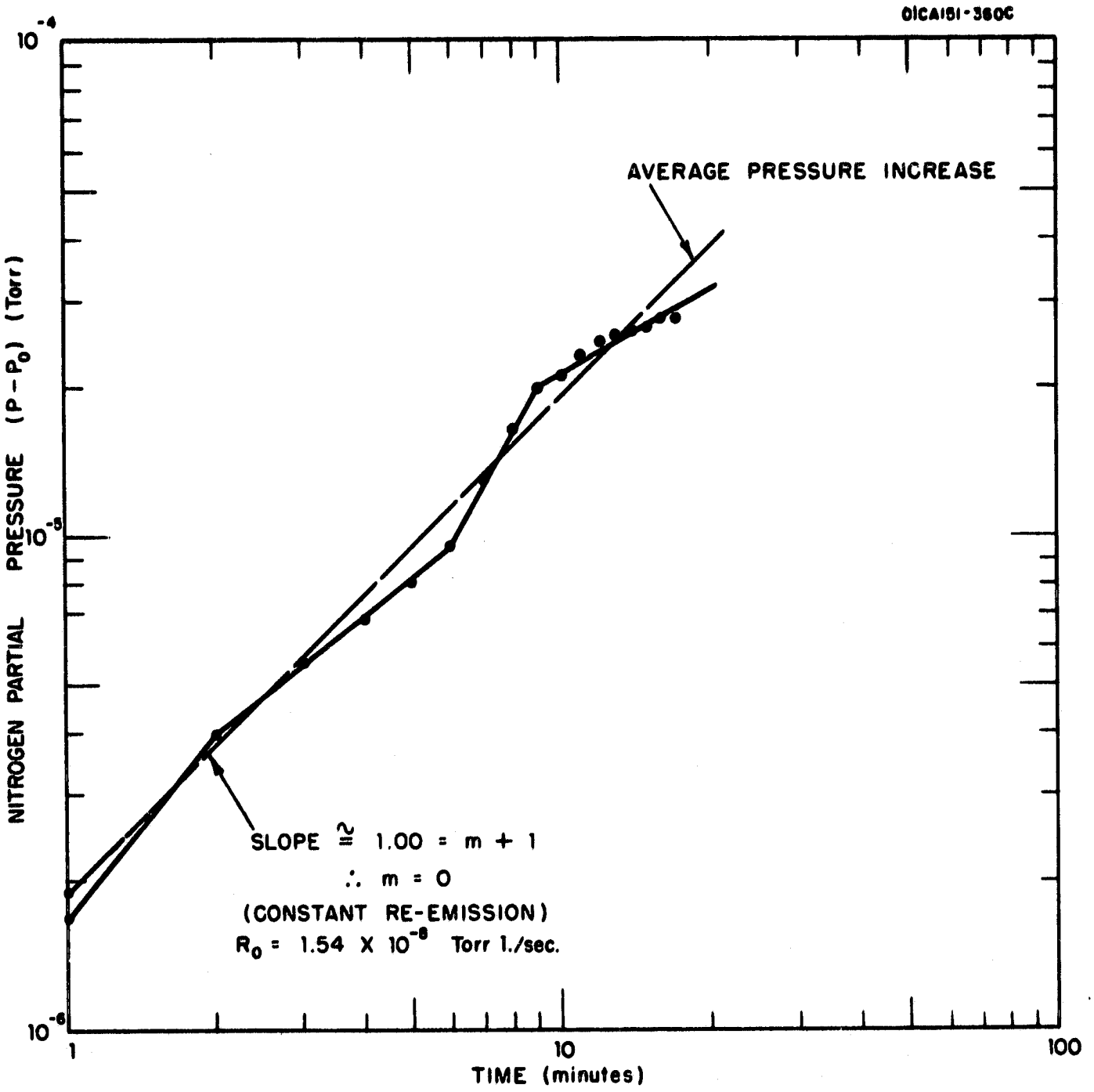

Figure 44. Pressure increase due to re-emission of nitrogen gas from an unbaked GCA model R-5 cold cathode gauge after 13 minutes of pumping, starting at a pressure of 1.45×10^{-5} torr.

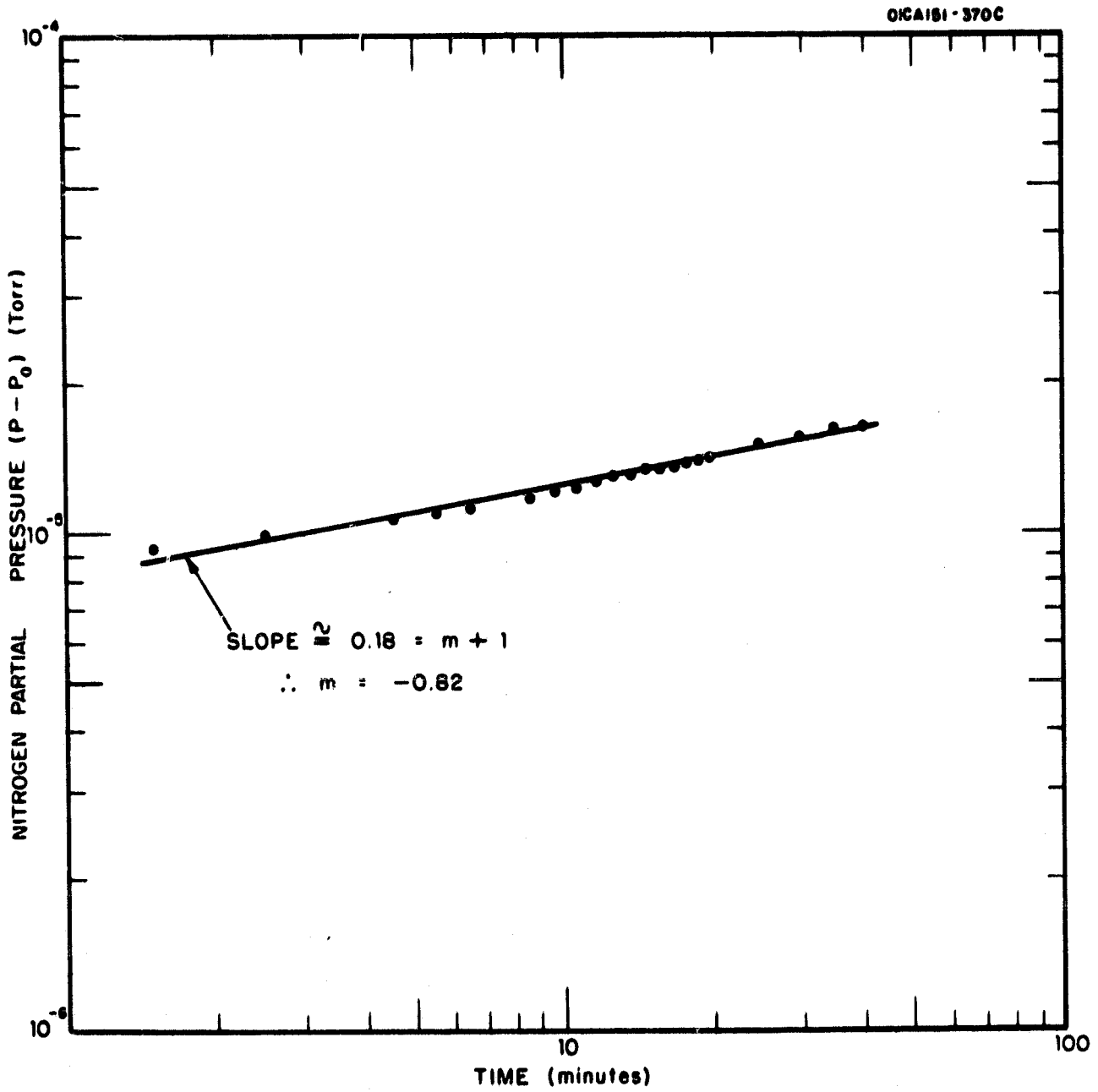

Figure 45. Pressure increase due to re-emission of nitrogen gas from an unbaked but well-pumped GCA model R-5 cold cathode gauge after 10-1/2 minutes of pumping, starting at a pressure of 7.20×10^{-6} torr.

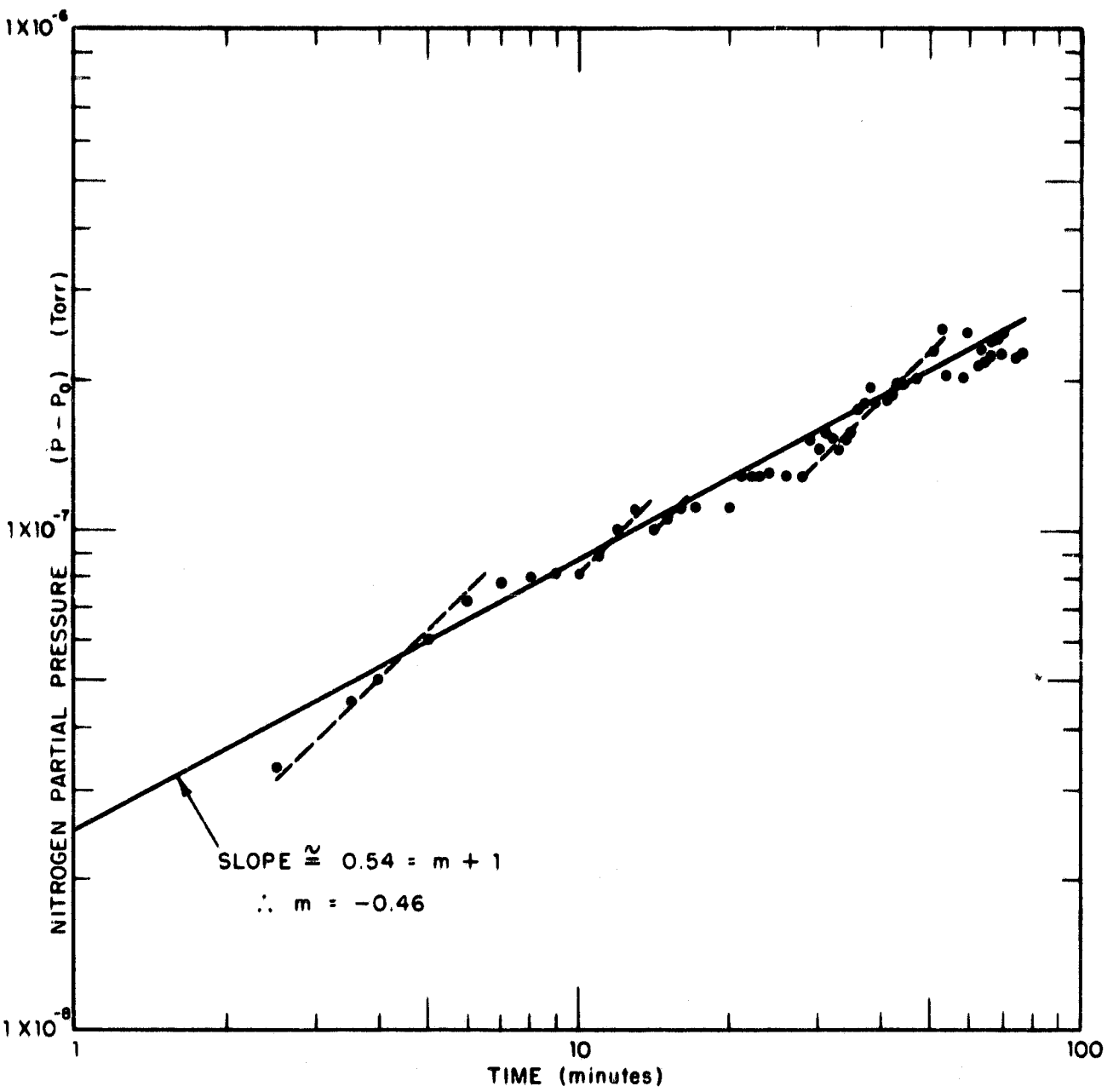

Figure 46. Pressure increase due to re-emission of nitrogen gas from a well-baked GCA model R-5 cold cathode gauge after 5-1/2 minutes of pumping, starting at a pressure of 5.1 x 10^{-6} torr.

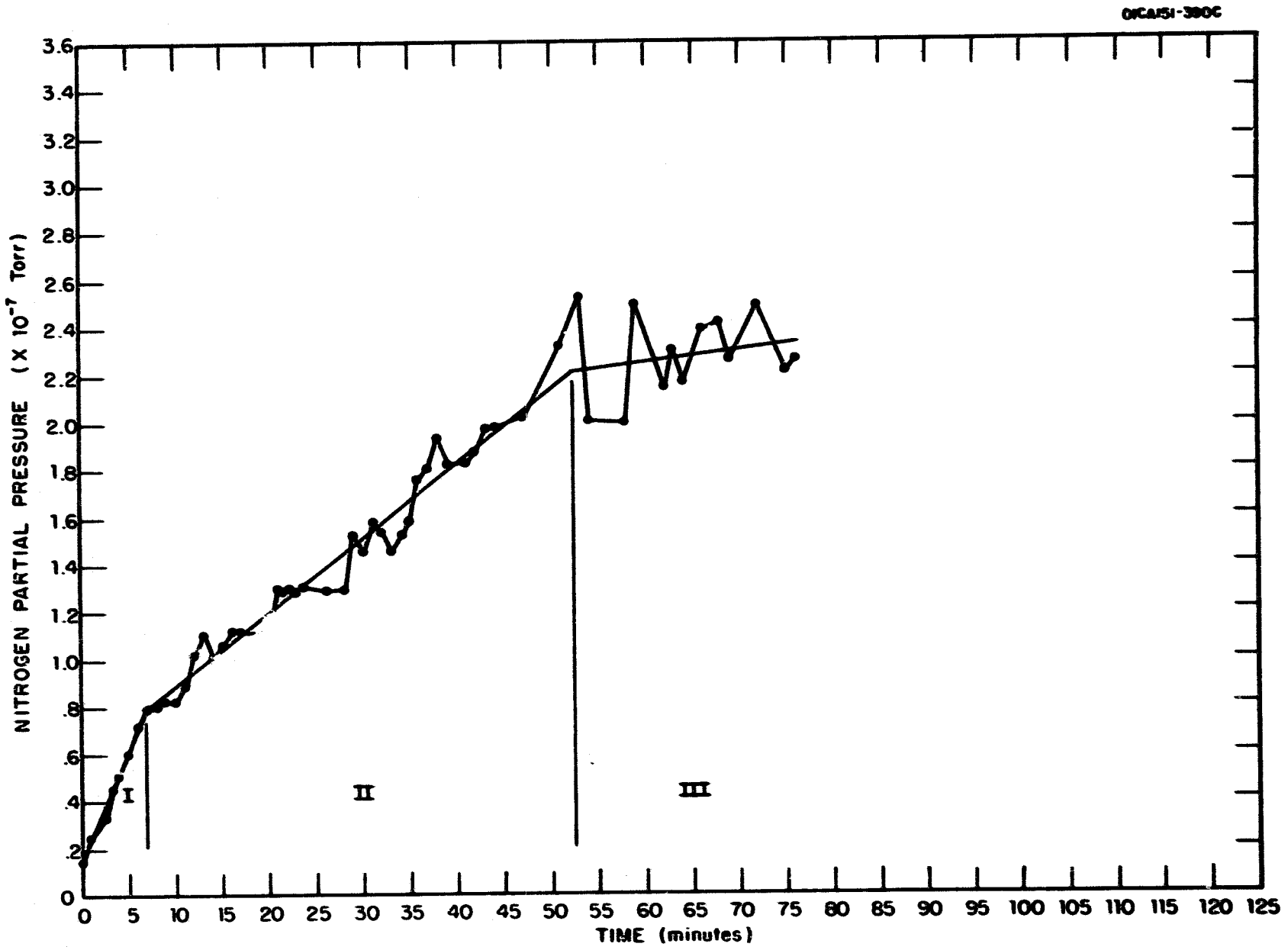

Figure 47. Linear plot of pressure increase due to re-emission of nitrogen gas from a well-baked GCA model R-5 cold cathode gauge after 5-1/2 minutes of pumping, starting at a pressure of 5.1×10^{-6} torr.

Taking the logarithm of both members of Equation (23), one obtains:

$$\log(p-p_o) = \log(R_o/V) - \log(n+1) + (n+1)\log t \qquad (24)$$

Thus, for a logarithmic plot, the slope of the $\log(p-p_o)$ versus log t curve represents the quantity (n+1) from which the value of the exponent n may be determined. The value of the exponent n is a function of the type of re-emission.

Returning now to the description of the results of the re-emission experiments, it should be pointed out that the data contained in the graphs of Figures 44 through 47 show not only the re-emission rate R(t) but also the total amount of gas that has been re-emitted during the period. For example, for the 17 minutes re-emission period that was recorded following the R-5 gauge pump-down of the first experiment, a total of 1.37×10^{-5} torr liters of nitrogen gas was re-emitted. If this quantity of gas is compared with the total nitrogen gas pumped by the R-5 gauge during the 13-minute pump-down period, a quantity of 5.87×10^{-6} torr liters, it becomes evident that more nitrogen was re-emitted than was pumped. The source of the additional nitrogen gas may have been the G.E. partial pressure analyzer, since the PPA was on during the initial admission of nitrogen gas to the test chamber. The source of additional nitrogen may also have been general outgassing from the cold cathode gauge and the walls of the closed volume. Whatever the source, the characteristic of the average re-emission for the short period of 17 minutes was that of a constant outgassing.

The re-emission results that were obtained for the second experiment are displayed in Figure 45. Here one can see that the re-emission of gas decreased with time according to the -0.82 power of the time. Such a rate is quite close to the 1/t dependence that is expected for ions that are distributed in a solid as a reciprocal function of the depth [11]. However, the circumstances under which the experiment was performed raise a serious question about the validity of the result. It will be remembered that during the second experiment, the PPA was turned on near the end of the pump-down phase. Turning on the PPA released enough gas into the closed volume to triple the pressure there. There is a good possibility that when the R-5 gauge was turned off the its re-emission started, the PPA could have been either strongly outgassing or even strongly pumping. The total amount of nitrogen gas re-emitted was measured to be 8.0×10^{-6} torr liters as compared with 3.46×10^{-6} torr liters of nitrogen that was pumped by the R-5 gauge. In this case, it is strongly suspected that the additional gas came principally from the PPA. As in the first experiment the re-emission cannot be said to be characteristic of the cold cathode gauge. The re-emission coefficient R_o was calculated to be 3.56×10^{-7} torr liters/$(\text{sec})^{n+1}$ for this experiment.

The re-emission results for the well-baked gauge that were obtained from the third experiment are displayed in Figures 46 and 47. Figure 46 shows that the re-emission in this case followed a $t^{-0.46}$ law, a value quite close to the

$t^{-1/2}$ law that is expected for ions that are uniformly distributed within a solid and for which the rate determining factor is the diffusion of these ions (or atoms) through the solid to the surface [12,13].

A closer look at the graph of Figure 46, however, reveals that the inverse square root time dependence appears to be an average of primarily two kinds of re-emission. The first kind of re-emission is re-emission at a constant rate. The short dashed line segments that joint data points on the graph and have a slope of unity belong to this category. The second kind of re-emission appears to be t^{-1} re-emission for which the data points on the graph form practically horizontal line segments. The two kinds of re-emission appear to alternate in time, as though there is first a diffusion of ions whose distribution varies inversely with depth (t^{-1} dependence), followed by a desorption at a constant re-emission rate. It appears to be most likely that what is really happening is that there is a continuous, low level constant diffusion of ions with a t^{-1} dependence upon which there is superposed bursts of constant re-emission.

A second way of presenting the re-emission data that was obtained in the third experiment is to plot the nitrogen partial pressure as a function of time on linear graph paper. This has been done in Figure 47. The data, as plotted in this fashion appears to consist of three regions of constant re-emission. The first region, extending in time from 0 to 7 minutes, is one of genuine constant re-emission. The second region, from 7 to 52 minutes, appears to be one in which there is an average constant re-emission but there are many fluctuations of re-emission about the average. In the third region, from 52 to 76 minutes, the average constant re-emission is not well defined because of very large fluctuations in the pressure. The "constant" re-emissions that can be calculated from Figure 47 are (a) 7.75×10^{-10} torr ℓ/sec in region I, (b) 2.61×10^{-11} torr ℓ/sec in region II, and (c) 4.53×10^{-12} torr ℓ/sec in region III. From the data of Figure 46 (the value of $n + 1 = 0.54$) one can compute the re-emission coefficient R_o for the entire re-emission period. The value of R_o is calculated to be 7.51×10^{-10} torr liters/$(\text{sec})^{n+1}$, a value which approximates the initial re-emission rate of region I since it is the actual re-emission for $t^n=1$, that is, for 1 second after re-emission has started.

The results obtained in the third experiment are believed to be an accurate measurement of the GCA model R-5 cold cathode gauge re-emission. The partial pressure analyzer was turned on and kept on during both the pump-down and the re-emission phases. There was no evidence that the PPA was either strongly outgassing or strongly pumping during either the pump-down phase or the re-emission phase. When the re-emission data was "corrected" for possible pumping by the PPA during this period, the result was an ever-increasing re-emission rate with time, an impossible situation. It is most likely that the PPA did some pumping during the pump-down phase, but since its measured pumping speed was 1.37×10^{-3} liters/sec for nitrogen compared with the R-5 gauge pumping speed of 3.08×10^{-2} liters/sec (for pumping phase I), it could not have pumped more than 5 percent of the total gas pumped. Thus, its re-emission must have been small also when compared with the R-5 gauge re-emission. It is worth noting that of the 2.54×10^{-6} torr liters of nitrogen that was pumped during the third experiment, only

1.10×10^{-7} torr liters was re-emitted in the 76-minute recovery period that was monitored. The re-emitted or recovered gas constituted 4.3 percent of the total that was pumped.

In summing up the re-emission work, it can be said that a technique for accurately measuring gauge re-emission was developed and applied to the measurement of the re-emission of nitrogen from a well-baked, all metal cold cathode ionization gauge. Earlier experiments showed how erroneous re-emission results could be obtained because of poor technique. The results obtained for the R-5 cold cathode ionization gauge indicated that re-emission in this case consisted of a superposition of constant re-emission and t^{-1} re-emission which together yielded a resultant $t^{-0.46}$ time dependency. Future experiments in this area should include work with gases such as argon and helium to see to what extent adsorption is responsible for the unique re-emission results obtained for nitrogen.

Calculations of the Model R-5 Gauge Equilibrium Pressure. As a simple exercise in applying some of the information that has been gained in the measurements of pumping speeds and re-emission rates, one can calculate the effective re-emission at the end of the gauge pumping period in the third experiment. The gauge pressure had decreased to a value of 8×10^{-9} torr and probably would have decreased further, but assume that this pressure was an equilibrium pressure between gauge pumping and gauge re-emission. From Table III, the pumping speed of the R-5 gauge for this last pumping phase was 4.85×10^{-4} liters/sec. At an equilibrium pressure P torr, the amount of gas removed by pumping at a constant speed S liters/sec must just be equal to the generation of gas within the system. If it is assumed that the gas entering the system is primarily that due to re-emission from the gauge, then the following equation holds:

$$R = PS \tag{25}$$

Using the values of P and S listed above, it is found that $R = 3.88 \times 10^{-12}$ torr liters/sec. This value compares favorably with the measured re-emission of region III of Figure 47, a value of 4.53×10^{-12} torr liters/sec. It is evident that the re-emission rate will depend on the amount of gas that has been pumped with a gauge (or ion pump). A knowledge of gauge and pump pumping speeds and re-emission rates will yield information about the lowest equilibrium pressures that can be achieved under various conditions.

VI. COLD CATHODE GAUGE RESPONSE TO CYCLING GAS PRESSURE

Methods of Obtaining Varying Pressures

Variation in Test Chamber Volume. As shown in Figure 48, one obvious method of changing the pressure in a test chamber is to change the physical volume of the chamber. This may be most easily done by using either a cylinder-piston or flexible bellows variable volume device. As the chamber volume is increased from its nominal value of V_1 liters to its maximum value of $V_1 + V_2$ liters, where V_2 is the added variable volume, the chamber pressure will decrease according to Boyle's Law. If there is a continuous flow of gas into the chamber through the conductance C and there is a continual removal of gas at a constant pumping speed, S, then pressure variations within the chamber will follow Boyle's Law (in the absence of absorption-desorption phenomena) only if the gas flow time constant V_1/C and the pumping time constant V_1/S are much greater than the bellows' oscillation period T. In other words, the volume of the test chamber must be varied at a rate that is faster than the rates at which gas can enter and leave the chamber. Accordingly, this method is ideally suited to the creation of high frequency pressure oscillation, provided that a suitable bellows or other volume changing device is available. The percent modulation of the base pressure will be determined by the ratio of the volumes V_1 and V_2.

The pressure variation system sketched in Figure 48 is very flexible in that the base pressure can be varied by varying either the gas flow into the chamber or the effective pumping speed S. Further, the pressure in the test chamber will be independent of the pumping speed of the gauges under test as long as the pumping speed S is much larger than the combined pumping speed of the gauges. The minimum value of S, say about 1 liter/sec, coupled with the maximum practical value of V_1, say about 1 liter, yields a maximum pumping time constant of 1 second. Such a chamber would be suitable for creating pressure oscillations of about 10 cps and higher.

One way to remove the frequency limitations of the pumping and gas flow requirements would be to use a closed test chamber. Practically speaking, this could only be done if the gauge pumping action is negligible. It is unlikely that a closed system would work well below pressures of 10^{-5} or 10^{-6} torr because of system outgassing and the generation of gas due to the motion of the variable volume elements. This kind of arrangement, however, could be used to create low frequency pressure variations as well as high frequency variations.

Variation of Test Chamber Pumping Speed. Referring to the sketch of Figure 49, it can be seen that the modulation of the effective pumping speed of a chamber (by a butterfly-type valve, for example), should vary the pressure within the chamber. Under steady-state conditions, an equilibrium pressure develops within the chamber such that the gas flowing into the chamber

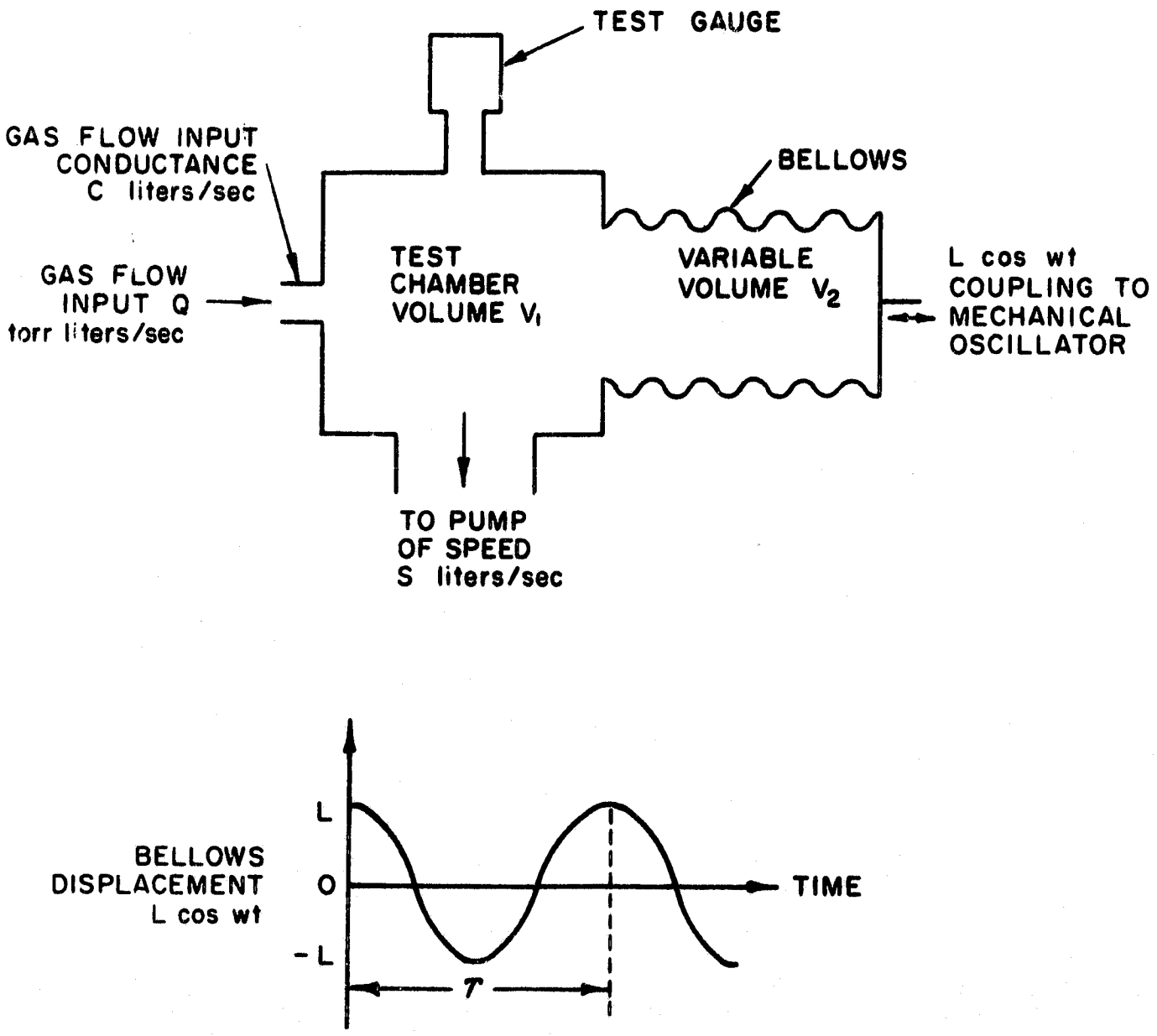

Figure 48. Volume variation method of changing the pressure in a test chamber.

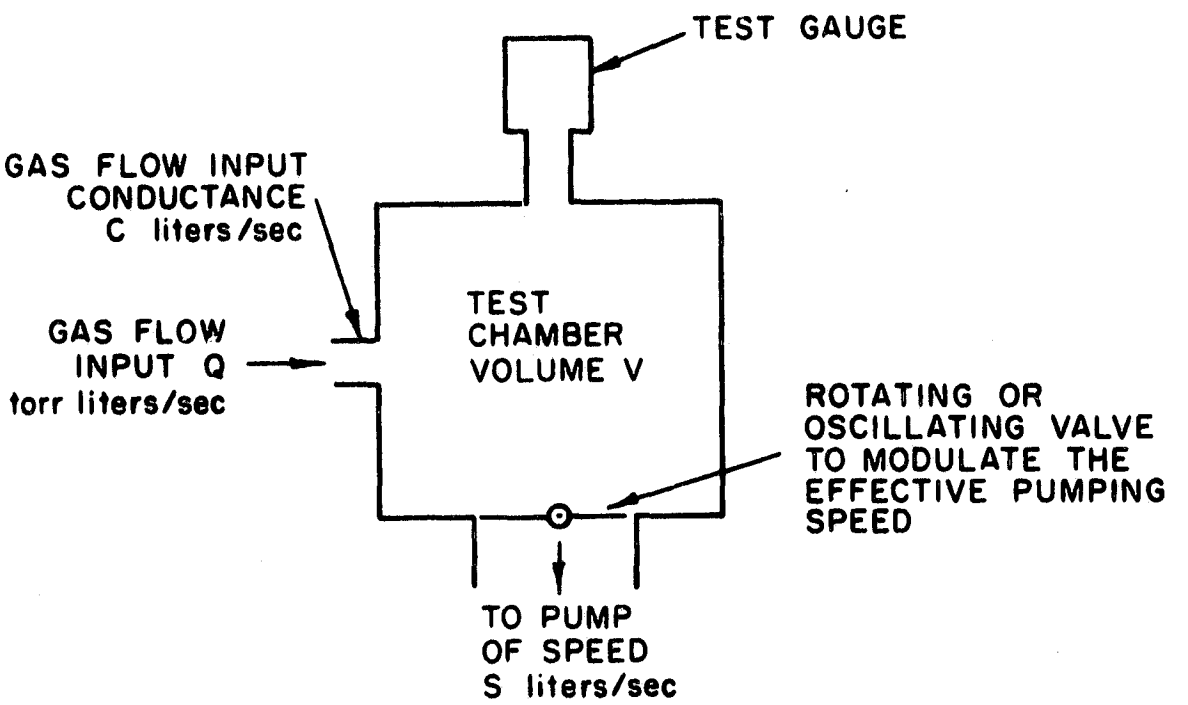

Figure 49. Variable pumping speed method of changing the pressure in a test chamber.

per unit time just equals the gas removed per unit time. If the pumping speed were suddenly decreased, the pressure in the chamber would start to increase, but the rate of increase would be regulated by the volume of the chamber and the conductance C through which the gas flows in. Thus, very rapid or high frequency oscillations of pressure in this kind of system are possible only if the conductance C is large. A large conductance implies a large gas flow into the pump, and it would either be necessary to have a large reservoir of gas at a low pressure to maintain the flow or else have a differential gas introduction system having short flow time constants throughout.

Variation of Gas Flow into a Test Chamber. The pressure in a test chamber of fixed volume and having a constant pumping speed may be varied by modulating the gas flow into the chamber. An arrangement for modulating gas flow is shown in Figure 50. As the amount of gas admitted from an external chamber (chamber no. 1 in the figure) into the test chamber is varied, the pressure in the test chamber will also vary, provided the time constants of the system are short enough. The values of the time constants V/S, V/C and V_1/S_1 must be small compared to the period of rotation or oscillation of the modulating value. In addition, the maximum value of the valve conductance C should be small compared with the value of C_1 so that the pressure in the external chamber will not change appreciably as the conductance C varies. Under these conditions, there will be a heavy gas flow into the pump of speed S_1 and only a small gas flow into the test chamber. It would seem that this method is useful primarily for low modulating frequencies.

Interruption of a Gas Beam. Another method of varying the pressure within a given region is illustrated in Figure 51. In this method, the pressure is varied within a region that encloses the gauge to be tested. A rotating or oscillating valve is used to interrupt a beam of gas than can flow directly into the test gauge enclosure. The test chamber is connected to a pump having a high pumping speed S such that there is a large pressure gradient between the front and rear surfaces of the test gauge enclosure. When the modulating valve is closed, gas at a low pressure P_2 can enter the enclosure through the rear venting apertures. When the valve is open, gas at a higher pressure P_1 can enter the enclosure from the front. The time constant of the enclosure volume V and the venting apertures of conductance C_V must be small. As can be seen, the technique here is to create a pressure gradient so that gas at different pressures, and even directly beamed molecules can alternately enter a region in which the test gauge is located. This method is closely related to the two chamber-cycling valve method to be described shortly. It is also related to the rotating orifice method described in the next section.

Variable Interception of Gas Beam by Rotating Gauge Orifice. If a beam of gas molecules is created by collimation in a cryogenic chamber, the orifice of a test gauge may be rotated or oscillated so that the subtended area of the beam varies. In this way, the number of gas molecules entering

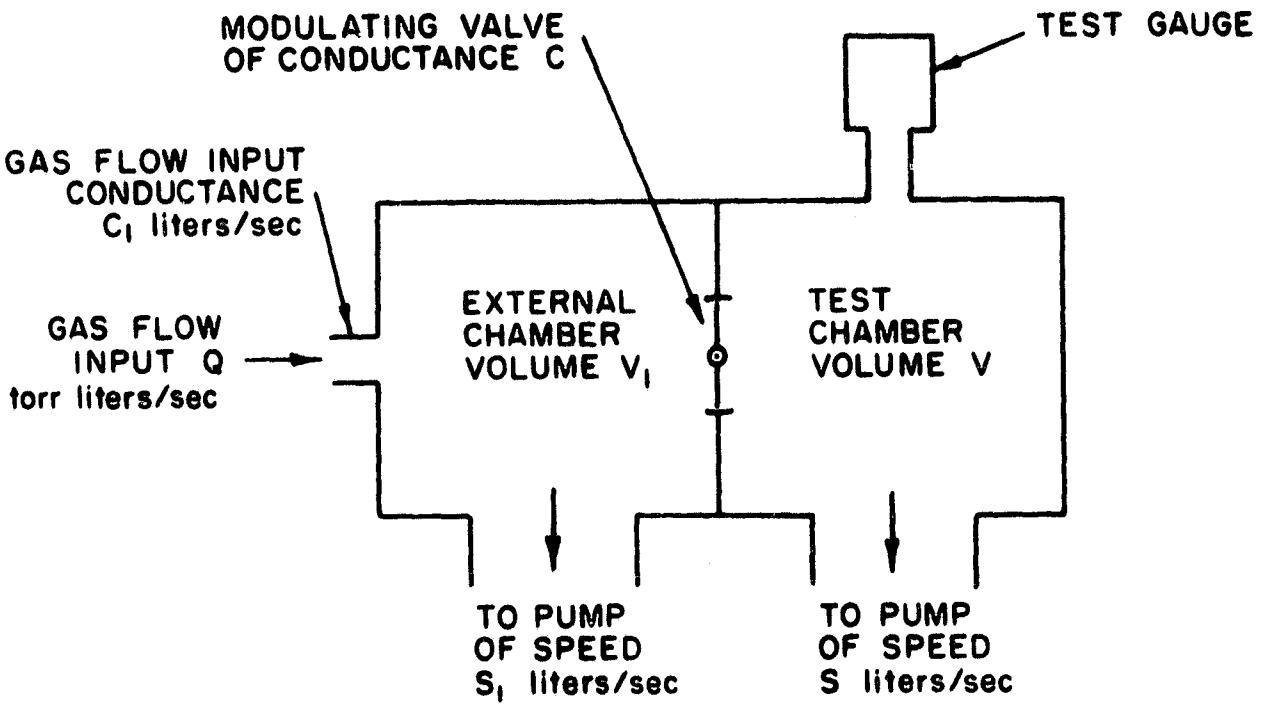

Figure 50. Variable gas flow method of changing the pressure in a test chamber.

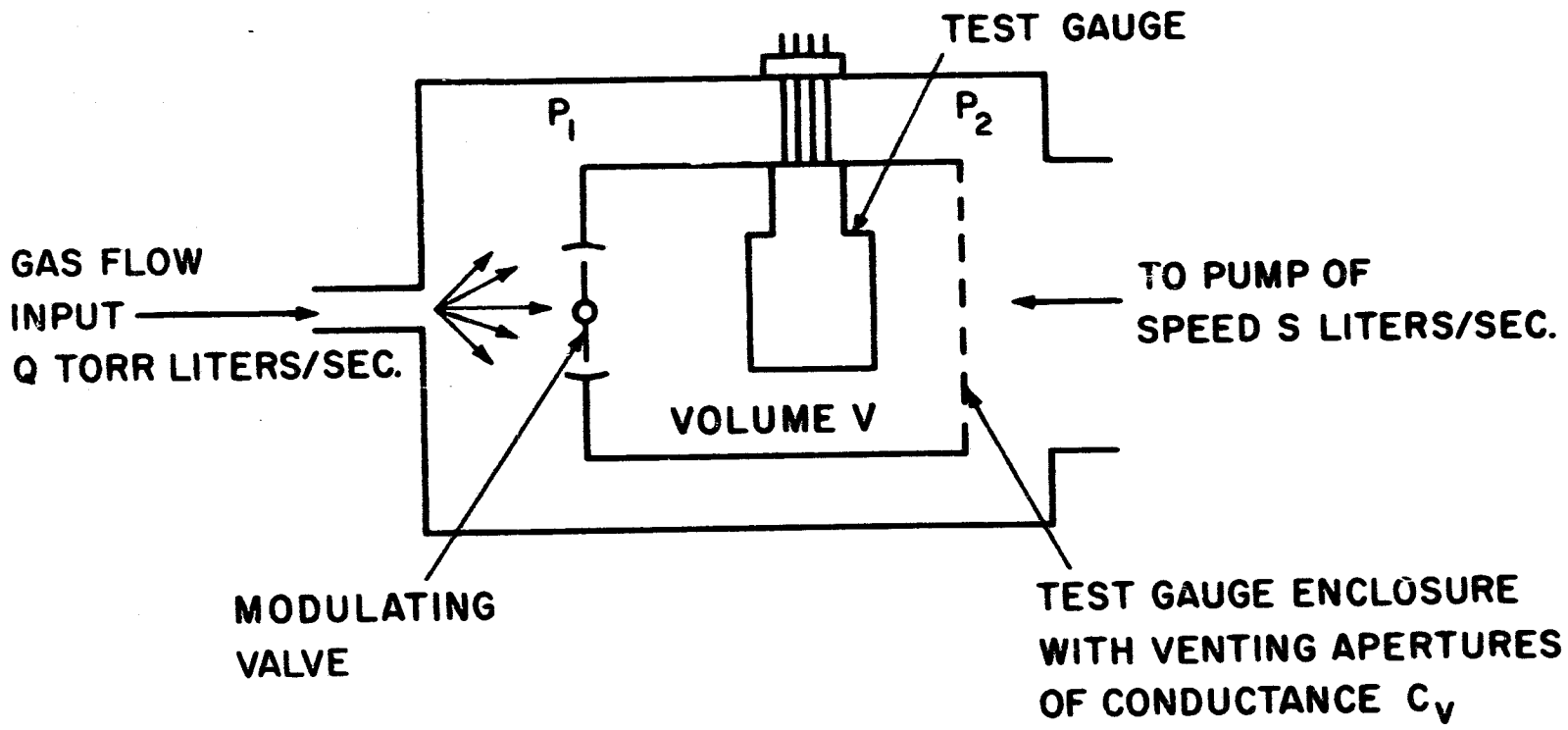

Figure 51. Interrupted beam method of varying the pressure within a gauge enclosure.

the gauge per unit time will vary and consequently, the pressure within the gauge will vary. If the gauge orifice is surrounded by pumping walls at a low temperature, the number of molecules that can enter the gauge when the orifice faces away from the direct beam will be small. The modulation frequency of the pressure in the gauge can be varied over a wide range with an arrangement of this sort. The high frequencies will eventually be limited by the conductance of the gauge orifice and the tabulation to the gauge. The pressure levels attained in the gauge can be changed by adjusting the strength of the gas beam. A system of this type would begin to approximate the manner in which molecules enter a gauge that is mounted on a spinning satellite. The detailed design and construction of such a system will undoubtedly involve a number of technical difficulties.

Two Chamber-Cycling Valve Method. A very flexible and general method of changing the pressure within a test gauge is to alternately connect the gauge to two chambers that are maintained at different pressures. The two chamber method is illustrated schematically in Figure 53. The basic idea of this method is to use either a rotating or oscillating valve mechanism (or even two separate valves) to connect the test gauge alternately to two chambers at different pressures. Rotating and/or oscillating valves are constructed so that there is no metal-to-metal contact between the components (rotor and housing) that define the degree of valve opening. The valve operates by providing a relatively large conductance (say 20 or 30 liters/sec) in the "open" position and a relatively small conductance (of the order of 10^{-3} liters/sec) in the closed position. The "closed" or leakage conductance of the valve is kept small enough so that a relatively large pressure difference can be maintained between the high and the low pressure chambers. The amount of gas that the valve transfers from the high pressure to the low pressure chamber per unit time is simply the product of the valve and test gauge volume V and the valve cycling frequency f. For example, if the volume V is 0.1 liter and the valve rotates at a frequency of 1 cycle per second, it will transfer 0.1 liter x 1/sec or 0.1 liter/sec of high pressure gas to the low pressure chamber. Another way of stating this is to say that the "effective operating conductance" C_E of the valve when operating at 1 cps is 0.1 liter/sec.

The maximum ratio of high pressure to low pressure that can be maintained in the two chambers depends on the "effective operating conductance" of the valve as defined above. Consider, for example, the flow of gas from the high pressure chamber to the cycling valve, to the low pressure chamber and then to the pump of the low pressure chamber. Equating the gas flow through the valve to the gas pumped out of the low pressure chamber (assuming that the external gas flow input Q to the low pressure chamber is zero), one obtains

$$\frac{P_1}{P_2} = 1 + \frac{S_2}{C_E} \tag{26}$$

the ratio of the high pressure P_1 to the low pressure P_2 may be 1000 or greater if the pumping speed S_2 of the low pressure chamber is large compared

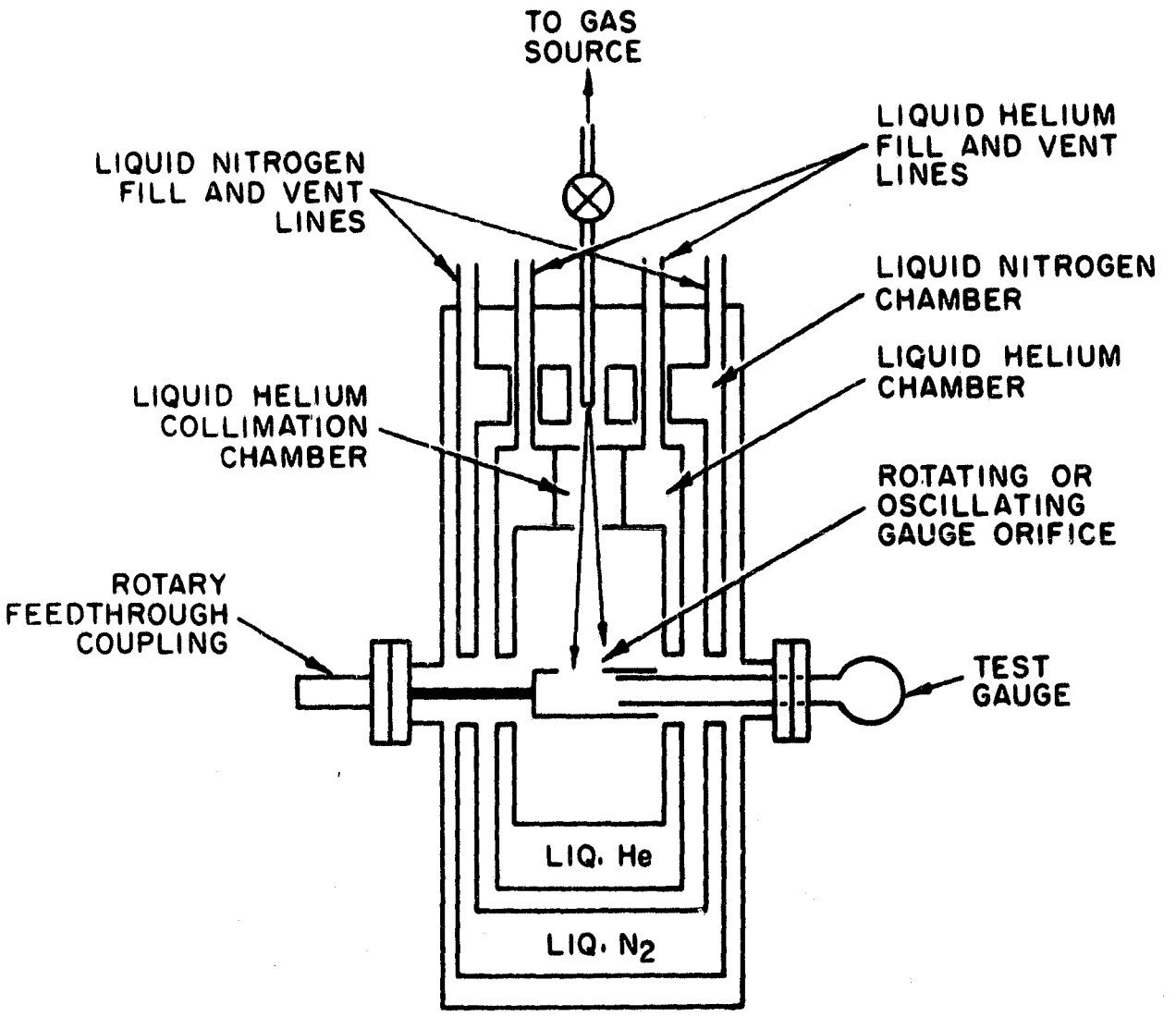

Figure 52. Variable interception of a gas beam by a rotating gauge orifice.

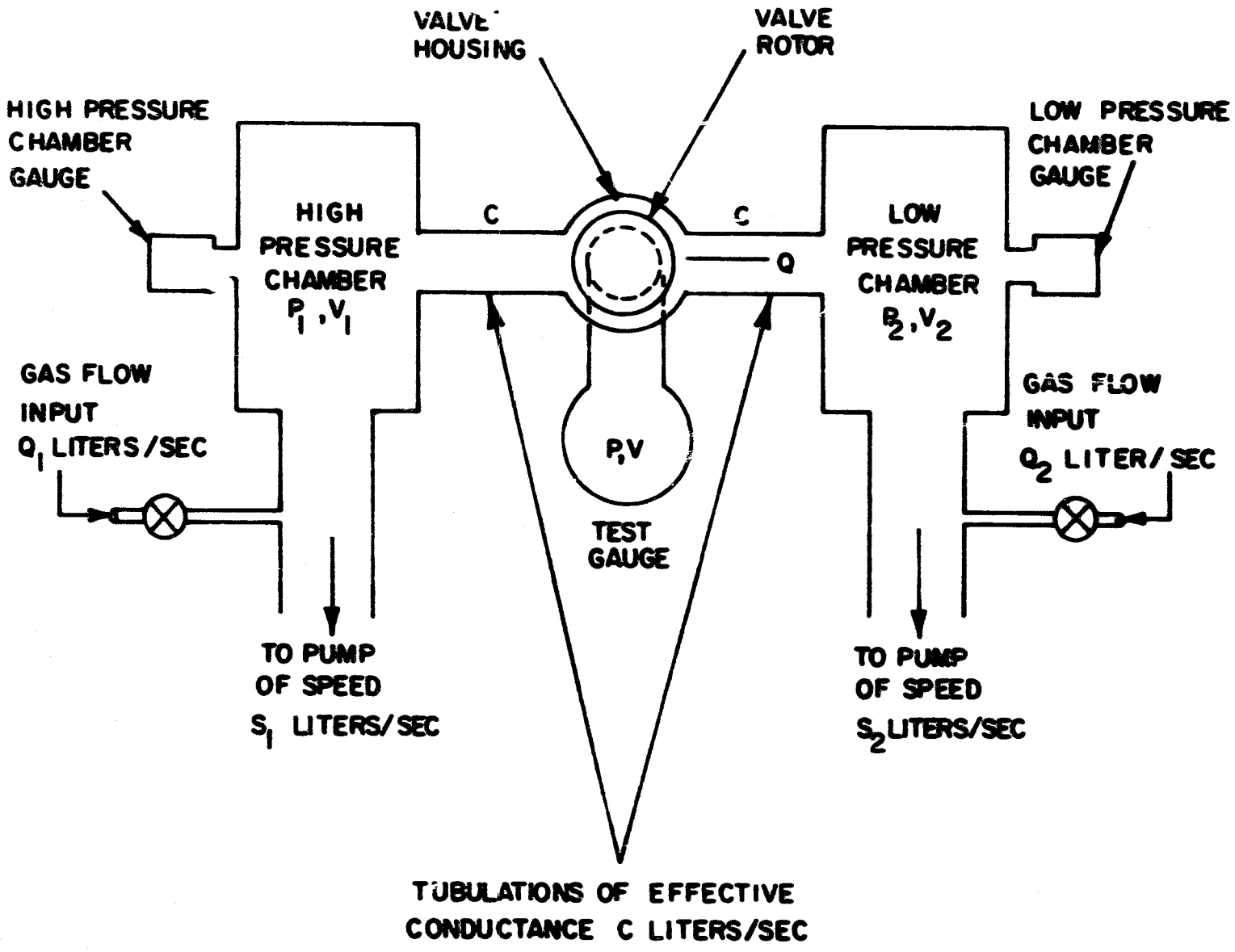

Figure 53. Variation of the pressure within a test gauge by alternate connections to separate pressure chambers.

to the effective operating conductance C_E of the valve. When the valve is in the closed position, the effective conductance C_E becomes the valve leakage conductance, which is much less than the effective operating conductance.

The operating time constant of the two chamber-cycling valve system may be derived in the following manner: Consider the situation that exists when the cycling valve and test gauge have been filled with a sample of high pressure gas at a pressure P_1 and the valve begins to discharge this high pressure gas into the low pressure chamber which is at a pressure P_2. The low pressure chamber then has gas flowing into it from two sources: a flow Q from the valve and test gauge and a gas flow input Q_2 from an external source. The pressure P_2 in the low pressure chamber will then be

$$P_2 = (Q + Q_2)/S_2 \tag{27}$$

The gas flow Q may be expressed in terms of the valve tubulation conductance C (see Figure 53) and the pressure difference $P - P_2$ across this conductance. If the gas flow Q is also equated to the change in the quantity of high pressure gas within the valve and test gauge, one has

$$Q = C(P - P_2) = -V \frac{dP}{dt} \tag{28}$$

the pressure P is the time varying pressure within the valve and test gauge and the volume V is the volume of the valve and test gauge. From the two equations above, one derives the equation

$$\frac{dP}{dt} + \frac{CS_2}{V(C + S_2)} P = \frac{CQ_2}{S_2} \tag{29}$$

The conductance C is really a function of time since it involves the changing aperture conductance of the valve. However, as a first approximation, assume that C has a constant average value during the valving cycle. The above equation then becomes a first order, linear differential equation with constant coefficients. If one imposes the initial condition that at time $t = 0$, $P = P_1$ the solution becomes:

$$P = \frac{Q_2V\ (C + S_2)}{S_2^2} + P_1 - \frac{Q_2V\ (C + S_2)}{S_2^2}\ e^{-\frac{CS_2}{V(C + S_2)}\ t} \tag{30}$$

The time constant for this exponential solution is:

$$\tau = \frac{V\ (C + S_2)}{CS_2} \tag{31}$$

Since ordinarily S_2 is much greater than C, one can write

$$\tau \simeq \frac{V}{C} \qquad S_2 \gg C \tag{32}$$

By making the valve orifice and valve tubulations sufficiently large and the valve and gauge volume small, the time constant can be made small. For example, if the average conductance C is 10 liters/sec and the volume V is 0.1 liter, then $\tau = 0.01$ seconds.

The two chamber-cycling valve method of changing the pressure in a test gauge has great potential usefulness because the pressure modulation amplitude and the modulation frequency can be varied over a wide range.

Design of Special Equipment

A Butterfly Valve for Pressure Cycling Experiments. As illustrated in Figure 54, a butterfly type valve was constructed to mount on the copper gasket that is used with a Varion 6-inch O.D. Conflat flange. Such a flange separates the liquid helium cryopump from the test chamber of the cryopump-ion pump test system. A similar flange was used to separate the test chamber of the metal mercury diffusion pump system from its pumping components (this system will be described in the next chapter). Thus, the butterfly valve was constructed to be used with either of these ultra high vacuum systems.

The butterfly test valve used gold plated ball bearings to support the shafts of the rotating central circular vane. These bearings were manufactured specifically for vacuum use, but as will be pointed out later, they had several shortcomings. The valve assembly was fabricated primarily of non-magnetic 304 stainless steel. The central circular flat vane of the valve was fastened to cylindrical shafts which, in turn, were mounted to the inner races of the ball bearings. The outer races of the ball bearings were supported and held fixed in position by bearing retainer blocks. Nickel cylinders (drive rotors) were pinned to the ends of the vane shafts. An external permanent magnet was used to couple magnetically to one of the nickel drive rotors as shown in Figure 54. A small variable speed motor was used to rotate the permanent magnet, and the rotational motion of the magnet was thus transferred to the circular vane of the valve. The clearance between the circular vane and the surrounding cylindrical housing was 0.003 inch so that any axial movement of the vane by this amount could cause the vane to bind or rub on the housing. The assembly of the valve had to be performed carefully to center the moveable vane and maintain the proper clearances between the vane shafts and the valve housing.

The butterfly valve was mounted within the test system as shown in the illustration. A mirror was mounted within the test chamber at an angle of approximately 45 degrees to the horizontal. A glass window that was mounted on one of the side tubulations of the test chamber permitted the operation

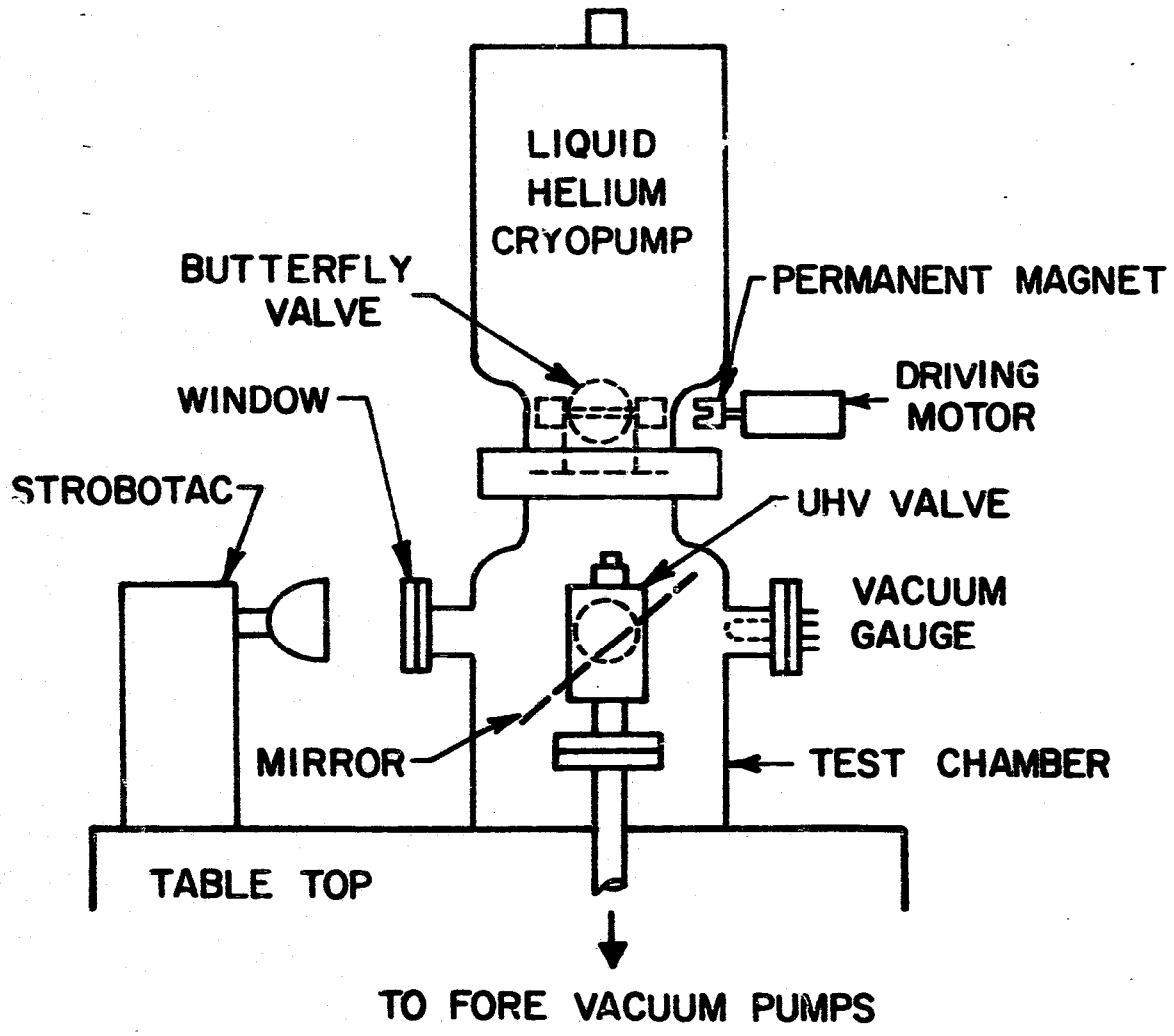

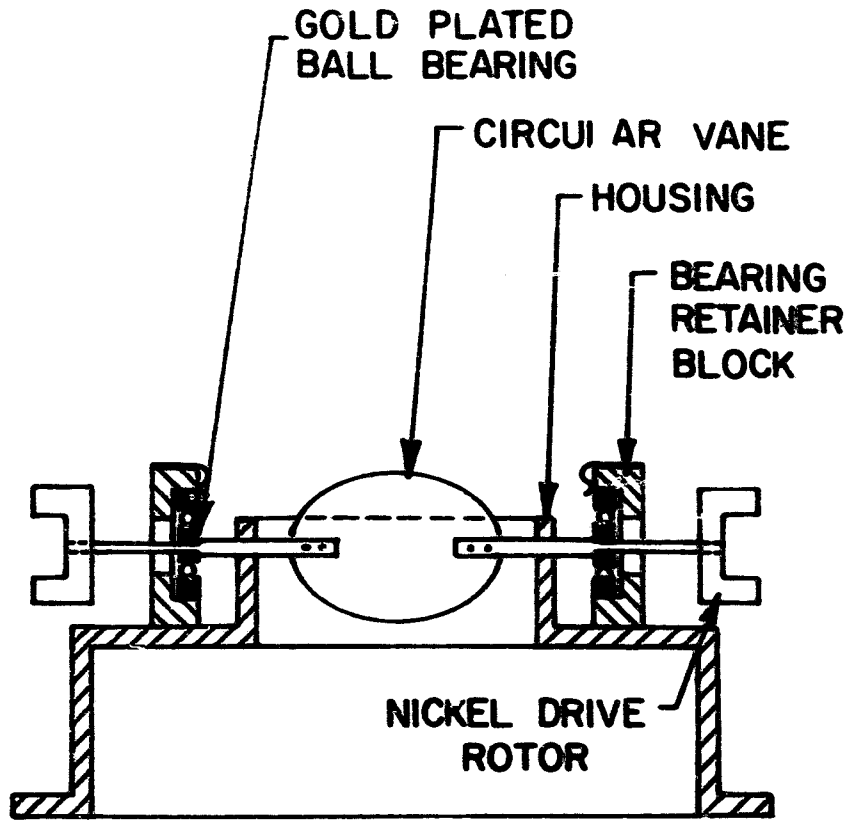

Figure 54. Schematic drawing of butterfly valve and its installation within the cryopump-ion pump test system.

of the valve to be observed. A General Radio Company Strobatac was used to measure the rotational speed of the valve. Pressures within the test chamber were measured with a Varian nude UHV-14 ionization gauge. Gas could be admitted to the test chamber via the UHV valve that connected the test chamber to the forevacuum portion of the test system.

A Rotary Cycling Valve For Use With a Two-Chamber Test System. Like the butterfly type valve, the rotary valve was designed to make use of gold plated ball bearings. Only ultra high vacuum materials could be used in its construction since it had to be bakeable at high temperatures and handle gases at very low pressures. The valve was designed so that there would be no metal-to-metal contact thus eliminating the possibility of cold welding and the spurious generation of gas due to surface abrasion. The "closure" of the valve would consist of the creation of a high resistance flow path.

As shown in Figure 55, the rotary valve consisted of a one-piece stainless steel cylindrical body with diametrically opposed inlet tubulations. A thin wall cylindrical rotor was mounted between two gold plated miniature precision ball bearings. The thin film of gold plating on these bearings serves as a lubricant in vacuum operation. The radial clearance between the rotor and the valve body was kept small to obtain a maximum open-to-closed vacuum conductance ratio. The design target for radial clearance was two mils. Mounted to the top of the valve rotor was the drive rotor, which, when acted upon by the field assembly, imparted the torque necessary to drive the valve rotor at the proper cycling speed. The lower end of the valve rotor and the lower ball bearing mount were perforated to allow the gas within the valve to reach the test gauge. The test gauge would be mounted to the valve assembly by a demountable flanged joint. A proximity pick-up (magnetic reed switch, for example) could be used to indicate the rotor position for inlet port identification and synchronization purposes.

The advantages of a rotary valve over that of other possible designs are its simplicity, small physical size and high conductance ratio. Its chief disadvantage is the presence of ball bearings within the vacuum. It has been learned from experience that these bearings are not completely reliable. They do have a tendency to seize-up and they can generate gas.

One type of two-chamber test system that could be used with the rotary valve is illustrated in Figure 56. This test system provides two identical test chambers, each chamber being pumped by separate ion pumps and titanium sublimation pumps or their equivalent. Nude ionization gauges of the Bayard-Alpert variety measure the pressure in each test chamber. A variable leak valve connected to each test chamber permits the pressure of each chamber to be adjusted independent of the pressure in the adjacent chamber. As shown, the two chambers can be connected together by means of an ultra high vacuum valve. Connection of the two chambers will make it possible to equalize the pressures in the chambers when this is required to obtain a zero pressure differential at the input of the rotary valve. It will also permit the readings of the test chamber nude ionization gauges to be compared. A high temperature bakeout oven can be used to bake the test chambers, the rotary valve and the test gauge. It is recommended that 1-liter bottles of pure gas

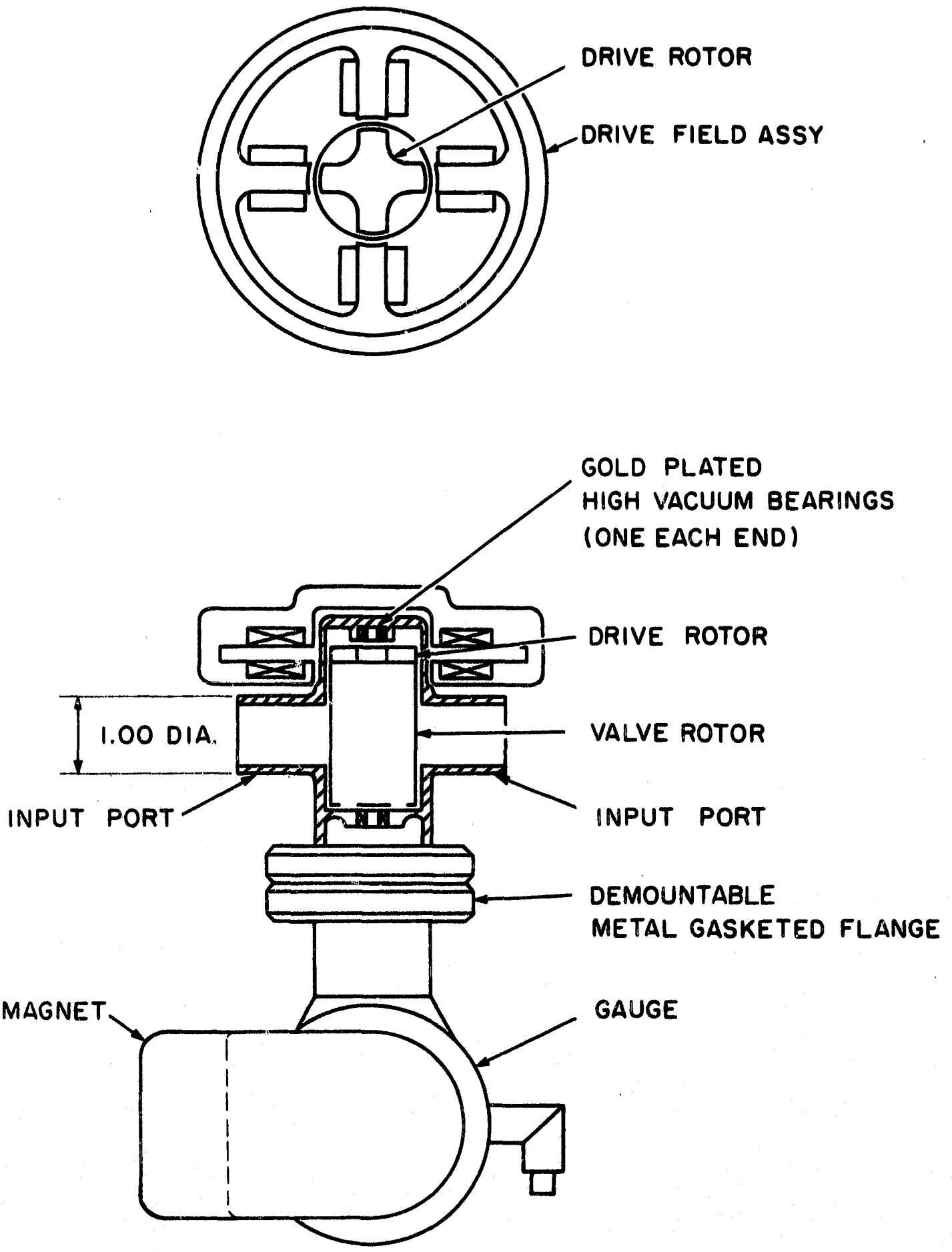

Figure 55. Rotary cycling valve and gauge assembly.

be connected to the variable leak valves to establish the desired working pressures in the test chambers. The use of zeolite type sorption pumps to pump down from atmospheric pressure to about 10^{-3} torr, at which point the ion pumps can be operated, will keep the system oil free.

Pressure Cycling Experiments

Modulation of Carbon Dioxide Pumping By A Cryopump. The butterfly valve described in the previous section was installed in the cryopump-ion pump test system as shown in Figure 54, for the purpose of varying the pressure in the test chamber by varying the test chamber pumping speed (method A 2 described earlier). The test system had previously been pumped for several days with the forevacuum ion pump with liquid nitrogen present in the cryopump. The background pressure in the test chamber was 6.6×10^{-8} torr as measured with the nude Varian gauge.

A flow of carbon dioxide gas into the test chamber from a small tank was initiated until a pressure in the low 10^{-5} torr region was established there. The butterfly valve was then opened and closed and the resulting test chamber pressures were observed. It was found that the test chamber pressures changed slowly after the valve position was changed. For example, it took 3 or 4 seconds for the chamber to reach a new lower equilibrium pressure after the valve had been opened suddenly. It took 6 or 8 seconds for the pressure to rise to its new equilibrium value when the valve was suddenly closed.

It was observed that the pressure in the test chamber changed from a value of 1.4×10^{-5} torr with the valve open to a pressure of 2.0×10^{-5} torr with the valve closed. The pressure in the forevacuum portion of the system was 3.0×10^{-5} torr, which set an upper limit on the pressure increase in the test chamber.

The calculated "open" conductance of the butterfly valve was 298 liters/sec for air at 20°C while its calculated "closed" conductance was 2.65 liters/sec for air at 20°C. The time constant of 3 to 4 seconds for the pressure decrease and the less than two to one pressure drop in the test chamber lead to the conclusion that the effective pumping speed of the liquid nitrogen cooled cryopump for carbon dioxide was quite low, in fact its speed would be only 1.15 liters/sec if the above-mentioned valve conductances were correct for carbon dioxide. The time constant of 6 or 8 seconds for the pressure rise indicates that this system was not suitable for the measurement of rapid pressure variations even if the pumping speed of the cryopump were to be increased--say by using liquid helium instead of liquid nitrogen in the cryopump.

Cold Cathode Gauge Response to Cycling Gas Pressures. Since a two-chamber test system was available in our laboratory, it was possible to make several tests of the response of a GCA model R-5 gauge to a sinusoidally-varying pressure of pure nitrogen gas. The test system was substantially of the type described in a previous section. Eighty liter-per-second getter-ion type pumps were used to pump each of the two test chambers. One-liter bottles of pure nitrogen gas were connected to the variable leak valves of the system.

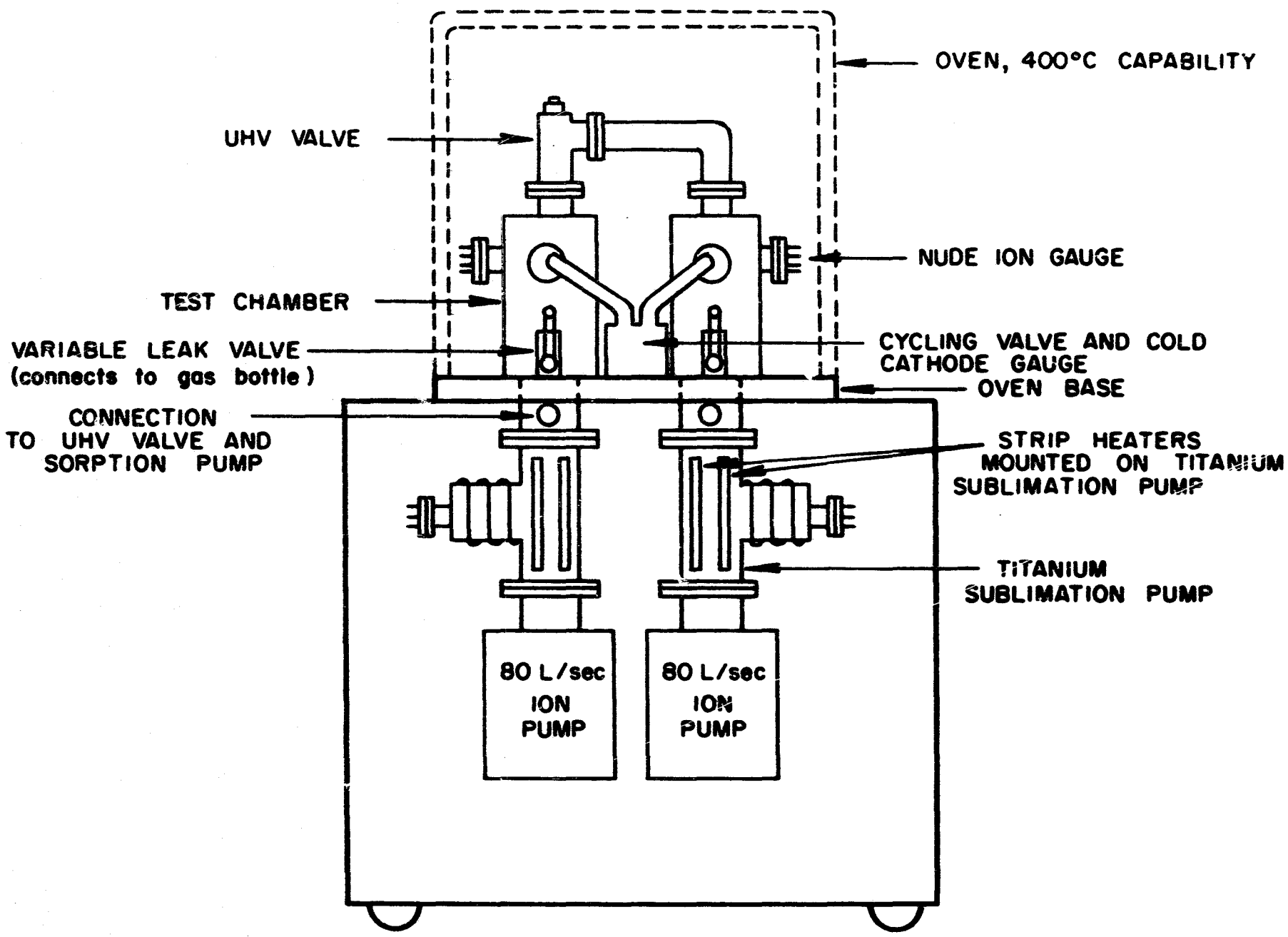

Figure 56. Two-chamber-type test system.

The model R-5 test gauge was connected to a rotary valve of the kind described earlier. The two tubulations of the rotary valve were flanged so that they could be conveniently connected to the two pressure chambers of the test system. The rotary valve was driven by magnetic coupling via an external permanent magnet. The permanent magnet was rotated by a Bodine model NSH-12R variable speed motor connected to a Minarick Electric Co. model SH-12 speed control. The high voltage to the cold cathode gauge was furnished by a J. Fluke model 408A power supply. The gauge output current was amplified by either a Keithley model 415 fast response linear electrometer or a Keithley model 412 logarithmic electrometer. The logarithmic electrometer was used when the range of pressures to be measured was greater than one decade. The output of the electrometers was recorded with either a Sanborn model 150 strip chart recorder or a Honeywell 906C Visicorder.

The results of the various pressure cycling experiments are displayed in Tables 4 through 7. Nitrogen gas was used as the test gas in all of the experiments. The same GCA model R-5 gauge and rotary valve were used for all the tests. Each table of data lists the maximum and minimum gauge currents for each cycling frequency. The frequency labelled zero represents the equilibrium gauge currents with the gauge connected to each of the two chambers for at least 5 or 10 minutes. The column labelled I_{MAX}- I_{MIN}, the difference between the maximum and minimum gauge readings, is the peak-to-peak amplitude from its largest value at equilibrium (zero frequency) represents an attenuation caused by the frequency dependence of the system response. It is this attenuation as a function of frequency that must be explained by pressure cycling theory. The average gauge current for each frequency has also been listed in each table. The average gauge current is a measure of the d.c. current level (d.c. pressure level) and shows if the pressure oscillations have shifted to a higher or lower pressure level. For example, in Table VI, it can be seen that the average current has continuously increased with frequency. Here, the corresponding continuous increase in I_{MAX} indicates either an outgassing process that increased with time or else a generation of gas within the rotary valve due to rubbing at the bearings or some other metal-to-metal contact points.

The data presented in Table 4 were obtained with a Keithley fast response model 415 electrometer. This data is probably the most reliable of all the data taken, since the rotary valve was operating properly up through a frequency of 4 cycles per second. Notice that the maximum current decreased with increasing frequency for frequencies of 2, 3 and 4 cycles per second. At the same time, the minimum currents increased with increasing frequency. This is exactly the sort of behavior that one would expect if the peak-to-peak amplitude is being limited by the time constant for gas exchange. Table 7 presents a somewhat different picture. Here the nitrogen pressure is relatively high and the pressure range for cycling was small. Apparently, the maximum pressure is attained in each cycle independent of the frequency but the minimum pressure (current) increased with increasing frequency. This kind of behavior indicates that gas exchange effects alone are not responsible for the attenuation but that desorption or re-emission of nitrogen gas prevented the gauge and valve from emptying completely at the higher frequencies.

TABLE 4

DATA AND RESULTS OBTAINED IN A TWO-CHAMBER CYCLING VALVE EXPERIMENT USING A GCA MODEL R-5 COLD CATHODE GAUGE EXPOSED TO AN 8.5 TO 1 NITROGEN GAS PRESSURE RATIO

Pressure Oscillation Frequency (cps)	I_{MAX} (Ampere)	I_{MIN} (Ampere)	$I_{MAX}-I_{MIN}$ (Ampere)	$\frac{I_{AVE}}{\frac{I_{MAX}+I_{MIN}}{2}}$ (Ampere)	Reduction in $I_{MAX}-I_{MIN}$ (Percent)	Remarks
0	9.75×10^{-8}	1.15×10^{-8}	8.60×10^{-8}	5.45×10^{-8}	0	Initial
2	9.75	2.00	7.75	5.87	9.9	Equilibrium
3	9.10	2.20	6.90	5.65	19.8	Levels
4	8.60	2.50	6.10	5.55	29.1	Gauge Anode
5	9.75	4.50	5.25	*7.12	38.9	Voltage of
6	9.20	4.50	4.70	*6.85	45.4	2.0 kV

*These increases in the gauge readings are believed to be due to gas generated within the rotary valve at the higher cycling frequencies.

TABLE 5

DATA AND RESULTS OBTAINED IN A TWO-CHAMBER CYCLING VALVE EXPERIMENT USING A GCA MODEL R-5 COLD CATHODE GAUGE EXPOSED TO A 25 TO 1 NITROGEN GAS PRESSURE RATIO

Pressure Oscillation Frequency (cps)	I_{MAX} (Ampere)	I_{MIN} (Ampere)	$I_{MAX}-I_{MIN}$ (Ampere)	$\frac{I_{AVE}}{\frac{I_{MAX}+I_{MIN}}{2}}$ (Ampere)	Reduction in $I_{MAX}-I_{MIN}$ (Percent)	Remarks
0	1.00×10^{-7}	4.00×10^{-9}	9.60×10^{-8}	5.20×10^{-8}	0	Initial Equilibrium Levels
2	7.00×10^{-8}	6.3	6.37	3.81	*33.7	
3	7.00	8.0	6.20	3.90	35.4	Frequencies Changed in Steps
4	6.6	1.2×10^{-8}	5.4	3.9	43.8	
5	6.0	1.7	4.3	3.85	55.2	
6	6.0	2.1	3.9	4.05	59.4	Gauge Anode Voltage of 1.0 kV
7	6.0	2.5	3.5	4.25	63.5	
8	5.7	3.0	2.7	4.35	71.8	Frequencies Changed continuously; *log electrometer used here
9	5.5	3.2	2.3	4.35	76.1	
10	5.5	3.4	2.1	4.45	78.1	
11	6.0	4.5	1.5	5.25	84.5	

*The time constant of the logarithmic electrometer used in this experiment has probably affected the gauge current readings.

TABLE 6

DATA AND RESULTS OBTAINED IN A TWO-CHAMBER CYCLING VALVE EXPERIMENT USING A GCA MODEL R-5 COLD CATHODE GAUGE EXPOSED TO A 1.63 TO 1 NITROGEN GAS PRESSURE RATIO

Pressure Oscillation Frequency (cps)	I_{MAX} (Ampere)	I_{MIN} (Ampere)	$I_{MAX}-I_{MIN}$ (Ampere)	$\frac{I_{AVE}}{\frac{I_{MAX}+I_{MIN}}{2}}$ (Ampere)	Reduction in $I_{MAX}-I_{MIN}$ (Percent)	Remarks
0	2.6×10^{-8}	1.6×10^{-8}	1.0×10^{-8}	2.1×10^{-8}	0	Initial Equilibrium Levels
2	2.6	1.8	0.8	2.2	20	
3	2.9	2.2	0.7	2.55	30	Gauge Anode Voltage of 2.0 kV
4	3.2	2.7	0.5	2.95	50	Noisy Recorder Signals
5	3.3	2.8	0.5	3.05	50	

TABLE 7

DATA AND RESULTS OBTAINED IN A TWO-CHAMBER CYCLING VALVE EXPERIMENT USING A GCA MODEL R-5 COLD CATHODE GAUGE EXPOSED TO A 1.2 TO 1 NITROGEN GAS PRESSURE RATIO

Pressure Oscillation Frequency (cps)	I_{MAX} (Ampere)	I_{MIN} (Ampere)	$I_{MAX}-I_{MIN}$ (Ampere)	$\frac{I_{AVE}}{\frac{I_{MAX}+I_{MIN}}{2}}$ (Ampere)	Reduction in $I_{MAX}-I_{MIN}$ (Percent)	Remarks
0	1.27×10^{-6}	1.05×10^{-6}	2.2×10^{-7}	1.16×10^{-6}	0	Initial Equilibrium Levels
2	1.27	1.095	1.75	1.183	20.5	
3	1.27	1.145	1.25	1.208	43	Gauge Anode Voltage of 1.5 kV
4	1.27	1.182	0.88	1.226	60	
5	1.27	1.195	0.75	1.233	66	

One should note that different gauge anode voltages were used in the different experiments. It is expected that different gauge voltages will lead to different gauge pumping and re-emission characteristics and will thus change the response.

The theory for the two chamber-cycling valve experiments has not been developed satisfactorily to date. However, a simplified version of the differential equation of the system has been derived and solved for rather special circumstances to obtain some idea of the parameters that would be involved.

Consider the volume V of the rotary valve and test gauge and the pressure P(t) within this volume. The pressure will change as gas is added to or removed from this volume. Gas is added to the volume by a flow from the high pressure chamber through a total effective conductance C(t) that varies with time. Gas is also added to the volume by desorption and re-emission R(t). Gas is removed from the volume by a flow to the low pressure chamber or by gauge pumping or surface adsorption. In both adsorption and pumping, the rate at which gas is removed is a function of the pressure P(t). Pumping and adsorption are combined in this development and are represented by a characteristic constant pumping speed S. Desorption and re-emission are also combined in this development. They both decrease with increasing time and are represented by the symbol R(t). If P_E is the external chamber pressure, the basic differential equation of the system may be written as

$$\frac{dP}{dt} + \frac{C(t) + S}{V} P = \frac{C(t)\ P_E}{V} + \frac{R(t)}{V} \tag{33}$$

Now, the conductance of the value C(t) depends on the shape of the apertures that move relative to one another. As a first order approximation, it will be assumed that the conductance C has a constant average value and that the external chamber pressure P_E is instantaneously shifted from one level to another every half cycle. Further, the period of time available for re-emission or desorption is so small that we shall consider R to be constant. With the above approximations, the solution to equation (33) is:

$$P(t) = \frac{C\ P_E + R}{C + S} + C_1\ e^{-\frac{C + S}{V}\ t} \tag{34}$$

The quantity C_1 is the constant of integration which is determined by the initial conditions. If we consider, now, only those cycling experiments in which the gauge pressure returns to its maximum value every cycle, then the initial pressure at t = o will have a constant maximum value P_H just as the external pressure P_E switches to its lower pressure level P_{EL}. Under these conditions, the solution is

$$P(t) = \frac{C\ P_{EL} + R}{C + S} + P_H - \frac{C\ P_{EL} + R}{C + S}\ e^{-\frac{C + S}{V}\ t} \tag{35}$$

As t becomes infinite, the pressure in the gauge and valve becomes equal to the first term of the right-hand member of the above equation. If the re-emission factor is small and the adsorption and pumping speed S can be neglected with respect to the conductance C, this limiting lower pressure is just the low pressure chamber level P_{EL}.

To simplify the remaining development, introduce the following abbreviations:

$$P_L = \frac{C\,P_{EL} + R}{C + S} \quad , \quad \frac{C + S}{V} = A \tag{36}$$

Next, form the ratio

$$\frac{P_H - P(t)}{P_H - P_L} = 1 - e^{-At} \tag{37}$$

The expression for the percentage reduction in the pressure amplitude for this special case can then be written as

$$100 \quad 1 - \frac{P_H - P(t)}{P_H - P_L} = 100\, e^{-At} \tag{38}$$

The percentage reduction is shown to depend on the cycling frequency through the time $t = T/2$ where T is the period of the pressure oscillation. All that remains to be done is to substitute the gauge currents that correspond to the various gauge pressures with the tacit assumption that the gauge is linear in the region of operation. The final equation is

$$\text{Percentage amplitude reduction} = 100 \quad 1 - \frac{(I_{MAX} - I_{MIN})_f}{(I_{MAX} - I_{MIN})_o} = 100\, e^{-At} \tag{39}$$

where the subscripts f and o refer to the pressure oscillation of frequency f and the equilibrium or zero frequency pressure levels respectively.

To test the above theory, apply it to the data of Table IV. For example, first determine the parameter A from the data obtained at 2 cps and the equilibrium current levels. It will be found that A = 9.20 ($t = \frac{T}{2} = 1/4$ sec here) in order to obtain the experimentally determined 9.9 percent reduction. Next, use this value of A and the appropriate values of $T/2 = 1/6$ sec for a frequency of 3 cps and $T/2 = 1/8$ sec for a frequency of 4 cps to obtain the percentage reduction values of 21.7 percent at 3 cps and 31.7 percent at 4 cps.

VII. ADDITIONAL EXPERIMENTS

Equipment

The test system that was used to study cold cathode gauge stability noise and the effect of cold traps on gauge calibration with nitrogen gas was quite different from the other test systems described previously. This new system used a specially designed, bakeable, stainless steel mercury diffusion pump patterned after the glass pumps that were first constructed by Venema [14]. This ultra high vacuum (UHV) pump was backed by a conventional mercury diffusion pump and rotary mechanical forepump. A water-cooled baffle and an isolation cold trap separated the two diffusion pumps. Between the UHV diffusion pump and the test chamber, a series of two non-level-sensitive cold traps were interposed to prevent migration of the mercury pumping fluid to the test chamber. The UHV diffusion pump, each of the non-level-sensitive cold traps, and the test chamber were fitted with large ConFlat flanges so that they could readily be disassembled. The system was constructed so that the major UHV components mentioned above could be baked out at high temperatures of at least 450°C. The test chamber was fitted with three smaller flanged tubulations to permit the attachment of vacuum gauges, mass spectrometers or other experimental equipment. A gas diffuser was installed within and near the flanged end of the test chamber to permit pure gases to be introduced. The gas diffuser was connected via calibrated capillary tubes to a small "gas inlet" chamber that was pumped by a separate mercury diffusion pump system. This arrangement permitted pure gases to be introduced into the gas inlet chamber in a continuous flow fashion. A wide range of pressures of pure gas could be established in the gas inlet chamber. Of the two capillary tubes used to join the gas inlet chamber and the gas diffuser of the test chamber, the larger bore tube was valved with an all-metal, bakeable valve. The smaller bore tube had such a smaller vacuum conductance (6.0×10^{-6} liters/sec for nitrogen at 20°C) that it would not limit the ultimate pressure attainable in the test chamber (with a gas inlet chamber pressure of 10^{-8} torr) until a pressure of 10^{-15} torr was reached.

Referring to the block diagram of Figure 57 and the photograph of Figure 58, it can be seen that all of the UHV components, the calibration capillaries, the gas inlet chamber, the bakeable valves, the gas inlet gauge, and the test chamber gauges were located above an insulated table top so that they could be conveniently baked out in the same oven. The components located below the insulated table top were not baked, with the exception of the tubing that joined the UHV diffusion pump to its isolation cold trap and the tubing that joined the gas inlet chamber to its isolation cold trap.

A Welch model 1402B 140 liter/min two-stage rotary mechanical pump was used to create a forepressure of the order of 10 to 20 microns for both the UHV pumping portion of the system and the gas introduction portion of the system. The mechanical pump was fitted with a vented exhaust to minimize the condensation of vapors and the subsequent contamination of the pump oil.

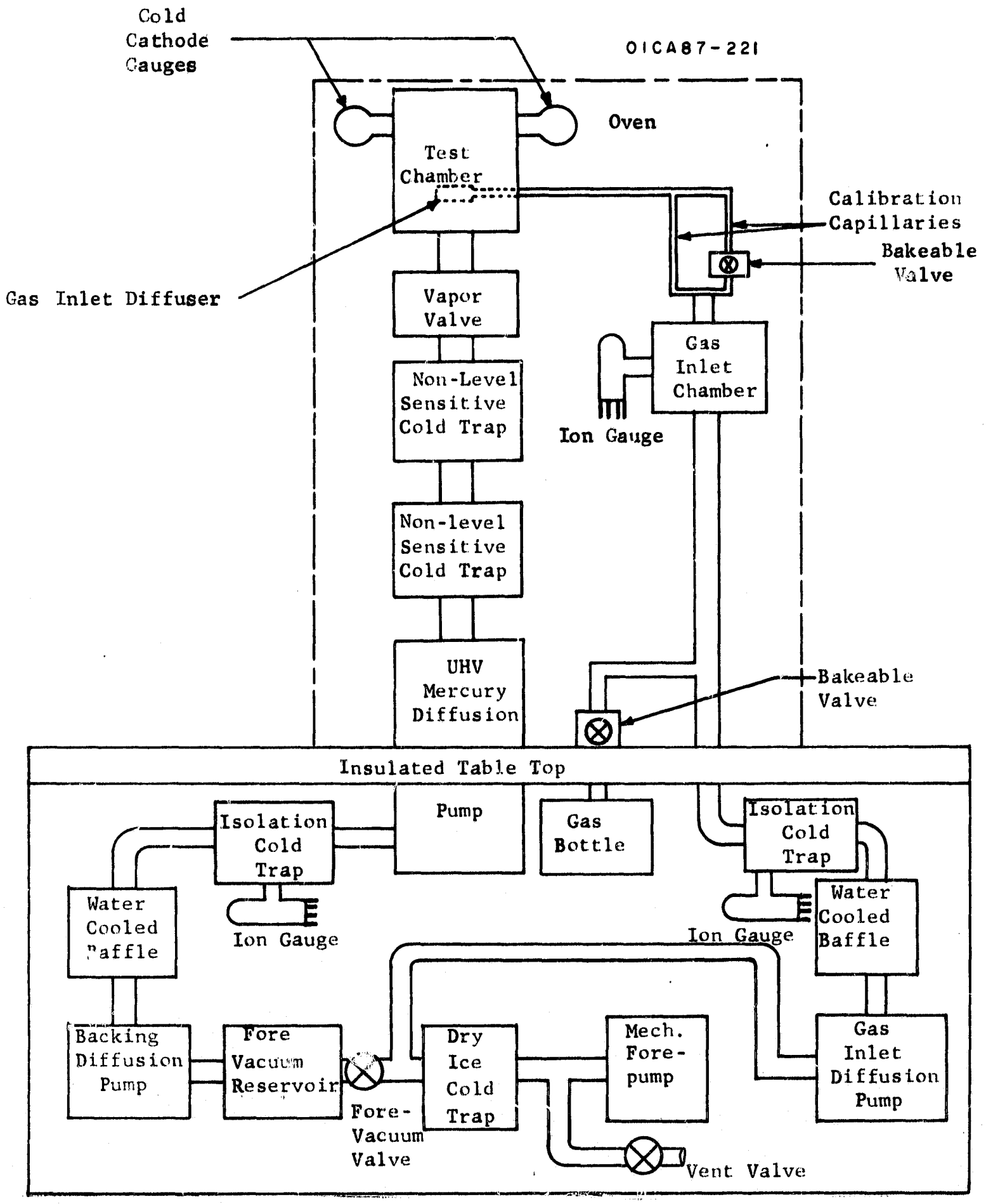

Figure 57. Block diagram of all-metal, UHV mercury diffusion pump system.

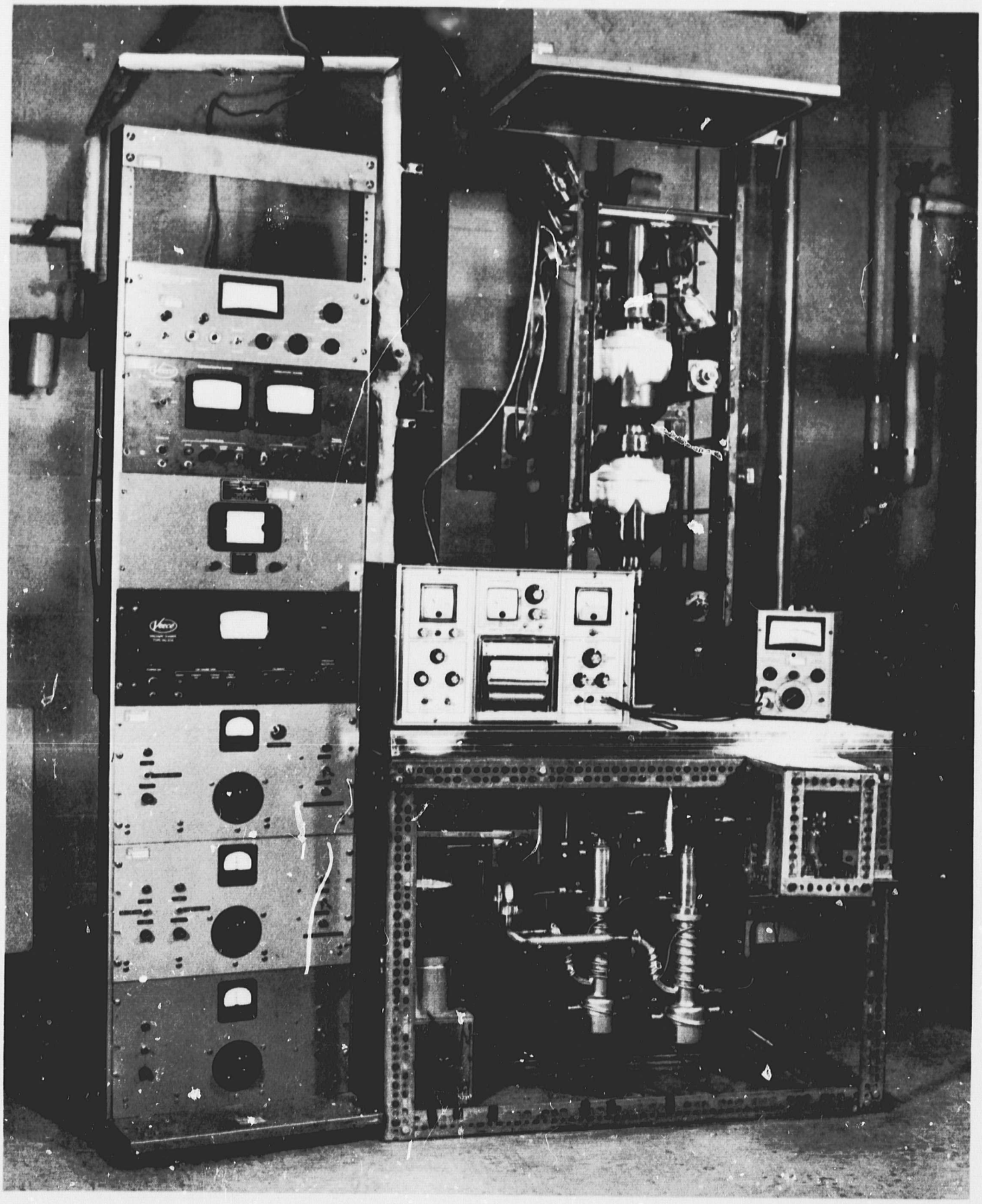

Figure 58. Photograph of mercury diffusion pump system.

The mechanical pump was separated from the rest of the system by a demountable glass vacuum trap that was cooled with dry ice. A stainless steel, bellows type valve using teflon gaskets and a zytel seat was connected between the mechanical pump and the dry ice cold trap to serve as a venting and leak testing valve.

A stainless steel, bellows type fore-vacuum valve was located between the dry ice cold trap and a 2-liter glass bulb that served as a fore-vacuum reservoir. The fore-vacuum valve could be closed to completely isolate the UHV pumping section from the gas introduction part of the system.

The backing diffusion pump and the gas inlet diffusion pump were Consolidated Vacuum Corporation Model NHG-40 metal mercury diffusion pumps. Specially designed water-cooled baffles fitted directly over the tops of the diffusion pumps and served the purpose of reducing the loss of mercury to the isolation cold traps. The latter traps were designed for a two-fold purpose: First, they isolated the flow of mercury from one pump to another in the UHV system, and kept mercury out of the gas inlet chamber. Second, they permitted ionization gauges to be installed in these portions of the vacuum circuit. The ionization gauges were particularly valuable during the bakeout cycle since they would indicate the degree of outgassing of those parts of the system within the oven.

The UHV mercury diffusion pump was designed so that the entire jet assembly could be baked out in the oven. The upper part of the pump containing the jets was located above the insulated table top, while the pump boiler was located well below the table top. This arrangement, combined with the design of the pump, permitted the upper part of the pump to be baked to temperatures of 450°C. The function of the two non-level-sensitive cold traps that were mounted between the top of the UHV diffusion pump and the bottom of the test chamber was to prevent any migration of mercury from the UHV pump into the test chamber. These two cold traps were normally filled with liquid nitrogen.

The gas inlet chamber to which the calibrated capillaries were attached was connected, via 1-inch diameter tubing to the isolation cold trap of the gas introduction system. A 1-liter bottle of pure gas was connected through a second bakeable valve to the 1-inch diameter tubing as shown in the block diagram. Notice that the gas bottle was located just below the insulated table top so that the complete tubulation to the gas bottle was baked out (before the seal-off tip on the gas bottle was broken). This arrangement guaranteed a minimum of contamination of the pure gas admitted to the system. The gas inlet chamber also contained a side tubulation to which a hot filament ionization gauge was connected. A McLeod gauge was also connected to this side tubulation to measure the pressure in the gas inlet chamber.

The system oven was of the forced draft variety and was designed to be used with the vacuum system. The temperature of the oven could be controlled to within a few degrees centigrade. During the system bakeout procedure, it was customary to bake out with the oven at several fixed positions above the

insulated table top. Under these conditions, it was necessary to seal off the open, bottom end of the oven with an insulating, demountable oven base.

A John Fluke model 408B high voltage power supply was used to provide the anode voltage to the GCA model R-5 cold cathode gauges that were being tested. Keithley model 600 battery operated electrometers were used to measure the positive ion current to the gauge cathodes. The standard permanent magnet that was used with the gauges had a cylindrical air gap that was 1-1/4 inches in diameter and 1-1/4 inches long. The magnetic field strength at the center of the air gap was about 1050 gauss. In the study of gauge stability and noise, a potentiometer type strip chart recorder was used to record the gauge output current. Only low frequency noise (of the order of a few cycles/sec was of concern in this study.

Study of Cold Cathode Gauge Stability and Noise

Measurements of the GCA model R-5 cold cathode gauge noise and instability as a function of anode voltage and magnetic field strength were made on several occasions. The R-5 gauge was mounted on the test chamber of the metal mercury diffusion pump system and had been under vacuum for several months. The upper part of the system including the gauge was baked at 400°C for 3 hours before each experiment. Measurements were made using the background gas in the system. The system pressure was varied within a narrow range by allowing the level of liquid nitrogen in the cold traps to change.

Two separate sets of stability measurements were made by starting with the gauge anode at 1.0 kV and increasing the anode voltage in steps of 200 volts about every 20 minutes. A normal magnetic field of 1050 gauss was used for one set of measurements, while a much weaker magnetic field of 800 gauss was used for the other set of measurements. The gauge currents were monitored and recorded continuously.

A resume of the results obtained with the normal magnetic field of 1050 gauss follows: Starting with 4.0 kV on the gauge anode as an operational check of the gauge, it was observed that the gauge current reading was 3.3×10^{-9} Ampere with 6 percent peak-to-peak noise. When the cold traps were filled and the anode voltage was reduced to 1.0 kV, the gauge signal decreased to $1.45 \times 10^{-}$ Ampere and became noise-free. At an anode voltage of 1.2 kV, the gauge signal increased slightly to 1.5 Ampere and a noise of about 4 or 5 percent developed as the pressure and gauge signal increased. When the anode voltage was changed to 1.4 kV, the signal was steady at first at 1.5×10^{-9} ampere, but after a minute or so, it developed positive going spikes that were approximately 15 percent of the signal magnitude. Soon thereafter, the spikes became a general noise of 15 percent and when the current reached a value of 1.7×10^{-9} Ampere, there was a sudden mode change to a lower noise-free current that varied from 0.8 to 1.1×10^{-9} ampere with changing pressure. When the anode voltage was increased to 1.6 kV and the cold traps were filled, the gauge current decreased to 0.8×10^{-9} ampere, developed about 10 percent noise, and then jumped to a higher current level of 2.0×10^{-9} ampere. At this new level, the gauge

developed large negative going excursions (current spikes or surges) down to 0.8×10^{-9} ampere, alternating with positive going excursions to 2.5×10^{-9} ampere. After about 2 minutes of this behavior, the gauge current returned to a lower level of 0.8×10^{-9} ampere with 10 percent noise. After another 2 minutes, the current increased to 0.9×10^{-9} ampere and became noise-free. When the cold traps were filled again about 5 minutes later, the gauge current again jumped to the higher current mode and began spiking positively and negatively as before. This behavior was repeated a third time upon filling the cold traps. When the anode voltage was increased to 1.8 kV, the gauge current increased from 0.9×10^{-9} to 2.3×10^{-9} ampere and was almost noise-free. When the current increased to 2.4×10^{-9} ampere due to the normal rise in the test chamber pressure, there was a mode change, and the current decreased suddenly to a value ranging between 1.1 and 1.25×10^{-9} ampere and remained noise-free for about 15 minutes. At that time, the current increased suddenly to a value of 2.8×10^{-9} ampere for 15 seconds and then dropped back to a value of 1.1×10^{-9} ampere. The two mode changes at 1.8 kV had nothing to do with the filling of the cold traps. At an anode voltage of 2.0 kV, the gauge current increased to 2.5×10^{-9} ampere and had 4 percent noise for about 2 minutes as the current increased to 2.7×10^{-9} ampere. At that time, the current suddenly dropped back to 2.5×10^{-9} ampere and became noise free. In the next 5 minutes, as the test chamber pressure increased, the gauge current increased, and when the current reached 3.4×10^{-9} ampere, it pulsed negatively to a value of 1.3×10^{-9} ampere several times. When the cold traps were filled, the same cycle of behavior repeated starting with a gauge current of 2.5×10^{-9} ampere having 4 percent noise.

After the 2.0 kV test, an operational check of gauge operation at 4.0 kV was made. The gauge signal varied from 2.0 to 3.0×10^{-9} ampere with about 10 percent noise and 20 to 25 percent positive spiking about every minute or two. The general noise level decreased as the signal increased.

At an anode voltage of 2.2 kV, the gauge signal started at a value of 3.25×10^{-9} ampere with about 2 percent peak-to-peak noise. As the gauge current increased to a level of 4.35×10^{-9} ampere, the noise increased to 3 percent. At this point, the signal became noise-free as it increased further up to a value of 5.2×10^{-9} ampere, at which time the cold traps were filled and the gauge current went as low as 2.9×10^{-9} ampere, and then generally repeated its behavior as the pressure increased. At an anode voltage of 2.4 kV, the gauge current started at 2.9×10^{-9} ampere, noise-free, after filling the cold traps and then gradually increased to a value of 4.7×10^{-9} ampere, at which time the cold traps were filled again. When the gauge current reached a value of about 3.7×10^{-9} ampere, it started to become noisy, and the noise signal increased gradually as the current increased until it had its maximum value of about 4 percent peak-to-peak when the gauge current was 4.7×10^{-9} ampere. When the anode voltage was increased to 2.6 kV and the traps were filled, the gauge behavior was similar to that at 2.4 kV. The current started out at 3.5×10^{-9} ampere, noise-free, as the current increased to its maximum value of 5.6×10^{-9} ampere it became more and more noisy, reading a maximum noise of almost 4 percent at 5.6×10^{-9} ampere. There were a few positive and negative current spikes present. At 2.8 kV

on the anode, the cold traps were filled and the current decreased to 3.6×10^{-9} ampere and then started to increase. At 4.0×10^{-9} ampere, the current became slightly noisy (about 2.5 percent) and when the current reached 4.2×10^{-9} ampere there was a mode change and the current decreased to a level of 3.45×10^{-9} ampere and became noise-free. When the cold traps were filled again, the current decreased to 3.1×10^{-9} ampere and then started to rise. It remained noise-free until it reached a value of 4.7×10^{-9} ampere, at which point it jumped upward to a higher mode at a level of 5.5×10^{-9} ampere and became noisy (4.5 percent noise) and spiked negatively about 14 percent. At an anode voltage of 3.0 kV there appeared to be three separate modes of operation. After filling the cold traps, the current started at 4.9×10^{-9} ampere with 2 percent noise and 14 percent negative spiking. As the current increased, the noise and spiking increased. At 5.2×10^{-9} ampere, the noise was 2.5 percent while the negative spiking had increased to about 25 percent. The current then dropped a small amount ot a new lower value of 4.8×10^{-9} ampere and became noise free. The noise-free condition persisted until the current reached a value of 5.5×10^{-9} ampere, at which time the current jumped up to a new noisy mode (5 percent noise) centered at 6.05×10^{-9} ampere.

An operational check of the gauge at 4.1 kV was made at this time. After filling the cold traps, the gauge current started at a value of 4.4×10^{-9} ampere and then increased gradually, becoming more and more noisy and spiking was as much as 25 precent. A mode change then occurred. The current decreased to 4.85×10^{-9} ampere and became noise-free. As the cold trap liquid levels fell, the gauge current increased to 8.5×10^{-9} ampere and remained noise free. There was a mode change at this point and the current decreased drastically to 2.55×10^{-9} ampere and became noisy (about 6 percent noise) and now exhibited positive spiking of about 15 percent. This mode persisted as the current increased to 3.3×10^{-9} ampere. This was the first time that a clear-cut relationship between noise-free, negative spiking and positive spiking operation was observed.

When the gauge anode voltage was reduced to 3.2 kV, two noisy modes of operation were observed. The high sensitivity mode current ranged from 5.0 to 6.0×10^{-9} ampere with about 6 percent peak-to-peak noise and about 10 percent negative spiking. The low sensitivity mode current ranged from 3.0 to 4.4×10^{-9} ampere and also had about 6 percent noise, but no spiking. At 3.4 kV on the gauge anode, the gauge current started at 2.7×10^{-9} ampere after filling the cold traps and then gradually increased. In this case, the current noise was about 7 or 8 percent initially and gradually decreased to a noise-free condition at a current level of 3.5×10^{-9} ampere, then became noisy once more from 3.5 to 4.0×10^{-9} ampere (about 5 percent noise), and finally became noise-free again from 4.0 to 4.4×10^{-9} ampere. There was no spiking. When the gauge anode was increased to 3.8 kV and the cold traps were filled, the gauge current decreased to 2.05×10^{-9} ampere and was noise free, but did have 20 percent positive spiking every 5 or 10 seconds. When the current had increased to 2.35×10^{-9} ampere, the positive spiking became more frequent up to the maximum current of 3.6×10^{-9} ampere. The cold traps were filled and the current decreased, again exhibiting the same dependence of spiking frequency on pressure (or current level). Finally, the gauge anode voltage was increased to 4.0 kV and two modes

of operation were observed. In the high sensitivity mode the current ranged from 7.6 to 8.1 x 10^{-9} ampere and was noise free. The current then decreased sharply to 2.4 x 10^{-9} ampere with about 4 percent noise. As the current signal increased to 3.3 x 10^{-9} ampere, the noise increased to a maximum of about 6 percent and there were 4 or 5 positive current spikes over a period of 4 minutes.

The test that was made with the 800 gauss magnet in position on the gauge did not include as many anode voltage values as the test with the normal 1050 gauss magnet. The currents measured with the weaker magnet in position were generally larger than those taken earlier with the normal magnet. Filling of the cold traps caused a very large change in gauge current when using the weaker magnet. For anode voltages from 1.0 to 1.6 kV two sets of measurements were taken with the weak magnet so that a wider current range was covered. A summary of results obtained with the weaker magnet follows:

With 1.0 kV on the gauge anode, during one test the gauge current ranged from 1.25 x 10^{-9} ampere to greater than 9.9 x 10^{-9} ampere. The signal was noise free up to 4.5 x 10^{-9} ampere, had positive spiking of about 9 or 10 percent up to 6.8 x 10^{-9} ampere, exhibited a mode shift to a current of 7.5 x 10^{-9} ampere, was noise free up to 8.5 x 10^{-9} ampere, and then exhibited negative spiking of about 5 percent up to 9.5 x 10^{-9} ampere. With 1.0 kV on the gauge anode during a second test, the gauge current varied from about 1 x 10^{-8} to 4 x 10^{-8} ampere and was noise free.

With 1.2 kV on the gauge anode, the gauge current during one test ranged from 2.5 to 5.0 x 10^{-8} ampere and was noise free. During a second test, the current ranged from 1.3 x 10^{-7} to 4.3 x 10^{-7} ampere and was noise free.

At 1.4 kV on the gauge anode, the gauge current was noise free from 2.8 to 8.5 x 10^{-8} ampere during one test and was also noise free from 3.6 to over 9.9 x 10^{-7} ampere during a second test.

At 1.6 kV on the gauge anode, the gauge current was noise free from 3.2 x 10^{-8} to over 9.9 x 10^{-8} ampere in one test.

With 1.8 kV on the gauge anode, the gauge current varied from 4.15 x 10^{-8} to over 9.9 x 10^{-8} ampere. The current was noise free until a level of 6.4 x 10^{-8} ampere was reached. At this point there was negative spiking up to a level of about 8.0 x 10^{-8} ampere, and the current became noise free above this level.

At an anode voltage of 2.0 kV, the gauge current signal had about 1 percent noise between 2.8 x 10^{-8} ampere and 3.1 x 10^{-8} ampere. The gauge current then became noise free as it increased up to about 9.9 x 10^{-8} ampere. There was a single negative spike at 6.45 x 10^{-8} and a single positive spike at 6.8 x 10^{-8} ampere. There appeared to be a small mode change from 3.7 to 4.5 x 10^{-8} ampere.

A gauge operational check was made at 4.0 kV after filling the cold traps. The gauge current was noise free from 2.65 x 10^{-8} ampere to 4.8 x 10^{-8} ampere. The current became noisy from 5.0 x 10^{-8} ampere to 9.4 x 10^{-8} ampere (about 4 percent noise) with some negative spiking.

With 2.6 kV on the gauge anode, the cold traps were filled and the gauge current decreased to 3.5×10^{-8} ampere. The current was noise free and then increased to 6.8×10^{-8} ampere at which point it became very noisy (about 5 percent noise), had 14 percent positive spiking, and decreased to 6.5×10^{-8} ampere. The current then increased in noise-free fashion to 8×10^{-8} ampere at which point it again had positive spiking (about 10 percent). The gauge current from 8×10^{-8} to 9.9×10^{-8} ampere was noise free.

After placing the gauge anode at 3.0 kV and filling the cold traps, the gauge current decreased to 3.5×10^{-8} ampere and then started to increase. The current was noise free until it attained a value of 6.8×10^{-8} ampere, at which point it became noisy and spiked positively in the same way that it did at 2.6 kV. The current decreased to 6.35×10^{-8} amps, then became noise free and increased to 8.0×10^{-8} ampere and spiked positively about 10 percent as before. The gauge current from 8×10^{-8} to 9.9 x 10-8 ampere was noise free.

Finally, at an anode voltage of 3.6 kV and with the weak 800 gauss magnet still in position, the gauge current increased from 1.9×10^{-8} ampere to 6.0×10^{-8} ampere in a completely noise-free fashion.

The results of a third noise and stability experiment that was performed with the same GCA model R-5 gauge are summarized in Table 8. The gauge current was in the 10^{-9} ampere region, a region which is known to be noisy and unstable for the R-5 gauge and which was chosen deliberately for this purpose. Measurements were made at intervals of 100 volts from 1.5 to 3.0 kV.

The use of a table to catalog the data of noise and stability measurements makes it easy to see the overall results. For example, Table 8 shows that multimode and single mode gauge operation alternated as the anode voltage was increased. There were as many as five modes of operation at 1.5 kV. All but one of these modes were noisy and both positive and negative spiking were observed. At 1.6 kV, there were two modes. The higher current mode was noisy and spiked negatively (toward the lower current mode). There was a single noise-free mode at 1.7 kV and two modes again at 1.8 kV. Here the higher current mode was noisy but the lower current mode spiked positively (toward the higher current mode). There were single modes at 1.9 and 2.0 kV. At 2.1 kV, there were 3 modes, one noise free, one with noise and one with negative spiking (toward the lowest current mode). There was a single mode at 2.2 kV. At 2.3 kV, three modes appeared again, one with negative spiking (toward the lowest current mode). The lowest current mode was noisy as before. At 2.4 and 2.5 kV, there was single mode operation. Three mode operation re-appeared at 2.6 kV. Here both negative and positive spiking occurred in two of the three modes. At anode voltages of 2.7, 2.8, 2.9, 3.0, 3.2, 3.4 and 3.6 kV, only single modes were present, and all but two of these were noise free.

The purpose of the noise and instability measurements was to obtain quantitative data concerning cold cathode gauge operation. It is expected that gauge noise, spiking and oscillation are intimately connected with the space

TABLE 8

SUMMARY OF A TYPICAL STABILITY AND NOISE EXPERIMENT

Anode Voltage (kV)	Time of Scan (min)	Gauge Current (Ampere)	Peak-to-Peak Noise (Ampere)	Spiking Amplitude (Ampere)	Remarks
1.5	29	1.60×10^{-9}	0.25×10^{-9}		No. 1 Mode
		1.20			No. 2 Mode
		2.80	0.25		No. 3 Mode
		1.40	0.10	0.30×10^{-9} (neg.)	No. 4 Mode
		1.00	0.10	0.30(pos.)	No. 5 Mode
1.6	15	$8.1\text{-}8.6 \times 10^{-10}$	0.30×10^{-10}	1.2×10^{-10} (neg.)	No. 1 Mode
		6.3-7.0			No. 2 Mode
1.7	15	$5.7\text{-}9.6 \times 10^{-10}$			Single Mode, Noise-free
1.8	15	$4.1\text{-}4.2 \times 10^{-9}$	0.20×10^{-9}		No. 1 Mode
		2.4-3.3		0.30×10^{-9} (pos.)	No. 2 spiking every 5-10 sec
1.9	12	$2.5\text{-}2.6 \times 10^{-9}$			Single Mode, Noise-free
2.0	8	$2.65\text{-}2.85 \times 10^{-9}$	0.10×10^{-9}		Single Mode
2.1	15	$3.15\text{-}3.6 \times 10^{-9}$			No. 1 Mode
		3.6-4.0		0.20×10^{-9} (neg.)	No. 2 Mode
		3.0-3.6	0.20×10^{-9}		No. 3 Mode
2.2	15	$3.3\text{-}3.6 \times 10^{-9}$			Single Mode, Noise-free

TABLE 8 (continued)

Anode Voltage (kV)	Time of Scan (min)	Gauge Current (Ampere)	Peak-to-Peak Noise (Ampere)	Spiking Amplitude (Ampere)	Remarks
2.3	10	$3.3\text{-}3.4 \times 10^{-9}$		0.20×10^{-9} (neg.)	No. 1 Mode
		3.1-3.6			No. 2 Mode
		2.95-3.15	0.20×10^{-9}		No. 3 Mode
2.4	5	$3.1\text{-}3.3 \times 10^{-9}$	0.20×10^{-9}		Single Mode
2.5	5	$3.1\text{-}3.35 \times 10^{-9}$	0.20×10^{-9}	0.7×10^{-9} (pos. + neg.)	Single Mode
2.6	12	$4.0\text{-}5.2 \times 10^{-9}$	0.20×10^{-9}	0.6×10^{-9} (pos. + neg.)	No. 1 Mode
		5.4-6.5		0.8 (neg.)	No. 2 Mode
		6.3-6.7	0.20	0.5 (pos. + neg.)	No. 3 Mode
2.7	10	$3.8\text{-}4.1 \times 10^{-9}$	0.40×10^{-9}	0.7×10^{-9} (pos. + neg.)	Single Mode
2.8	7	$4.2\text{-}5.4 \times 10^{-9}$			Single Mode, Noise-free
?	5	$4.0\text{-}5.0 \times 10^{-9}$			Single Mode, Noise-free
3.0	5	$3.8\text{-}4.4 \times 10^{-9}$			Single Mode, Noise-free
3.2	5	$3.7\text{-}4.2 \times 10^{-9}$			Single Mode, Noise-free
3.4	5	$3.6\text{-}4.1 \times 10^{-9}$			Single Mode, Noise-free
3.6	1	1.10×10^{-9}	0.30×10^{-9}		Single Mode

charge distribution within the gauge and with the physical processes that occur in the discharge. Thus, in the eventual formulation of a detailed theory of gauge operation, all of the phenomena of noise and instability should be accounted for.

Some of the observations that can be made on the basis of the noise and instability measurements are listed below:

(1) There can be many modes of operation at one anode voltage setting.

(2) Different modes of operation are associated with different gauge currents (pressures).

(3) There can be some overlap between the modes, that is, the gauge can operate in different modes at the same anode voltage and current.

(4) The modes of operation change with changes in the magnetic field as well as with changes in the anode voltage and the gas pressure.

(5) Mode changes to either higher or lower currents occur very rapidly.

(6) A mode can be noise free, contain random noise, contain positive and/or negative spiking, or have both noise and spiking.

(7) The amplitude of current excursions (spiking) is usually much greater than peak-to-peak noise amplitudes.

(8) Current excursions usually move in a direction toward another current mode.

(9) There can be small changes in gauge current accompanied by transitions from a noisy to a noise-free condition or vice versa.

(10) Noise and spiking patterns as a function of anode voltage, magnetic field strength and gauge current are repeatable.

(11) In a noisy mode, the noise can become larger or smaller as the gauge current increases.

(12) Gauge current can go from a noisy condition to a noise-free condition as a function of current (pressure) with any sharp mode (current) changes.

(13) When there are two distinct modes at different current levels, the higher current mode usually spikes negatively while the lower current mode usually spikes positively.

(14) The frequency of spiking can vary with the gauge current.

(15) There were large mode changes at the higher anode voltages but only small mode changes at the lower anode voltages.

(16) Gauge operation was more nearly noise free with an 800-gauss magnet (and higher currents) than with a 1050-gauss magnet (and lower currents).

Additional work that should be performed in connection with noise and stability studies is the development of one or more noise models that might explain the origin of the random noise and spiking. These models would then be used to plan new noise tests. As stated earlier, the eventual goal is to understand the detailed operation of the gauge.

Demonstration of the Pumping Effect of Liquid Nitrogen Cooled Traps During Low Pressure Nitrogen Gas Gauge Calibration

It has long been suspected that liquid nitrogen cooled cold traps which are used with diffusion pumped systems and other pumping systems have a strong effect on nitrogen gas calibrations that are made at pressures of 10^{-9} torr and below. The basis for this suspicion is the unusually long time that is required to obtain an equilibrium pressure in the test or calibration chamber at these pressures.

At low pressures, it is often assumed that an equilibrium pressure will be reached as soon as a monolayer of gas has formed on the surfaces. It is known that nitrogen gas adsorbs on tungsten, molybdenum and iron surfaces at room temperature. Atomic nitrogen is adsorbed on nickel surfaces at room temperature. No specific data is available on the adsorption of nitrogen gas on 300 series stainless steel surfaces at liquid nitrogen temperature.

It is known that the sticking probability for nitrogen on tungsten, and for other chemically active gases on metal surfaces in general, has a high initial value between about 0.1 and 1.0 at low surface coverage (very low pressures). As the surface coverage increases and a monolayer is approached, the sticking probability decreases to values less than 10^{-3}. The time required to form a monolayer on a surface is proportional to the rate at which molecules strike and stick to the surface as well as the number of adsorption sites. This relation is expressed simply as:

$$t = n/\beta\gamma \qquad (40)$$

where t is the time to form a monolayer, n is the number of adsorption sites, β is the sticking probability, the fraction of molecules striking the surface that are adsorbed, and γ is the impingement rate, the number of molecules striking each square centimeter of surface per second. Obviously, as β becomes small, the time to form a monolayer increases. However, even if the sticking probability were unity, it would take over 1 hour to form a monolayer at a pressure of 1×10^{-9} torr and over 10 hours at a pressure of 1×10^{-10} torr. It is not necessarily true that a complete monolayer will form since it is possible to attain an adsorption-desorption equilibrium at coverages of less than a monolayer.

Since adsorption-desorption phenomena are strongly affected by temperature, it was reasoned that a change in the temperature of the cold traps would greatly change the time required to reach an equilibrium pressure in the test chamber during low pressure calibration work with nitrogen gas. A very simple (but expensive) method of increasing the cold trap temperature to a constant higher value is to use a cryogenic liquid having a higher boiling point that that of liquid nitrogen. Liquid argon appears to be ideal for this application, since its boiling point is -185.7°C as compared with the boiling point of liquid nitrogen at -195.8°C, about 10°C lower. It was decided to start a low pressure calibration with the metal mercury diffusion pump system in the usual way, with the exception that liquid argon would be used in the two non-level sensitive cold traps in place of liquid nitrogen. It would then be possible to compare the behavior of the system with the two different cryogenic fluids.

The metal mercury diffusion pump system had been baked up to 450°C overnight several days prior to the experiment. The two non-level-sensitive cold traps were initially filled with liquid nitrogen and the test chamber pressure was measured to be in the 10^{-12} torr region. Several hours before the experiment began, the top cold trap was blown out and warmed up to room temperature and then filled with liquid argon. It was noticed that the liquid argon boiled off more rapidly than liquid nitrogen and the cold traps had to be "topped off" more frequently. In addition, it appeared that the background pressure in the system was not as low as it had been with liquid nitrogen in the cold traps, but the pressure measurements were not completely comparable and this finding is not conclusive.

The test chamber background pressure was 1.2×10^{-11} torr as measured with the GCA model R-5 gauge operated with 4.0 kV on the gauge anode and using an estimated gauge sensitivity of 2 amperes/torr. The background pressure in the gas inlet chamber was 1.7×10^{-7} torr as measured with a hot filament Bayard-Alpert gauge. The gas bottle line had been pumped out to a pressure of 1 to 2×10^{-7} torr, after which the nitrogen gas bottle seal-off had been broken. It was decided to use the small 0.2 mm diameter capillary (nitrogen conductance at 20°C equal to 6×10^{-6} ℓ/sec) to introduce the nitrogen from the gas inlet chamber to the test chamber. Since the conductance limited pumping speed of the diffusion pump at the test chamber was about 25 liters/sec for nitrogen, a pressure of 5×10^{-4} torr nitrogen in the gas inlet chamber would eventually establish a test chamber pressure of about 1×10^{-10} torr.

The nitrogen gas bottle valve was opened to allow nitrogen to flow into the gas inlet chamber. It took about 5 minutes to establish a pressure of 5.4×10^{-4} torr in the gas inlet chamber by slowly adjusting the gas bottle valve. During this five-minute period, the test chamber pressure increased from 1.2×10^{-11} torr to 3.4×10^{-11} torr. Fourteen (14) minutes after the nitrogen gas bottle valve was first opened, the gas inlet chamber pressure had stabilized at a value of 5.60×10^{-4} torr and the test chamber pressure reached an equilibrium value of 4.5×10^{-11} torr (at an estimated sensitivity of 2 amperes/torr). The test chamber pressure and gas inlet chamber pressure were then monitored for a period of one hour and were found to be unvarying. The gas bottle valve was closed and the test chamber pressure decreased very quickly to a value of 1.6×10^{-11} torr within 8 minutes.

Upon comparing the results of the experiment described above with the many hours required to reach equilibrium test chamber pressures when using liquid nitrogen cooled cold traps in the same situation, it is apparent that a liquid nitrogen cold trap has an appreciable "transient pumping speed" for nitrogen gas at low pressures. The transient pumping speed decreases continuously with time (as the surface coverage and pressure increase). Previous experiments have shown that carbon monoxide, carbon dioxide, methane and water vapor are all either adsorbed or condensed on liquid nitrogen cold traps. Since these gases often constitute a large percentage of a low pressure background environment, it would appear that all low pressure calibration work can best be done without the use of liquid nitrogen cold traps. The effective pumping speed of a liquid nitrogen trapped pumping system must be carefully measured for each gas species as a function of pressure.

REFERENCES

1. Kreisman, W. S., "Development of Cold Cathode Ionization Gauges for Space Vehicles," GCA Report No. 64-17-N, prepared for NASA, Goddard Space Flight Center, Greenbelt, Maryland under Contract No. NAS5-3353 (November 1964).

2. Kreisman, W. S., "Yaw Attitude Sensor," GCA Report No. 67-19-N, prepared for NASA, Goddard Space Flight Center, Greenbelt, Maryland under Contract No. NAS5-9642 (December 1967).

3. Penning, F. M., Physica 4, 71 (1937).

4. Redhead, P. A., Can. J. Phys. 37, 1260 (1959).

5. Young, J. R. and Hession, F. P., Transactions of the Tenth National Vacuum Symposium of the American Vacuum Society, The Macmillan Co., New York, p. 234 (1963).

6. Beck, A. H. and Brisbane, A. D., Vacuum 2, 137 (1952).

7. Haefer, R., Acta. Phys. Austriaca 7. 52 and 251 (1953); 8, 213 (1954).

8. Redhead, P. A., Can. J. Phys. 36, 255 (1958).

9. Spargenberg, K. R., Vacuum Tubes, McGraw Hill Book Co., Inc., New York, p. 642 (1948).

10. Kreisman, W. S., "Measurement of the Lowest Pressures in Space and the Laboratory," NASA Contractor Report NASA CR-154, p. 40 (February 1965).

11. Carmichael, J. H. and Knoll, J. S., Transactions of the Fifth National Vacuum Symposium, Pergamon Press, New York, p. 18 (1958).

12. Blodgett, K. B. and Vanderslice, T. A., Proceedings of the Second International Vacuum Congress, Washington, D. C., Pergamon Press, New York, p. 400 (1961).

13. Carter, G. and Leck, J. H., Transactions of the Seventh National Vacuum Symposium, Pergamon Press, p. 339 (1960).

14. Venema, A. and Bandringa, M., Philips Tech. Rev. 20, 145 (1958-59).